U U 0 4 3 0 7 2 2 1

LBL-4029
c. 1

MASS MEASUREMENTS OF HIGHLY NEUTRON-EXCESS NUCLEI IN THE LIGHT ELEMENTS

Kenneth Hugh Wilcox
(Ph. D. thesis)

RECEIVED
NOV 13 1975
LIBRARY AND
DOCUMENTS SECTION

May 1975

Prepared for the U. S. Energy Research and
Development Administration under Contract W-7405-ENG-48

For Reference

Not to be taken from this room

LAWRENCE BERKELEY LABORATORY
UNIVERSITY OF CALIFORNIA
BERKELEY

LBL-4029
c. 1

DISCLAIMER

This document was prepared as an account of work sponsored by the United States Government. While this document is believed to contain correct information, neither the United States Government nor any agency thereof, nor the Regents of the University of California, nor any of their employees, makes any warranty, express or implied, or assumes any legal responsibility for the accuracy, completeness, or usefulness of any information, apparatus, product, or process disclosed, or represents that its use would not infringe privately owned rights. Reference herein to any specific commercial product, process, or service by its trade name, trademark, manufacturer, or otherwise, does not necessarily constitute or imply its endorsement, recommendation, or favoring by the United States Government or any agency thereof, or the Regents of the University of California. The views and opinions of authors expressed herein do not necessarily state or reflect those of the United States Government or any agency thereof or the Regents of the University of California.

0 0 0 0 4 3 0 7 2 2 2

E. ^{15}B 67
V. Comparison with Theory 78
A. Masses 78
^{25}Ne 78
$^{43-46}Ar$ 78
^{10}Li 78
B. Level schemes 80
^{25}Ne 80
$^{43,45}Ar$ 80
VI. Conclusion 84
Acknowledgments 86
Appendix I - Predictions of proton-excess nuclei 88
Appendix II - Low-cross section reactions 90
References 93

MASS MEASUREMENTS OF HIGHLY NEUTRON-EXCESS NUCLEI IN THE LIGHT ELEMENTS

Contents

Abstract iv

I. Introduction 1

II. Theory 3

A. The calculation of nuclear masses 3

B. Semiempirical mass methods 4

Liquid drop 4

Semiempirical shell model 5

General nuclidic mass relations 7

C. Modified shell model mass relation 9

Description of the mass relation 9

Comparison with transverse relation 11

Prediction of neutron-excess nuclei 14

Prediction of proton-excess nuclei 21

III. Experimental Technique 22

A. General considerations 22

B. Recoil techniques 24

C. Heavy ion considerations 27

D. Cyclotron 28

E. Beam transport and experimental area 31

F. Targets 31

G. Detectors and electronics 34

Singles electronics 37

Coincidence electronics 39

H. Data acquisition and analysis 41

IV. Experimental Results 44

A. ^{25}Ne 44

B. ^{43,45,46}Ar 46

C. Cl and S isotopes 53

D. ^{10}Li 55

techniques. Contamination problems only permitted determining a ground state cross section upper limit of 50 nb/sr.

A simple mass relation is derived, similar in approach to the Garvey-Kelson method but taking more explicit account of shell effects. Comparison is made with the Garvey-Kelson relation, and predictions of masses and of the stability of neutron-excess light nuclei are given for both methods. The modified mass relation is shown to often better account for highly neutron-excess nuclei, including the values reported here for ^{25}Ne and ^{43,45,46}Ar.

MASS MEASUREMENTS OF HIGHLY NEUTRON-EXCESS NUCLEI IN THE LIGHT ELEMENTS

Kenneth Hugh Wilcox

Lawrence Berkeley Laboratory
University of California
Berkeley, California 94720

ABSTRACT

The $^{26}Mg(^{7}Li,^{8}B)^{25}Ne$ reaction at 78.9 MeV was used to measure the mass-excess of ^{25}Ne (-2.18 ± 0.10 MeV) and several low-lying excited states. Mass-excesses for ^{43}Ar (-31.98 ± 0.07 MeV), ^{45}Ar (-29.727 ± 0.06 MeV), and ^{46}Ar (-29.732 ± 0.07 MeV) were determined from the $^{48}Ca(\alpha,^{9,7}Be)^{43,45}Ar$ reactions at 77.7 MeV and the $^{48}Ca(^{6}Li,^{8}B)^{46}Ar$ reaction at 80.1 MeV. Several excited states of ^{43}Ar and ^{45}Ar were observed. These and the excited states of ^{25}Ne are compared with theoretical predictions. Ground state differential cross sections are given for all reactions, ranging from 0.1 to 1 μb/sr at forward angles. Upper limits of about 1 to 25 nb/sr were determined for the ground state cross sections of the reactions $^{48}Ca(\alpha,^{8,10,11}B)^{44,42,41}Cl$ and $^{48}Ca(\alpha,^{10-13}C)^{42-39}S$ at 110 MeV.

Recoil coincidence techniques were used to measure the mass-excess of the particle-unbound nucleus ^{10}Li(33.83 ± 0.25 MeV) by the $^{9}Be(^{9}Be,^{8}B)^{10}Li$ reaction at 121 MeV; the ground state cross section was 30 nb/sr. The $^{14}C(^{9}Be,^{8}B)^{15}B$ reaction at 120 MeV was also investigated using coincidence

I. INTRODUCTION

Mass measurements of nuclei far from the region of β-stability are interesting for several reasons. Most of these reasons can ultimately be reduced to a desire for basic knowledge about nuclear structure and forces. A principal emphasis here will be on the measurement of unknown masses as a means of testing various mass prediction schemes, and thus their underlying models. There is a substantial divergence in the predictions of some models as we move to increasingly-large neutron excess in the light elements. One such important prediction is the onset of particle instability of nuclei.

Valuable spectroscopic information may sometimes also be obtained in experiments producing nuclei far from stability. Due to the nature of these experiments, spins and parities of levels are hard to measure. Certain information about the location and spacing of levels may nevertheless be acquired. Since calculated level spacings have a high degree of sensitivity to the nature of the two-body interaction used, knowledge of the two-body interaction may be thereby gained.

Until about four years ago, no masses were known for $T_z = (N-Z)/2 \geqslant 5/2$ nuclei through Z = 15. Since then ground state masses in this region have been determined for the $T_z = 5/2$ nuclei ^{11}Li and ^{21}O through ^{35}P, as well as for the more-highly neutron-rich nuclei ^{22}O and $^{28-32}$Na. (Masses and references are given for all these nuclei in Table I, Sect. II) This has already made it possible to show that a simple modified shell model mass formula can predict the masses of these $T_z \geqslant 5/2$ nuclei significantly better than the widely-used Garvey-Kelson formalism. The modified model also accounts better for the heavy argon isotopes ^{43,45,46}Ar,

reported here. A discussion of the model appears in Section II.

Level schemes are known for even fewer highly neutron-excess nuclei with $Z \leqslant 15$. $T_z = 2$ nuclei with several excited states known are ^{20}O, ^{24}Ne, ^{28}Mg, and ^{32}Si (summarized and treated theoretically in ref. 1). Only two $T_z \geqslant 5/2$ nuclei fit this category: ^{25}Ne (ref. 2 and this work) and ^{29}Mg (ref. 3). Above Z = 15, level schemes are known for all $T_z = 5/2$ nuclei and many of higher neutron excess. The principal reason for the paucity of level data in the lighter-mass region is that most of the limited number of techniques available to produce nuclei in this region can not be used to measure excited states.

The technique employed in this work, described in Section III is in-beam particle identification using solid state detectors. One important advantage is the ability to measure excited states in the product nuclei.

Multiparticle transfer reactions must be used to produce nuclei far from β-stability, due to the lack of stable target materials close to the nuclei of interest. Usually this requires heavy ion (nuclei heavier than α particles) beams and exit particles. Associated with heavy ion experiments is a whole set of characteristic experimental difficulties, notable among them being low beam intensities, high angular momentum transfers, and relatively poor energy and mass resolution. Multiparticle transfer reactions tend to involve such additional difficulties as low cross sections, highly negative Q values, and severe target contamination problems. Experimental considerations such as these are discussed in Section III.

Many of the experiments presented in this work involved the detection of ^{8}B exit particles. ^{8}B is a particularly suitable heavy ion for particle identification due to a number of reasons. Both ^{7}B and ^{9}B are particle-

unbound, so ^{8}B should be well separated from neighboring reaction products despite the spreading effect of Landau fluctuations in their energy loss. ^{8}B has no particle-bound excited states to complicate interpretation of energy spectra or to overlap with higher levels in the residual nucleus. And, finally, ^{8}B is the lightest particle-bound, $T_z = -1$ nucleus, permitting large ΔT_z transfers and thus production of nuclei with large neutron excess.

The experimental results are presented in Section IV. Measured mass-excesses and level schemes are compared with theory in Section V.

II. THEORY

A. The Calculation of Nuclear Masses

Calculating nuclear masses directly from fundamental principles is not generally practical at present. No exact theory for the finite many-body problem and nucleon-nucleon interaction exists. Some successes have been obtained by making assumptions based on an independent-particle description of the nucleus. The excellent results of the shell model calculations of Cohen and Kurath[4] in the 1p shell are just such a case. However, these methods generally have a very restricted region of applicability. In particular, for nuclei far from the valley of β-stability either the necessary two-body matrix elements are unknown or the number of configurations involved is too large for the calculation to be realistic.[5] Consequently, no general expression for nuclear masses has been generated in this fashion.

We must therefore adopt a less fundamental view. A nuclear model is used to determine the form of the functional dependence of mass on various nuclear parameters. Coefficients are then adjusted freely by fitting the equation to the experimental data. The resulting equation is known as a

semiempirical mass equation. Of course, some care must be exercised in using such a procedure. In order that local trends in experimental data, or even erroneous data, do not cause extrapolation errors, it is important to check whether the coefficients so determined seem to contradict the model or generally accepted notions of the nucleus.[6]

A somewhat different approach is also possible. Although nuclear masses can not usually be reliably calculated directly, the differences between closely adjacent masses may perhaps be understood from general physical considerations. The resulting expression is often referred to as a mass relation to distinguish it from a mass equation, which attempts to calculate masses directly. Mass relations are the more reliable of the two approaches. A less global approach is taken, and the most relevant known masses are used in predicting the desired nuclear masses.[5]

B. Semiempirical Mass Methods

Three semiempirical approaches given the widest attention in recent years will be mentioned here. They are the liquid drop picture of the nucleus, the shell model, and various nuclidic mass relations employing mass difference equations. Since the methods of many authors contain elements from more than one of these descriptions (the models are not unrelated), their classification into models is to some extent artificial and nonunique.

Liquid drop — At the center of the liquid drop model (and its more realistic generalization, the droplet model) is a description of the nucleus as a macroscopic, incompressible nuclear liquid drop. Although this model leads to a smooth behavior for the nuclear mass surface, a number of rapid deviations or oscillations are experimentally observed.

Single-particle effects are responsible for these fluctuations, which arise because the single-particle levels in the nucleus are not smoothly distributed. The most important of these deviations is due to shell effects; the next most important is associated with nuclear pairing.[7]

To account for these effects, a method often referred to as the shell-correction approach has evolved.[8] It is a macroscopic-microscopic synthesis largely developed by Strutinsky.[9-11] To the smoothly-varying liquid drop terms are appended, in somewhat arbitrary fashion, nuclear pairing and shell effect terms.

Many investigations have been made using the corrected liquid drop model (LDM) to predict masses. They differ in the methods used to determine the shell and pairing correction terms (see ref. 12 for a discussion of several methods) and in the possible inclusion of additional, higher-order corrections. Comparisons of some of the more successful of these attempts, among themselves as well as with other types of models, are given, for example, by the papers of Wing[13,14] and Comay et al..[12]

The best fits to the experimental data tend to have a mean deviation of several hundred keV to 1 MeV. In the light nuclei, up through the 2s1d shell, fits are significantly worse, since single-particle effects become very large. Overall results of the LDM in this region of masses are not as good as those obtained with some other models, such as the semiempirical shell model and nuclidic mass relations. While much light can be shed on nuclear structure by the LDM, it does not at present appear to be the best tool for predicting masses of unknown nuclei in the light elements, our primary concern here.

Semiempirical shell model— The shell model is an independent-particle

model. In this model the sum of all the nuclear interactions is assumed to create a potential well within which each particle moves freely. Their energies and wave functions are found by solving the corresponding one-particle problem, with the potential determined on an empirical basis.

The best-known attempt to calculate masses based on a semiempirical shell model (and one of still very few such attempts) is the work by Zeldes et al..[6,15,16] They assumed that the residual interaction varies linearly with the number of particles in the valence shell. Configuration interactions among subshells were included, thus allowing for deformation energy. An equation of the many-parameter type results (parameters numbered in the hundreds), compared to the few-parameter (parameters numbered in the tens) liquid drop equations. For nuclei beyond the 1p shell, a fit to known masses gave a mean deviation[6] of 170 keV (although significantly worse deviations occurred in the light nuclei), much better than any LDM fit has been able to produce. Much of the improvement, however, should be ascribed to the increased number of parameters.

Recently the model has been extended[17] to account for new experimental evidence. Lowest seniority (strong pairing) requirements have been relaxed, and configuration mixing among major shells has been allowed, among other changes. The mean deviation of fit is comparable to that previously found and to the Garvey-Kelson relations (described below). However, remedy has been at least partially obtained for several previous deficiencies, including strong discontinuities at shell boundaries, a failure to preserve magic numbers far from stability, and a systematic deviation from several nuclei discovered in the interim.

Predictions by this model in the light elements are not nearly as

successful as in the heavier elements. Strong charge-dependent nuclear terms in the mass equation may be responsible.[18] It is thus not clear whether continued refinement will ever permit this particular model to be very useful in this mass region.

General nuclidic mass relations — A well-known general nuclear mass relation is the Garvey-Kelson (GK) formalism,[18,19] which is also based on an independent-particle model. A key assumption is that single-particle wave functions and residual interactions are only slowly-varying functions of atomic number. Each single-particle level is four-fold degenerate with respect to isospin conjugation and time reversal, corresponding to two protons and two neutrons in each level.

Equations consisting of sums and differences of closely-neighboring nuclei are constructed in such a way that all two-body interactions (nn, np, and pp) cancel in the limit of slowly-varying potentials. This can be accomplished for all nuclei having $N \geqslant Z$ except $N = Z =$ odd. In their general form, the equations may be expressed as recursion relations. Two such independent general relations have been formulated, the transverse and longitudinal equations. It has been shown[18] that the equations are consistent with several existing independent-particle models. This relatively high degree of model independence, stemming from the dearth of assumptions, apparently accounts[5] for the high degree of accuracy with which the GK approach reproduces the experimental data. Further discussion of this topic will be made later.

The utility of this model in predicting the masses of unknown nuclei with large neutron excess is very great. Each unknown mass can be expressed in terms of well-known masses in that general region of the chart

of the nuclides. It should be noted, however, that the same simplicity which is responsible for the GK formalism being a powerful mass-prediction tool also renders it essentially useless as a source of information on nuclear models.

Recently Jänecke and Behrens have noted[20-22] small systematic errors in the GK fits superimposed on the much larger random fluctuations. Neglect of the dependence of the residual neutron-proton interaction I_{np} on T_z or A (for the transverse and longitudinal relations, respectively) is responsible. Although small, these systematic deviations accumulate rapidly as one extrapolates away from the region of β-stability, approximately as ΔT_z to the third or fourth power.[22]

I_{np} is experimentally observed to decrease with increasing A, to fluctuate, and to exhibit shell effects.[15,23] Its dependence on T_z is complicated* and not fully understood. Because of the neglect of this I_{np} dependence, GK probably underestimates[22] masses for $T_z \gg 0$.

In order to account for the I_{np} dependence Jänecke and Behrens have developed a generalized nuclidic mass relation (containing GK as a limiting case) which contains a corrective term for I_{np}. Several different functional dependencies of the term, extracted from various macroscopic and microscopic models, have been investigated by Jänecke and Eynon[25] for their ability to reproduce the known masses.† Fits to the known masses could be greatly improved by the addition of this correction term. It was believed that predictive value would also improve somewhat, especially for nuclei far from the line of β-stability, if the I_{np} expression used was substantially correct. (The reliability of predicting unknown nuclei far from stability depends entirely on the underlying physical assumptions, and

*Although apparently I_{np} depends on $|T_z|$ rather than T_z, supporting the charge-symmetry property of nuclei.[24]

†While I_{np} can be extracted from experimental data, it cannot be used in the generalized-relation because it will reduce to an identity.[21]

accurate reproduction of the known masses is by no means a sufficient condition. For example, the transverse and longitudinal relations of GK[18] fit the known masses equally well, but lead to strongly diverging predictions[22] for N>>Z.) However, the authors caution[25] that, at least for the present state of development, their corrected mass relations should only be used for A≥70. Below that, the dependence of I_{np} on shell model configurations becomes too important.

Another attempt to extend the utility of the GK mass relations was made by Bassichis and Ali.[26] A literal interpretation of GK was used to relate various experimental deviations from GK. This information became the basis for predicting unknown masses. It was shown that the large discrepancies between experimental and predicted masses of some light $T_z = 5/2$ nuclei were removed in this way.

C. Modified Shell Model Mass Relation

Description of the mass relation— Goldstein and Talmi[27] developed an early simple shell model approach to calculate nuclear ground state energies. No specific assumptions were made on the nature of the two-body interaction, except that it was constant over nuclei in which the same shells were being filled. The energy of the closed shells of these nuclei was also considered constant, and equal to the binding energy of the nucleus with no particles beyond the closed shells. Although initially meeting with some degree of success,[27] the model has not been widely used partly because of the lack, until very recently, of sufficient experimental data in the light nuclei to determine the parameters in more than a few restricted regions.

Following their approach, the mass of a neutron-excess, doubly closed-

shell nucleus M_o is related to that of a nucleus $M(\pi j^m \nu j'^n)$ with m additional protons in the j shell and n additional neutrons in a higher j' shell by the equation

$$M(\pi j^m \nu j'^n) = M_o + V(\pi j^m) + V(\nu j'^n) + V(j^m, j'^n). \qquad (1)$$

In this expression $V(\pi j^m)$ represents the kinetic energy, interaction with the closed shells, and mutual interaction of the m protons in shell j; $V(\nu j'^n)$ that of the n neutrons in shell j'; and $V(j^m, j'^n)$ the interaction between the protons and neutrons.

Simplification is possible in Eq. (1) since the values of $V(\pi j^m)$ and $V(\nu j'^n)$ can each be expressed in terms of just three parameters (as noted below). However, as was indicated in the previous section, other configurations besides that of the simple shell model are generally important in describing the ground state wave function of a nucleus. Some allowance for such configuration mixing can be made by regarding $V(\pi j^m)$ and $V(\nu j'^n)$ as separate parameters for each value of m and n. This is equivalent to replacing $M_o + V(\pi j^m) + V(\nu j'^n)$ by the sum of arbitrary point functions U(Z) and W(N) of the number of protons and neutrons, respectively. Furthermore, if no odd-odd nuclei are considered, then $V(j^m, j'^n)$ depends only on an average interaction potential V(jj') through the relation[28] $V(j^m, j'^n) = mn\, V(jj')$. Hence, with the restriction of no odd-odd nuclei and rewriting $M(\pi j^m \nu j'^n)$ as M(Z,N), Eq. (1) is then equivalent to

$$M(Z,N) = U(Z) + W(N) + mn\, V(jj') \quad [mn \text{ even}]. \qquad (2)$$

This mass equation can be generalized to include neutron-excess nuclei from several configurations $\pi j_i \nu j_k$, though still with the requirement that the neutron shell νj_k lie higher than the proton shell πj_i. In this more general case the mass M(Z,N) is given by what will be called the

modified shell model mass relation (denoted M),

$$M(Z,N) = U(Z) + W(N) + \sum_{ik} m_i n_k V(j_i j_k) \; [m_i n_k \text{ even}] . \tag{3}$$

The m_i and n_k are the number of protons and neutrons in the shells πj_i and νj_k, respectively, and the sum $\sum_{ik}$ is over the neutron-proton interaction parameters $V(j_i j_k)$.

For comparison, in the simple shell model M(Z,N) is given by

$$M(Z,N) = M_o + \sum_i V(j_i{}^{m_i}) + \sum_k V(j_k{}^{n_k}) + \sum_{ik} m_i n_k V(j_i j_k) \; [m_i n_k \text{ even}] . \tag{4}$$

Each function of the form $V(j^q)$ represents the interaction energy of q identical nucleons and assumes minimum seniority can be expressed as

$$V(j^q) = qe_j + q(q-1)a_j/2 + [q/2]b_j ,$$

where $[q/2]$ is the integer less than or equal to q/2, and e_j, a_j, and b_j are three interaction parameters.[28]

Comparison with transverse relation-- Equation (3) is similar to the Garvey-Kelson transverse mass relation[18] (denoted T), which can be written in the form

$$M(Z,N) = F(Z) + G(N) + H(A) , \tag{5}$$

where F, G, and H are arbitrary functions of the number of protons, neutrons, and nucleons, respectively. Comparison with Eq. (3) shows that the two methods differ mainly in their parameterization of the residual neutron-proton interaction. In the method of Garvey et al.[18] much of this interaction is given by the function H(A), while in Eq. (3)

more explicit account is taken of shell structure by the term $\sum_{ik} m_i n_k V(j_i j_k)$. Also, implicit in Eq. (5) is the assumption, mentioned previously, that I_{np} is independent of T_z.

The differences in assumptions allow T to be more general than M, both in predicting masses of odd-odd nuclei and in being able to predict masses farther from stability. In both cases predictions are carried out by determining the parameters of the mass relations by a least-squares fit to known masses. For Eq. (5), all known masses of $N \geq Z$ nuclei can be included (except N = Z = odd), while for Eq. (3) only those which possess configurations $\pi j_i \nu j_k$ and which are not odd-odd can be used. (Although not all known nuclei need be used as input to Eq. (5), there are certain minimum requirements. In particular, it is not possible to exclude all odd-odd nuclei when predicting $T_z = \tau$ nuclei if only $T_z < \tau$ nuclei are used as input, thus making a direct comparison between T and M difficult.)

As a means of comparing the results of the modified mass relation with the transverse mass relation in the light neutron-rich nuclei, the masses of the $T_z = 5/2$ nuclei in the sd shell have been predicted. Their relative agreement with the experimental values is shown in Fig. 1. For these nuclei the predicted values arising from T were taken from the calculations of Thibault and Klapisch[29], which is an update of the Garvey et al.[18] work to include more recent experimental masses. Input included only known $T_z \leq 2$ nuclei. For the other predictions M was used except for the values for ^{21}O and ^{23}F, where Eq. (4) from the simple shell model was employed, since insufficient masses are known for Eq. (3) to be used. Only known non-odd-odd $T_z \leq 2$ nuclei, together with ^{29}Na, with configurations $\pi p_{1/2} \nu d_{5/2}$, $\pi d_{5/2} \nu s_{1/2}$, $\pi d_{5/2} \nu d_{3/2}$, and $\pi s_{1/2} \nu d_{3/2}$ were included

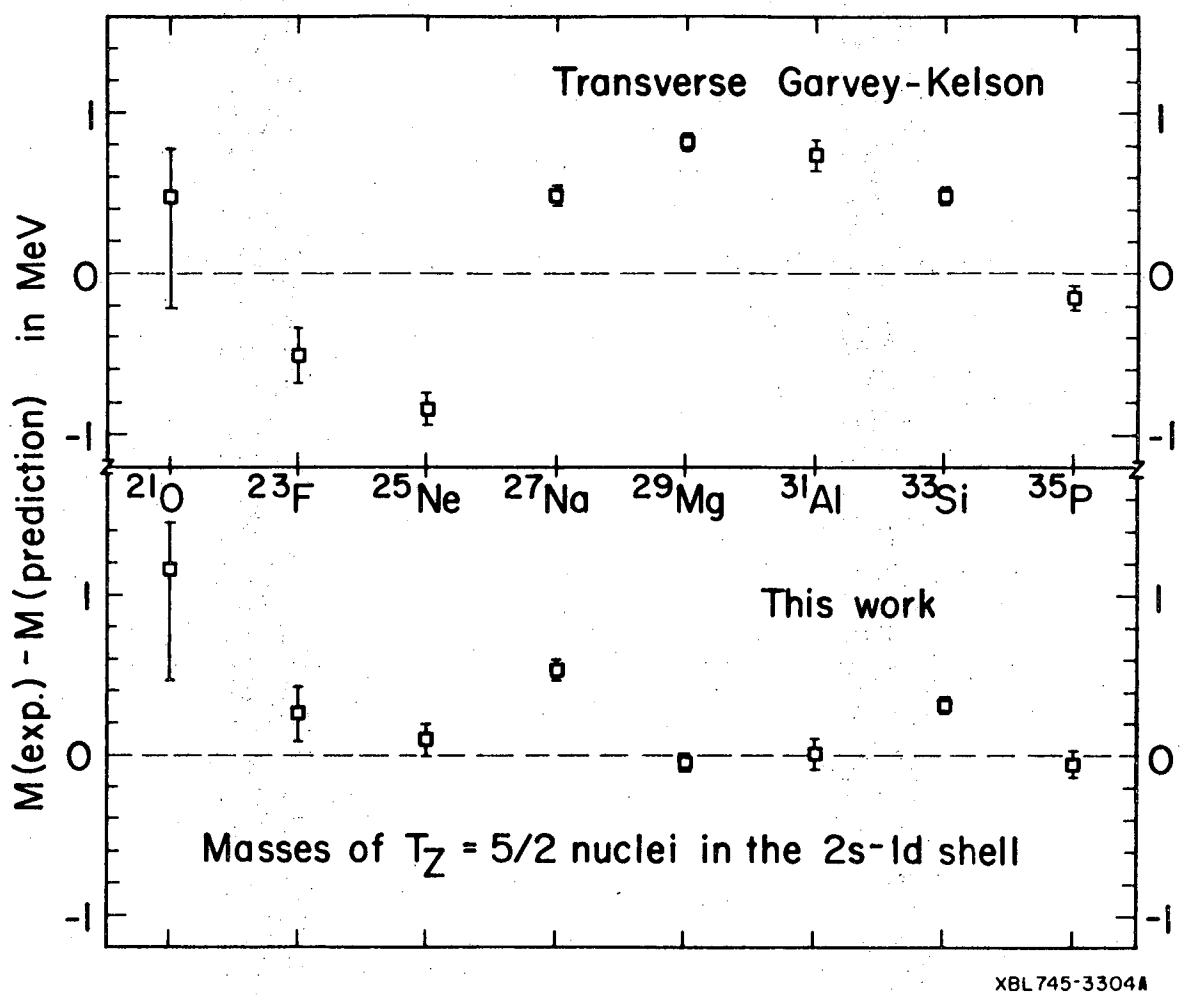

Figure 1. Two comparisons of the differences between experimental and predicted mass-excesses for the $T_z = 5/2$ nuclei in the 2s1d shell. Upper: Eq. (5), Garvey-Kelson transverse relation (T). Lower: Eq. (3), modified shell model mass relation (M), except for ^{21}O and ^{23}F (see text).

as input. (The mass of ^{29}Na is needed to determine the interaction parameter $V(\pi d_{5/2}\nu d_{3/2})$.)

As seen in Fig. 1, considerably better agreement was obtained with the approach of this work than with the transverse mass relation. Quantitatively the rms deviations between experiment and calculation are 260 keV and 620 keV, respectively (excluding the mass of ^{21}O because of its large error). A further comparison is afforded using the simple shell model, Eq. (4), alone. This yields a rms deviation of 390 keV, illustrating the importance of configuration mixing, which to some extent is allowed for in Eq. (3).

Another example that can be used as a means of comparing the predictions of M and T with experimental data for large neutron-excess nuclei is the heavy argon isotopes. Better agreement is also found using M, as presented in Section V.

Prediction of neutron-excess nuclei — Table I presents predictions of mass-excesses and one- and two-neutron binding energies of selected neutron-excess nuclei at or just beyond the limits of current investigation obtained with M, as well as through a recalculation with T. Experimental values are given when available; those nuclei only known to be bound or unbound are indicated by the symbol "B" or "U". A complete tabulation of the results is given in Ref. 30.

Calculated T and M values in Table I arise from a least-squares fitting program which employed with equal weight the appropriate particle-stable nuclei[31] with $N \geqslant Z$ whose mass-excesses are known to $\leqslant$ 200 keV; those known with less accuracy were not used in these calculations and are shown in the table enclosed in parentheses. All known nuclei(271)

Table I. Comparisons with experiment of the predictions of the transverse (T) and the modified (M) mass-equations.

				Mass Excess (MeV±MeV)			Binding Energy (MeV)					
							1 Neutron			2 Neutron		
				Experimental	Calculated		Experimental	Calculated		Experimental	Calculated	
Z	N	EL	A		T	M		T	M		T	M
2	6	HE	8	31.57±.03[a]	31.57	31.57	2.61			2.17		
2	7	HE	9	U ≡ unbound	42.61	43.49		-2.97	-3.85		- .36	
2	8	HE	10	U	51.00	52.34		- .32	- .78		-3.29	-4.62
3	7	LI	10	U	33.25			- .21			3.84	
3	8	LI	11	40.94±.08[b]	40.94	41.14				.17		
3	9	LI	12	U	52.94			-3.93			-3.55	
3	10	LI	13		61.56	60.34		- .55			-4.48	-3.05
4	8	BE	12	25.03±.05[c]	25.02	24.75	3.22			3.72		
4	9	BE	13	U	35.39	34.60		-2.31	-1.77		.94	1.84
4	10	BE	14	B ≡ bound	40.72	41.09*		2.74	1.58		.44	- .20
5	9	B	14	23.66 ±.03[d]	23.66		.98			5.86		
5	10	B	15	B	28.75	29.89		2.97			3.97	2.66
5	11	B	16	U	37.97			-1.14			1.83	
5	12	B	17	B	44.36	43.62		1.67			.53	2.41
6	11	C	17	B	21.27	20.86		.50	.90		4.75	5.34
6	12	C	18	B	25.50	24.57		3.84	4.36		4.34	5.27
6	13	C	19	B	33.47	32.41		.10	.24		3.94	4.60
7	12	N	19	B	16.27	15.32		5.07			7.74	8.51
7	13	N	20	B	21.60			2.75			7.82	
7	14	N	21	B	24.50	24.11		5.17			7.92	7.35
8	13	O	21	$\left(9.3^{+.3}_{-.7}\right)^{e}$	8.74	8.39**		3.08	3.48		10.80	11.09
8	14	O	22	$\left(11.5^{+.2}_{-.5}\right)^{e}$	9.42	9.35**		7.39	7.11		10.47	10.59
8	15	O	23	B	15.48	15.40		2.01	2.02		9.40	9.13
8	16	O	24	B	19.70	19.44		3.85	4.04		5.87	6.06

(continued)

0 0 0 0 4 3 0 7 2 3 1

Table I (continued)

				Mass Excess (MeV±MeV)			Binding Energy (MeV)					
							1 Neutron			2 Neutron		
				Experimental	Calculated		Experimental	Calculated		Experimental	Calculated	
Z	N	EL	A		T	M		T	M		T	M
9	14	F	23	3.36±.17[f]	3.40	3.36	7.54			12.74		
9	15	F	24	B	8.04			3.44			10.89	
9	16	F	25	B	11.75	11.26		4.36			7.80	8.24
10	15	NE	25	-2.16 ±.10[g]	-1.95	-2.12	4.28			13.15		
10	16	NE	26	B	.17	- .27		5.95	6.23		9.89	10.43
10	17	NE	27	-	6.52	6.58		1.73	1.21		7.68	7.44
11	15	NA	26	-6.90 ±.02[b,h]	-6.94		5.62			14.63		
11	16	NA	27	-5.62 ±.06[b,i,j]	-5.71	-5.73	6.79			12.41		
11	17	NA	28	-1.14 ±.08[b,i]	-1.02		3.59			10.38		
11	18	NA	29	2.65 ±.10[b,i]	2.32	2.66	4.28			7.87		
11	19	NA	30	8.37 ±.20[b,i]	8.50		2.35			6.63		
11	20	NA	31	(10.6 ±.8)[b]	12.70	14.38		3.87			5.76	4.42
11	21	NA	32	(16.4 ±1.1)[b]	21.02			- .25			3.62	
11	22	NA	33	B	26.90			2.19			1.94	
11	23	NA	34		35.08			- .11			2.08	
12	17	MG	29	-10.75±.05[k]	-10.70	-10.75	3.80			12.31		
12	18	MG	30	B	- 9.37	- 9.21		6.75	6.54		10.56	10.42
12	19	MG	31		- 3.73	- 3.17		2.43	2.03		9.18	8.56
13	18	AL	31	-15.01±.10[l]	-15.00	-15.05	7.19			12.94		
13	19	AL	32	B	-11.14			4.21			11.50	
13	20	AL	33	B	- 9.34	- 8.65		6.27			10.49	9.75
14	19	SI	33	-20.57 ±.05[m]	-20.71	-20.67	4.55			13.76		
14	20	SI	34	B	-20.57	-20.32		7.93	7.72		12.77	12.42
14	21	SI	35	B	-15.02			2.51			10.45	
15	20	P	35	-24.94 ±.08[n]	-24.90	-24.81	8.46			14.74		
15	21	P	36	B	-20.88			4.05			12.46	
15	22	P	37	B	-18.98			6.17			10.22	

(continued)

Table I (continued)

Z	N	EL	A	Mass Excess (MeV±MeV) Experimental	Calculated T	Calculated M	Binding Energy (MeV) 1 Neutron Experimental	1 Neutron Calculated T	1 Neutron Calculated M	2 Neutron Experimental	2 Neutron Calculated T	2 Neutron Calculated M
16	23	S	39	B	-23.07	-23.21		4.33	4.35		12.24	12.31
16	24	S	40	B	-22.50	-22.64		7.50	7.51		11.83	11.85
16	25	S	41		-18.31	-18.42		3.88	3.85		11.38	11.36
17	24	CL	41	B	-27.43	-27.39		7.84			13.65	13.67
17	25	CL	42	B	-24.68			5.32			13.16	
17	26	CL	43		-23.64	-23.61		7.03			12.35	12.36

*Assumed value, see text

**Calculated using equation 4

[a] J. Cerny, N. A. Jelley, D. L. Hendrie, C. F. Maguire, J. Mahoney, D. K. Scott and R. B. Weisenmiller, Phys. Rev. C10, 2654 (1974).

[b] Ref. 34.

[c] H. H. Howard, R. H. Stokes and B. H. Erkkila, Phys. Rev. Lett. 27, 1086 (1971); G. C. Ball, J. G. Costa, W. G. Davies, J. S. Forster, J. C. Hardy and A. B. McDonald, Phys. Lett. 49B, 33 (1974).

[d] G. C. Ball, J. G. Costa, W. G. Davies, J. S. Forster, J. C. Hardy and A. B. McDonald, Phys. Rev. Lett. 31, 395 (1973).

[e] Ref. 33.

[f] D. R. Goosman and D. E. Alburger, Phys. Rev. C10, 756 (1974).

[g] Ref. 2; D. R. Goosman, D. E. Alburger, and J. C. Hardy, Phys. Rev. C7, 1133 (1973).

(continued)

0 0 0 0 4 3 0 7 4 3 2

Table I (continued)

[h] E. R. Flynn and J. D. Garrett, Phys. Rev. C9, 210 (1974).

[i] R. Klapisch, R. Prieels, C. Thibault, A. M. Poskanzer, C. Rigaud and E. Roeckl, Phys. Rev. Lett. 31, 118 (1973).

[j] D. E. Alburger, D. R. Goosman and C. N. Davids, Phys. Rev. C8, 1011 (1973).

[k] Ref. 3; D. R. Goosman, C. N. Davids and D. E. Alburger, Phys. Rev. C8, 1331 (1973).

[l] D. R. Goosman and D. E. Alburger, Phys. Rev. C7, 2409 (1973).

[m] D. R. Goosman, C. N. Davids and D. E. Alburger, Phys. Rev. C8, 1324 (1973).

[n] D. R. Goosman and D. E. Alburger, Phys. Rev. C6, 820 (1972).

$2 \leqslant Z \leqslant 35$ and $4 \leqslant N \leqslant 50$ were used in obtaining the T values. Compared to the recent calculation of Thibault and Klapisch,[29] the ten known sd shell, $T_z \geqslant 5/2$ nuclei given in Table I were the additional nuclei included. For M the known non-odd-odd nuclei (74) with configurations $\pi p_{3/2}\nu p_{1/2}$, $\pi p_{3/2}\nu d_{5/2}$, $\pi p_{1/2}\nu d_{5/2}$, $\pi d_{5/2}\nu s_{1/2}$, $\pi d_{5/2}\nu d_{3/2}$, $\pi s_{1/2}\nu d_{3/2}$, and $\pi d_{3/2}\nu f_{7/2}$ were employed. Lack of sufficient known masses required assuming values for the mass-excesses of ^{21}O, ^{22}O and ^{14}Be. For ^{21}O and ^{22}O the values from Eq. (4) were used. To determine the interaction parameter $V(\pi p_{3/2}\nu d_{5/2})$, the mass-excess of ^{14}Be (known to be bound[32]) was taken to equal $^{12}Be + 2n = 41.09$ MeV, close to the value obtained with T of 40.72 MeV.

In order to compare how well these two approaches account for known masses, one can evaluate[28] the rms deviation defined as $[\sum_i \Delta_i^2/(N-P)]^{1/2}$, where the Δ_i are differences between the calculated and experimental masses, and N and P are the number of known nuclei and parameters, respectively. For nuclei with $2 \leqslant Z \leqslant 17$ T yields an rms deviation of 220 keV (N = 82, P = 66) and M yields 200 keV (N = 51, P = 36). Though these values are very similar it does not necessarily follow that the predictive validity of the two approaches will be the same. (Compare the results in Fig. 1.)

Several comments on nuclei at or near the current limit of experimental accessibility can be made from Table I. It appears that the differences between the T and M approaches observed in the sd shell for the $T_z = 5/2$ nuclei persist to lighter nuclei, since the predictions for ^{9}He, ^{13}Be, ^{15}B, and ^{19}N differ by more than 750 keV. In the sd shell the reported ^{22}O mass-excess[33] is much less bound (by 2.1 MeV) than is calculated

by either the transverse or the simple shell model mass relations. Since the β-decay end-point measurement employed by Artukh et al.[33] could possibly suffer from a systematic error in this direction, an additional measurement of the mass-excess of ^{22}O is of great interest. Similar conclusions apply to ^{21}O, reported in the same paper,[33] for which the predictions of M, T, and Bassichis and Ali[26] (mentioned previously) are all about 1 MeV more bound than the reported value.

Recent experimental measurements of ^{31}Na and ^{32}Na imply that these nuclei are more tightly bound than predicted. Experimentally,[34] the mass-excesses of ^{31}Na and ^{32}Na are 10.6 ± 0.8 and 16.4 ± 1.1 MeV, respectively, while the transverse mass relation predicts 12.7 and 21.0 MeV. This effect for ^{31}Na is even more striking when compared with the predicted mass-excess of 14.4 MeV arising from the modified mass relation. It has been pointed out[34] that this behavior can be explained by Hartree-Fock calculations which predict the sudden onset of a region of deformation, in sharp contrast to the well-known spherical nature at neutron number 20 in the calcium region.

These mass-excess calculations permit predicting which nuclei lie on the edge of stability. Limits yielded by this recalculation with the transverse relation differ from those of Ref. 29, which did not employ any $T_z \geqslant 5/2$ nuclei from the sd shell, in that a) ^{23}N, ^{26}O, ^{40}Mg, ^{43}Al, and ^{48}Si are now predicted to be the last nucleon stable isotopes, compared[29] to ^{25}N, ^{28}O, ^{42}Mg, ^{45}Al, and ^{46}Si; and b) ^{28}F, ^{29}Ne, and ^{37}Mg are predicted to be the first unbound isotopes, compared[29] to ^{30}F, ^{31}Ne, and ^{41}Mg. Results from the modified mass relation are less extensive than those from the transverse relation, generally not predicting the

edge of stability. For the lighter nuclei ^{26}O is calculated by Eq. (3) to be unbound by 240 keV, predicting ^{24}O as the last stable oxygen isotope. ^{29}F is calculated to be unbound to 2n decay by 910 keV, compared to the prediction of the transverse relation that it is bound by 770 keV.

Prediction of proton-excess nuclei — Kelson and Garvey[35] have employed relations based on the charge symmetry of nuclear forces to predict quite successfully the masses of proton-excess nuclei through the titanium isotopes. Since the results depend on the values used for neutron-excess nuclei, it was deemed desirable to repeat their calculation. Appendix I tabulates results for mass-excesses and one-and two-proton binding energies from the recalculation of T_z = -2, -5/2, and -3 nuclei, employing current known masses and predictions for neutron-excess nuclei from the transverse relation where necessary. Although many masses change considerably in this recalculation, the only revision[36] in their predictions of the onset of nuclear instability is that ^{31}Ar is now expected to be unbound.

III. EXPERIMENTAL TECHNIQUE

A. General Considerations

In order to investigate the properties of a nucleus Y, a target X is bombarded with projectiles a to initiate the nuclear reaction X(a,b)Y. For all experiments considered here, the standard technique is employed of identifying the exit particle b and measuring its emission angle and energy. It is then a simple matter to deduce the identity of the residual nucleus Y from nucleon conservation, and its energy by means of two-body kinematics based on energy and momentum conservation.

Reactions producing new nuclei far from stability usually have quite low cross sections (less than 1 μb/sr), so that the desired particles b are only a very small fraction of the total particle flux passing through the detectors. With a counting rate of 10^4 events/sec (a reasonable upper limit set by electronic dead time and pulse pileup), only a few events/sec or less may be of interest. Fairly sophisticated electronic and experimental procedures are then necessary. In particular, it is important to employ double particle identification with a stringent comparison between the two identifications, a technique to be discussed in Section III G.

If the target contains contaminants or if it is not monoisotopic, it is necessary to be able to tell when the exit particle b was produced by the reaction W(a,b)Z, for every W present to a significant degree. If the level structure of Z is well known, as it usually is, this identification is possible provided that the energy levels are far enough apart to permit good separation. Unfortunately, the reaction Q values for these interfering reactions are usually much less negative than the

desired reaction, so that their exit particle energies are higher. Thus the ground state of Y often coincides in kinetic energy with a high excitation region of the contaminant*, whose levels are then so close together as to form a continuous background. Furthermore, since the cross section for the reaction (a,b) is usually much higher on the contaminants than it is on X, a very small amount of a contaminant may account for most of the b particles produced. The net effect of all this is that the levels due to Y may be completely obscured by the contaminant reactions.

The most common contaminants are ^{12}C and ^{16}O. Targets which oxidize rapidly, such as calcium, are particularly difficult; a good vacuum is always necessary. The worst contaminant, however, is usually ^{12}C. Reactions of interest almost invariably proceed a great deal more rapidly on ^{12}C than on any other isotope present. Carbon is ubiquitous; pump oil and other organic vapors in the vacuum system are cracked by the beam and a thin layer of carbon tends to build up on the target during the course of an experiment. Liquid nitrogen traps are use to reduce these organics, but removal is never complete.

Fortunately, when the main target isotope is more massive than ^{12}C and ^{16}O, it is possible to overcome this contamination problem by going to larger detection angles. Due to kinematic effects, the particle energy decreases more rapidly with increasing angle for lighter targets. Beyond a certain angle, the peaks due to levels of Y are of higher energy than the contaminants and no longer obscured. A stiff price must be paid,

---

*Henceforth, the term "contaminant" will be considered to include not only isotopes originating in target manufacture or bombardment (such as ^{12}C and ^{16}O), but also other isotopes of the same element (^{40}Ca in a ^{48}Ca target) and other constituents of a nonelemental target (Si in SiO_2 used as an oxygen target).

however, since the cross sections for these multiparticle transfers also tend to drop off rapidly with increasing angle.

B. Recoil Techniques

Going to larger angles to avoid ^{12}C contamination is not possible in the $^{9}Be(^{9}Be,^{8}B)^{10}Li$ reaction because the target is lighter than ^{12}C, nor in the $^{14}C(^{9}Be,^{8}B)^{15}B$ reaction because the angles necessary are very large, and the cross section and particle energy become too low. Since the exit particles b (^{8}B in these cases) from target and contaminant can not be distinguished, it is necessary to use more sophisticated experimental techniques and also measure the recoiling residual nucleus.

The problem of target contamination by ^{12}C is particularly severe for the $^{14}C(^{9}Be,^{8}B)^{15}B$ experiment. Several percent ^{12}C is present in the purest ^{14}C material commercially available,[37] and additional ^{12}C builds up on the target surface throughout the experiment. The detection system needs to be very efficient in discriminating between ^{15}B and the ^{13}B recoil from ^{12}C in order to reduce contamination effects to manageable levels. This is difficult because mass, charge, and energy, the factors determining how a particle behaves in a solid-state detector, are so similar for ^{13}B and ^{15}B in this experiment.

The method employed was to require a coincidence between the ^{8}B nucleus detected in a 3-counter telescope and the recoiling ^{15}B residual nucleus, detected in another counter. Fig. 2 shows schematically the location of the detectors in the scattering chamber. For a ^{8}B detection angle of 14 degrees in the laboratory system and a Be beam energy of 120 MeV, ^{15}B recoils produced in the ground state are predicted to be emitted at 32 degrees and ^{13}B ground state recoils at 39 degrees. ^{13}B recoils

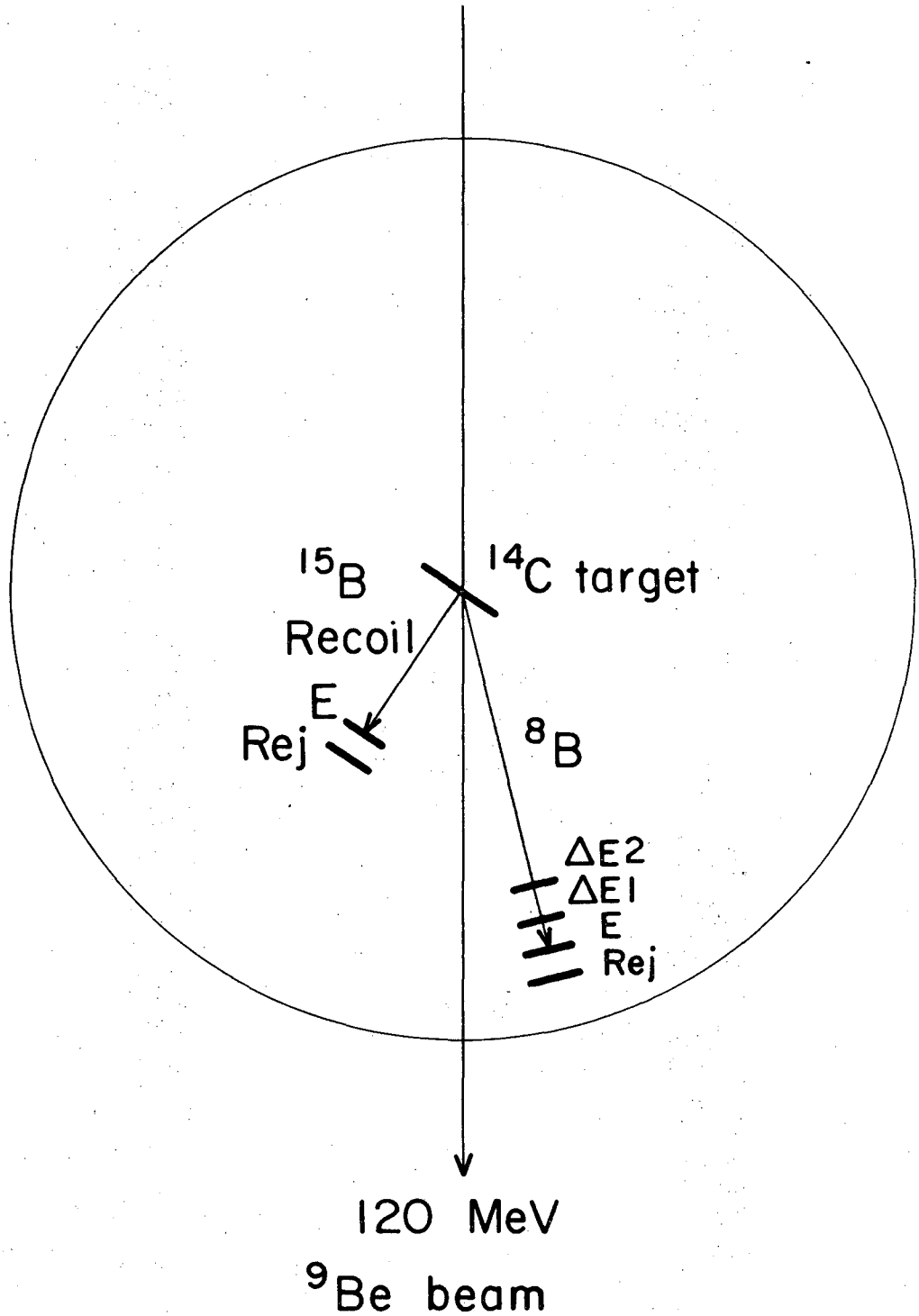

XBL7410-4478

Figure 2. Schematic drawing of scattering chamber showing orientation of detectors and target for ^{15}B experiment.

of about 8.4 MeV excitation, however, are emitted at the same angle as ^{15}B ground state recoils. Luckily, these ^{13}B particles are unbound to neutron emission by approximately 4.9 MeV, and because they decay in flight ($t_{\frac{1}{2}} = 10^{-22}$ sec), the ^{12}B daughters may be deflected from their original direction of travel. The opening angle of the resultant ^{12}B breakup cone is about 21 degrees. If the acceptance angle of the recoil detector is much smaller than this, most of the ^{12}B particles will not be detected, so the ^{8}B particles corresponding to these recoils will be rejected. It was hoped that in this way a sufficiently large fraction of the background events arising from contaminants could be eliminated to enable observation of ^{15}B.

The ^{15}B ground state recoils, although not decaying in flight, are also emitted in a cone, of substantially smaller opening angle, due to finite beam spot size and ^{8}B acceptance angle. Reducing the recoil acceptance angle to eliminate more ^{13}B events will therefore, beyond a certain point, also begin eliminating ^{15}B events. This serious problem will be further discussed in Section IV E.

Since it was foreseen that an appreciable fraction of the ^{13}B events might not be eliminated by the recoil detector if the ^{15}B detection efficiency was to be kept high, a further technique for background reduction was introduced. Subnanosecond timing was done between the detected ^{8}B particle and its associated recoil nucleus. This is a measure of the difference in time of flight from target to detector for the two particles, and should be different for every reaction. Expected time differences for the reactions on ^{14}C and ^{12}C are calculated in Section IV E.

In the $^{9}Be(^{9}Be,^{8}B)^{10}Li$ experiment, also, a recoil detection system

was used to reduce ^{12}C contamination background. However, two important differences from the ^{15}B experiment dictated adopting a different approach.

The first difference is that, unlike ^{15}B, ^{10}Li is particle unbound and decays into a ^{9}Li plus a neutron, in our case with a breakup cone of a few degrees opening angle. The angle depends on the breakup energy, and thus the mass of ^{10}Li, which was of course unknown at the time. (It turned out to be about 9 degrees.) Although it could be anticipated that the break-up cone angle would be smaller for ^{10}Li than for the ^{13}B contaminant, it was very unlikely to be sufficiently smaller to allow adequate discrimination between the two particle types purely by geometric considerations.

The second difference is that the rates of energy loss, dE/dx, of the contaminant and desired recoils are no longer very similar. For the ^{12}B (about 9 MeV) dE/dx = 3.5 MeV/mg-cm^2; for the ^{9}Li (about 12 MeV) dE/dx = 1.2 MeV/mg-cm^2. It then becomes possible to differentiate between the two by using a 2-counter recoil telescope. (See Section III G.) If the first detector is about 11 μm thick, the ^{12}B particles from ^{12}C reactions are completely stopped, while the ^{9}Li recoils from ^{9}Be reactions lose only about one third of their incident energy in this detector. A total separation of the contaminants from the desired reaction is thereby accomplished.

C. Heavy Ion Considerations

All of the experiments discussed here involved the detection of heavy ions, and most of them used heavy ion beams. This aggravates certain problems which are usually not such serious considerations with light ions.

The dE/dx of heavy ions can be very large, since at high energies (several MeV/nucleon) it is proportional to MZ^2/E. Energy deposited in the target then results in a large energy spread for the exit particles, especially for thick targets. Frequently an even larger contribution to the energy spread comes from the rapid variation of particle energy with detection angle, $dE/d\theta$. (Particles are accepted over a certain angular range due to finite beam spot size and angular acceptance of the detector geometry.) From kinematic considerations, when the exit particle and residual nucleus have comparable mass, $dE/d\theta$ becomes quite large. Among the experiments considered here, the $dE/d\theta$ of 1 MeV/degree for the $^{9}Be(^{9}Be,^{8}B)^{10}Li$ reaction at 14° was the highest encountered.

The sum of these two effects, dE/dx and $dE/d\theta$, leads to poorer energy resolution, usually a few hundred keV full width at half maximum (FWHM). Any attempts to improve the resolution by decreasing the target thickness or angular acceptance must be paid for by a decrease in the already-low counting rate.

The large dE/dx dictates the further requirement of thin, uniform transmission detectors, which are difficult and expensive to make. Thinner detectors also provide poorer particle resolution (see Section III E). Because of the highly negative Q values (about -20 to -40 MeV), a beam energy near the highest obtainable (for a charge state produced in sufficiently high yield by the ion source) was usually employed.

D. Cyclotron

The Berkeley 88-Inch Cyclotron is a variable-energy, sector-focused cyclotron with a maximum energy in MeV for particles of charge Q and mass A of 140 Q^2/A for heavy ions, and slightly less for alpha particles. Beams of many elements up through $krypton^{38}$ have been successfully accelerated.

The alpha-beam experiments described below utilized a standard hot filament source.[39] Lithium and beryllium beams, developed for these experiments, were produced by a Penning Ion Gauge (PIG) type source[38] with arc-heated cathodes.

Since no gaseous Li compounds are available for source material, a solid must be used. LiF was fused into many small slits cut into a tantalum sleeve which was then inserted into the anode chamber (see Fig. 3). Heating by the arc caused the LiF (boiling point = 1676°C) to slowly vaporize over a period of several hours, thus providing a continuous supply of Li vapor for ionization and subsequent acceleration. To provide a further supply of Li and thus increase the beam intensities attainable, lower cathode buttons were made by pressing a mixture of 40% LiF and 60% finely powdered Ta by weight into a Ta shell at 40,000 lb/in^2. Erosion of the cathodes by sputtering throughout the life of the source thereby provided additional slow Li release. Typical source life was 4 hours of 200 namp (2+) of beam on target.

The beryllium PIG source was similar to the lithium source, but with solid Ta cathode buttons rather than doped ones and with no anode sleeve. Instead, a small piece of Be metal about 3 mm square was mounted opposite the extraction slit, just outside of the arc. (Using a solid slug rather than mixing powdered Be into the cathode buttons minimized the toxicity problems associated with handling Be.) A massive support gas, such as Xe or Ar, introduced Be into the arc via sputtering, where it was ionized by the arc and extracted by the puller. Sources typically produced beam levels of 80 namp (3+) on target for 4 hours.

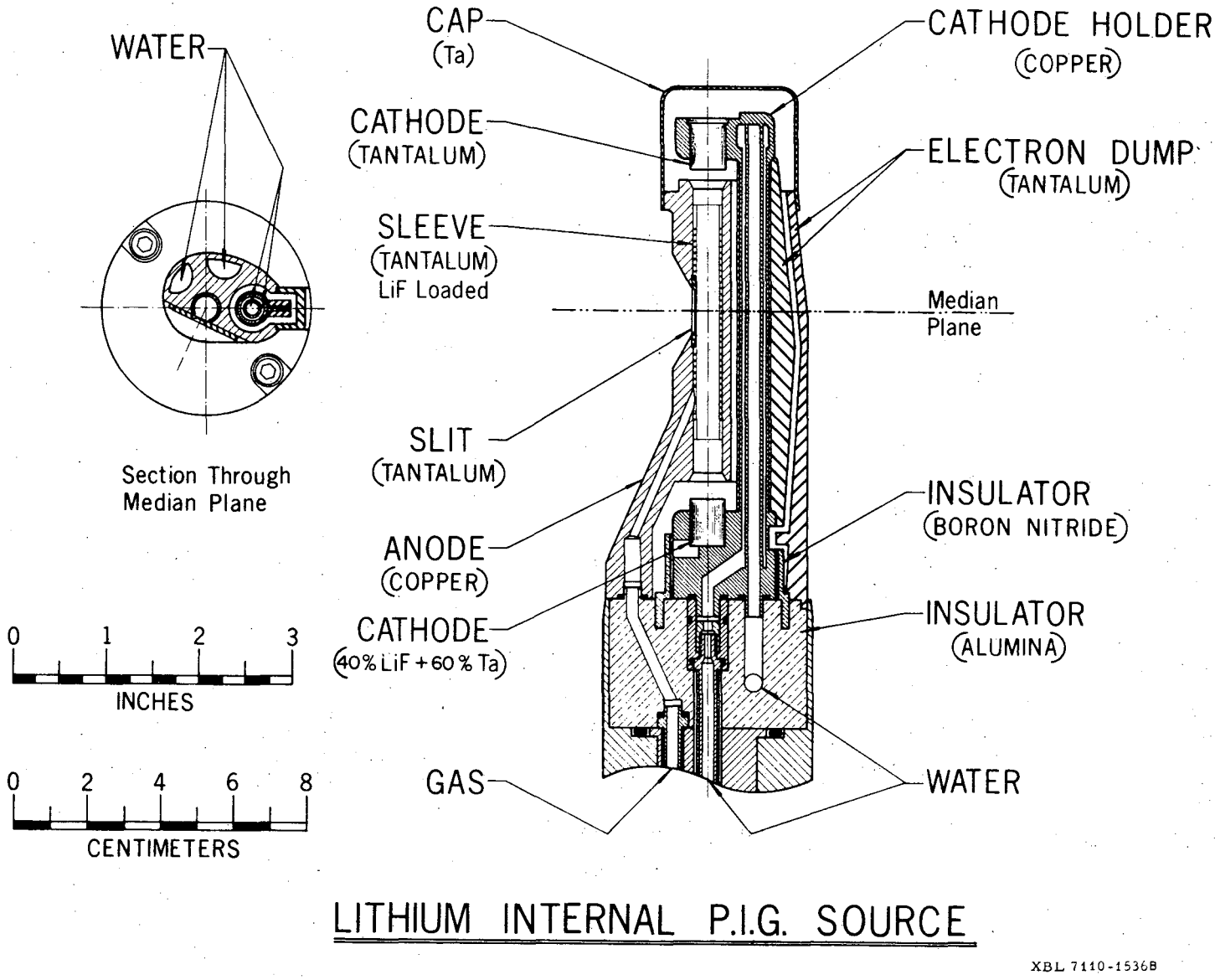

Figure 3. Section through internal PIG source showing sleeve insert for lithium ion generation.

E. Beam Transport and Experimental Area

The cyclotron, beam transport system, and experimental area are shown in Fig. 4. Beam energy analysis of dE/E ~ 0.14% was provided by the switching magnet and analyzing slit, normally set at 1.5 mm width. Typical beam spot dimensions on target were 2 mm wide by 2.5 mm high. Detectors were mounted about 12 cm from the target on two independently-movable platforms in the horizontal plane, one on either side of the beam. A tantalum housing shielded the detectors from scattered beam and a 600 Gauss permanent magnet in front of the collimator deflected low-energy electrons produced by the beam in the target. In some of the experiments the detectors were cooled to -20°C by a thermoelectric cooler to reduce thermal noise. Absolute beam energies were measured with a high-precision analyzing magnet[40] (dE/E = 0.02%) in an adjacent experimental area not illustrated in Fig. 4.

F. Targets

The ^{26}Mg target used in the ^{25}Ne experiment was a 99.4% isotopically-enriched self-supporting foil of thickness 150 μg/cm^2. The ^{48}Ca targets, also self-supporting, were 96.25% isotopically enriched and of thickness 410 μg/cm^2. To minimize oxidation they were made, transported, and stored under vacuum. The ^{9}Be target was a foil of either 680 (^{10}Li experiment) or 150 (^{15}B experiment) μg/cm^2.

^{14}C targets were made[41,42] using the apparatus shown in Fig. 5. Methyl iodide vapor containing carbon enriched to 94% in ^{14}C (the purest commercially available[37]) was introduced at low pressure into the vacuum chamber. Molecules passing between the electrodes were cracked by a high voltage (~ 1kV) radio frequency glow discharge. The carbon plated out

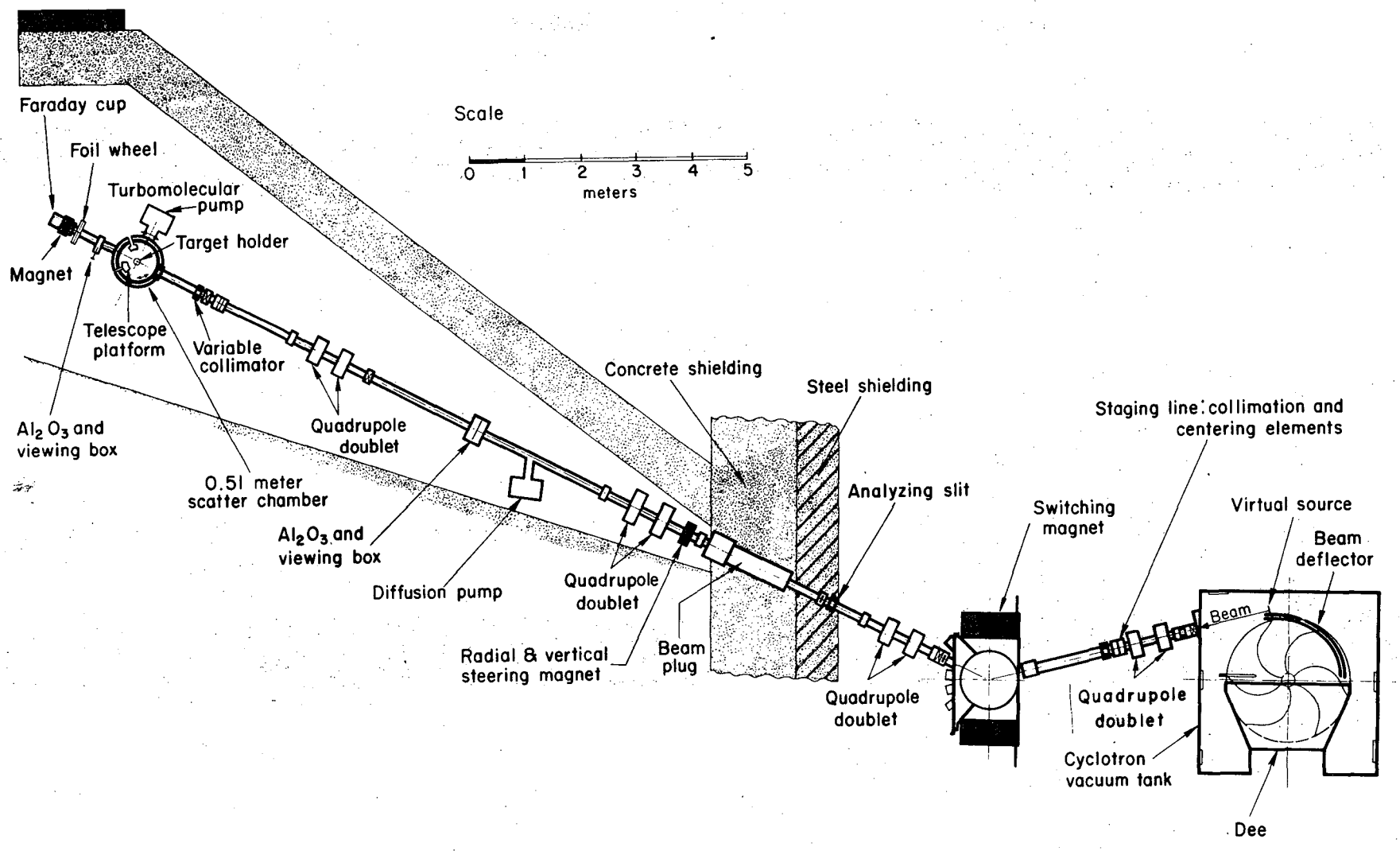

Figure 4. Schematic diagram of the cyclotron, beam transport system, and the cave 2 experimental area.

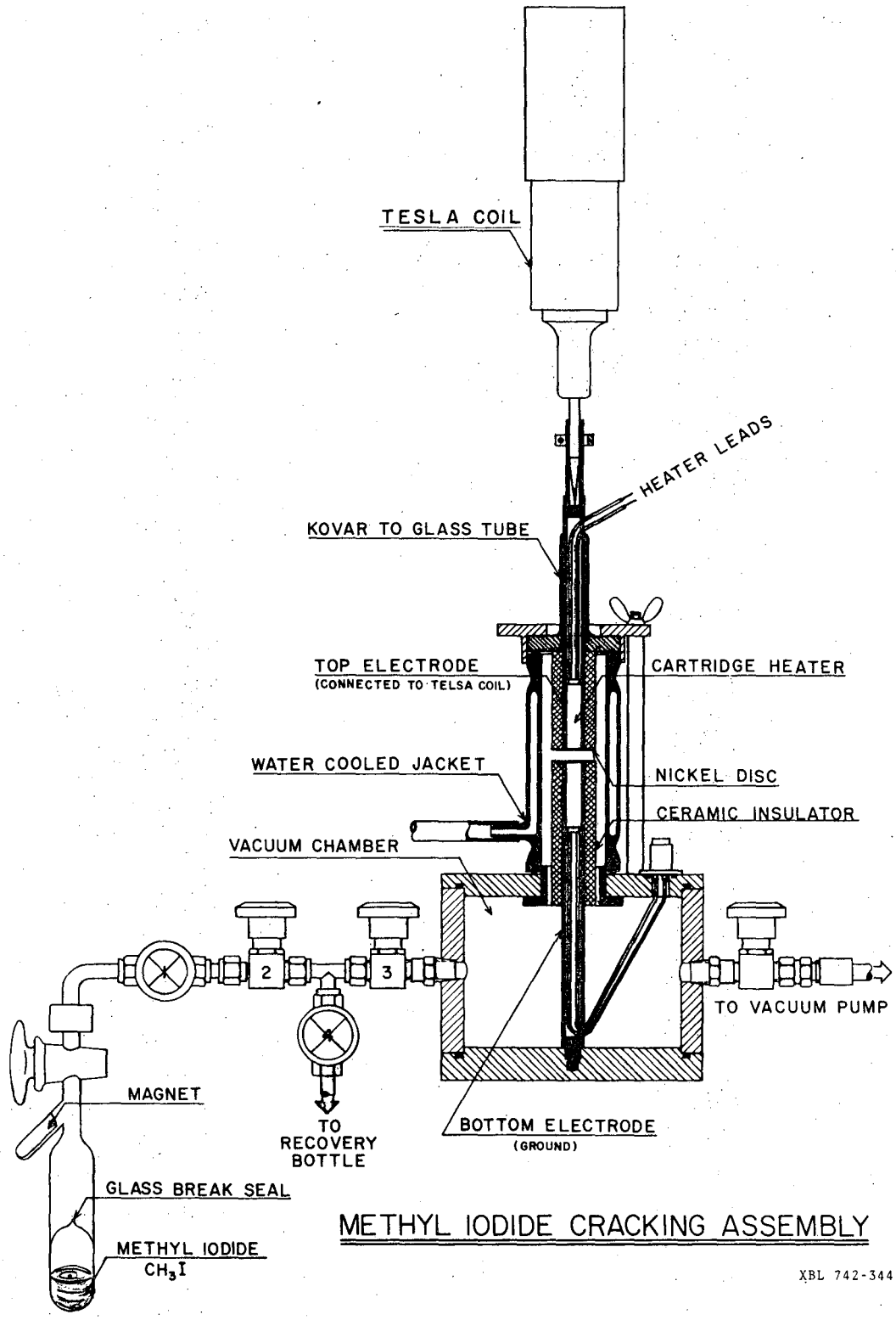

Figure 5. Methyl iodide cracking assembly for ^{14}C target manufacture.

onto two nickel discs, attached to the electrode faces, which had been previously flashed with 100 to 200 μg/cm^2 of gold to strengthen the finished target. Foils were floated off the discs in water and mounted over 8 mm holes in polyethylene frames. In this manner gold-backed targets were produced which contained (by subsequent analysis) about 80 μg/cm^2 of ^{14}C, 70 μg/cm^2 of I, and an undetermined small amount of H (from incomplete cracking). Apparently the system introduced considerable contaminant ^{12}C, because the approximately 20 μg/cm^2 of ^{12}C content in the freshly-made targets (determined by measuring a reaction of known cross section) was considerably greater than the 5 μg/cm^2 to be expected on the basis of a 6% ^{12}C content supposedly in the CH_3I sample.

^{14}C methyl iodide is unstable at room temperature, and decomposition is further catalyzed by impurities and by light. It must be kept at liquid nitrogen temperatures and in the dark. Even so, it degrades seriously in only a few days, soon becoming useless. There is also a serious stability problem with the finished targets, both from shelf life and especially from beam bombardment. In the belief that this was due to sublimation of the iodine from the target, heaters were added to the electrodes to prevent the iodine from building up during carbon deposition. Unfortunately, this reduced the reliability of the target making process, already very difficult to control, and was abandoned. (The cost of ^{14}C dictates obtaining maximum possible reliability.) By building up several carbon layers by successive cracking steps, however, some targets of 300 to 450 μg/cm^2 total carbon thickness were produced which were reasonably strong and durable.

G. Detectors and Electronics

All experiments employed the Goulding-Landis[43,44] 3-counter, double

particle identification system. This system is based on the empirical relationship that above a certain energy threshold (which increases with particle mass) the range of a nuclear particle in a detector is given by

$$R = AE^b.$$

A is a constant characteristic of particle type, E is the energy dropped in the detector, and b is a dimensionless number which varies very slowly with particle type. For boron isotopes[45] b is about 1.6. If the particle passes through a transmission detector (denoted ΔE) of thickness T and stops in a thicker (E) counter, it can be shown[46] that

$$T/A = (E + \Delta E)^b - E,$$

where ΔE and E are the energies deposited in the respective counters and T/A is a constant characteristic of particle type. T/A is generated by an analog circuit employing a logarithmic element, and b is optimized at the beginning of each experiment.

If we now add a second transmission counter, $\Delta E2$, as shown in Fig. 6, two separate determinations of particle type (A and B in Fig. 6) can be made. Should the energy dropped in one of the counters depart from the normal range of values due to nonstatistical fluctuations (caused for example by counter nonuniformity, channeling, or blocking), the ratio A/B will also depart from its normal range. Thus by rejecting those "bad" events in which A/B varies by more than some chosen percentage from the norm, we can substantially improve the particle identification and energy resolution. The percentage is usually made sufficiently small to also exclude the largest of the statistical fluctuations. Typically, some 20% to 40% of the events were eliminated in this manner.

The ΔE and E detectors were backed by an anticoincidence detector

Three counter particle identifier

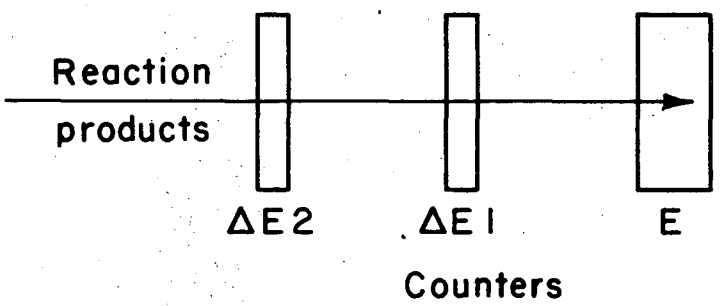

Different identification modes of the particle identifier

	ctr(s) used as "ΔE" ctr	ctr(s) used as "E" ctr
A.	ΔE2	ΔE1 + E
B.	ΔE1	E

if the ratio A/B is within a chosen percentage, then the final output is C

C.	ΔE2 + ΔE1	E

MUB-9885

Figure 6. Schematic illustration of the three-counter particle identifier, describing mode of operation.

to reject any events that passed entirely through the E counter. All ΔE and E counters were phosphorous-diffused silicon detectors made at LBL except for detectors 15 μm or thinner, which were surface barrier silicon detectors purchased from ORTEC, Inc.[47] Reject counters were in all cases 500 μm lithium-drifted silicon, made at LBL. All singles experiments employed two identifier telescopes of similar thicknesses except for the experiments leading to Cl and S isotopes, which used one thinner telescope to detect carbon particles and one thicker telescope for boron isotopes. Coincidence experiments used only one three-counter telescope. The ^{10}Li experiment employed in addition a two-counter single-identification telescope for recoil detection, while for ^{15}B detection only a single counter was used. In both cases the recoil detectors were also backed by reject counters.

The electronics will be discussed separately for the singles and coincidence experiments.

Singles Electronics—The signals from the detectors were amplified by charge-sensitive preamplifiers and transmitted to the electronics in the counting area, shown in Fig. 7. Here the signals feed amplifiers with matched gains and a pileup rejector (PUR) with 50 nsec resolving time which restricted events to one beam burst. Energy signals were shaped by 800 nsec delay lines and restricted to the amplitude of interest by single channel analyzer (SCA) windows. If a coincidence was detected between all three detectors (resolving time = 40 nsec), with no event in the reject counter and no subsequent or previous particle within 1 μsec, the signals were stretched to 5 μsec and sent to the particle identifier (PI). The output of the PI passed through a 4-channel router, where SCA windows could be set around as many as

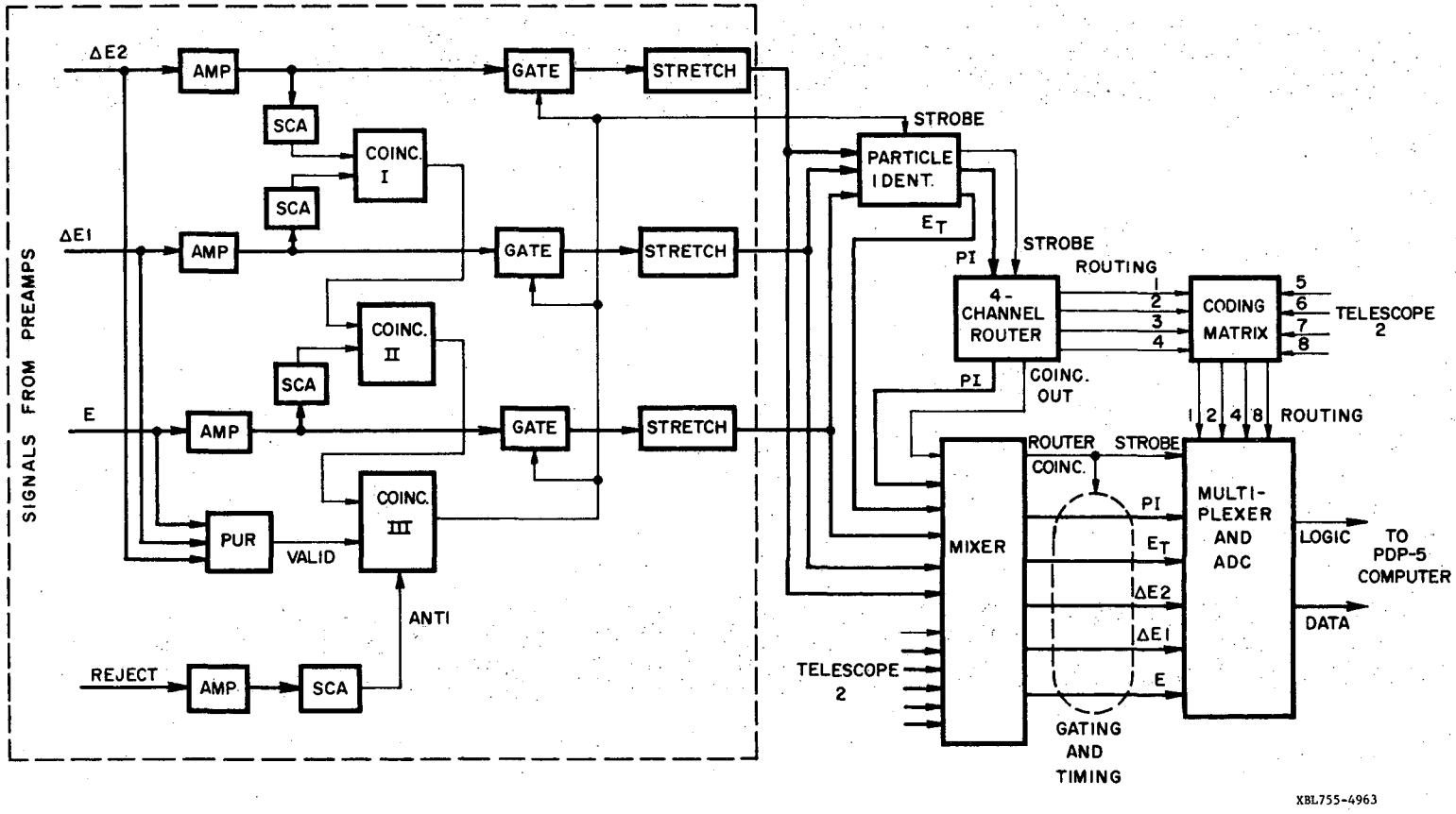

Figure 7. Electronic block diagram for singles experiments employing two three-counter telescopes.

four particle groups. For these events of interest, the three individual energy signals, total energy ($E_T = \Delta E2 + \Delta E1 + E$), PI and routing signal were sent to a multiplexer and 4096-channel ADC, and thence to an on-line PDP-5 computer. Periodic stability checks of the electronics were obtained and linearity was established by utilizing a high-precision pulser, which had been calibrated by α particles from a ^{212}Pb source. The beam energy was monitored with an NMR probe of the magnetic field of the switching magnet.

Coincidence Electronics — A block diagram of the electronics used in the ^{10}Li experiment is shown in Fig. 8. (The region enclosed by dashed lines is the same in Fig. 7 and Fig. 8). If coincident events were detected within a 1 μsec resolving time in both the ^{8}B and recoil telescopes, a single particle identification was performed using the ΔE and E signals from the recoil telescope. A time to amplitude converter (TAC) was also triggered which generated an output proportional to the difference between the flight time of the two particles from target to detector. This produced a peak of about the width of one beam burst (15 nsec full width) for true coincident events, plus a series of smaller peaks separated by the inter-beam burst time (125 nsec) arising from chance coincidences of particles from different beam bursts. An SCA window was set to accept particles from only the real coincidence peak plus one other (the latter to determine the contribution of the chance coincidence background to the energy spectra).

All three-counter telescope events belonging to particle types of interest were accepted whether or not they were in coincidence with a recoil. When there was also a recoil coincidence and a TAC signal, the

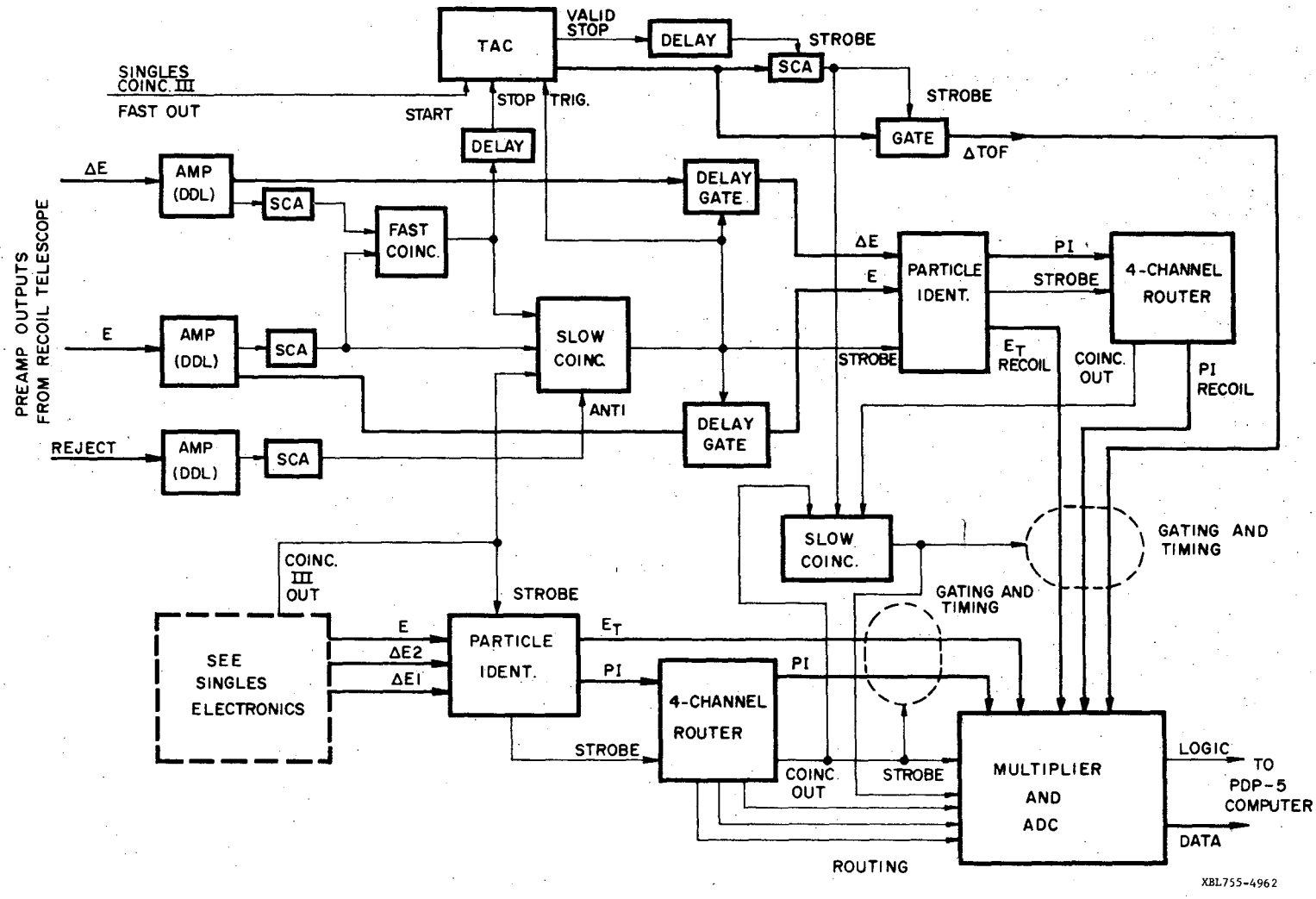

Figure 8. Electronic block diagram for ^{10}Li recoil-coincidence experiment. Area enclosed by dashed lines is the same in Fig. 7 and this figure.

event was routed differently, and the PI and E_T signals for both telescopes plus the TAC signal were sent to the computer. In other cases only the singles PI and E_T were accepted.

A block diagram of the ^{15}B experiment electronics is shown in Fig. 9. Both the $\Delta E2$ and recoil detectors were equipped with dual output fast-slow preamplifiers. The slow output was used as the energy signal and the fast output to derive a timing signal for time of flight information. Amplified fast signals had a rise time of about 1 to 4 nsec, depending on the capacitance of the detector used. To minimize time walk, the timing signal was generated by a constant fraction discriminator (CFD), whose output is independent of pulse amplitude. The $\Delta E2$ timing signal drove the start of a TAC, and the recoil timing signal, suitably delayed, provided the stop. The TAC output signal is thus the difference in time of flight (ΔTOF) from target to detector between the exit particle and its recoil.

As was done in the ^{10}Li experiment, the parameters (PI, E_T, $\Delta E2$ and $\Delta E1$ in this case) for three-counter telescope events were always sent to the computer. In addition, the E-recoil and ΔTOF signals were taken when the event was a ^{8}B with a recoil coincidence, and the event was then routed differently. For typical counting rates of 10^4 events/sec in the $\Delta E2$ counter, 1 ^{8}B event/5 sec was identified, about 1% of these ^{8}B events with a recoil coincidence.

H. Data Acquisition and Analysis

Events were sent from the ADC to an on-line PDP-5 computer and written on magnetic tape in unsorted form. The E_T and PI parameters for each event as it arrived were additionally sorted into arrays in memory which could be viewed on an updating CRT screen.

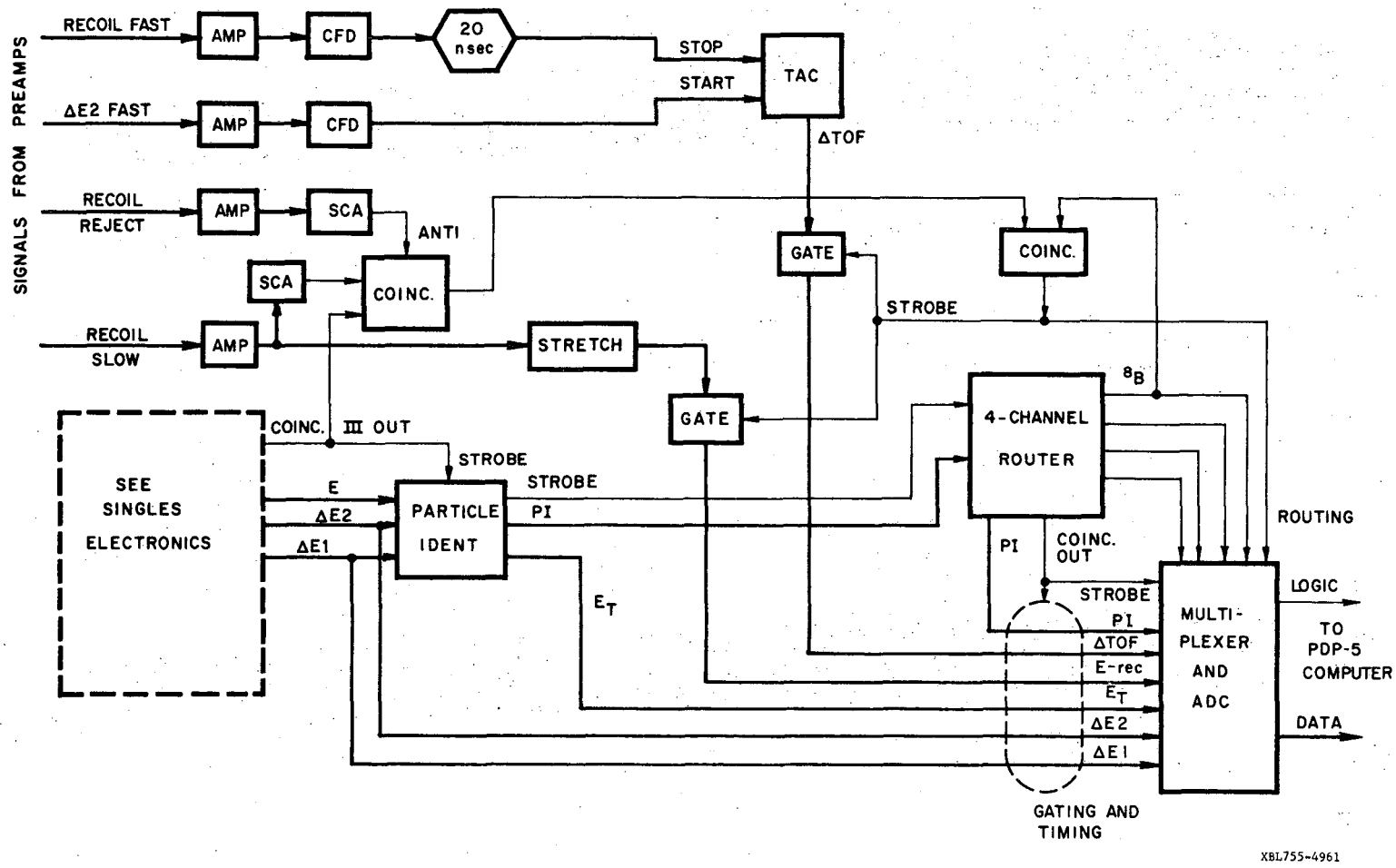

Figure 9. Electronic block diagram for ^{15}B recoil-coincidence experiment. Area enclosed by dashed lines is the same in Fig. 7 and this figure.

The data were later sorted off-line and bad events eliminated by a SCC-660 computer using the program CHAOS[48]. Gates were then set around PI peaks and energy spectra projected out. Analysis of these energy spectra was performed with the interactive, Gaussian peak-fitting program DERTAG[49]. Centroids, widths, and integrals were obtained for each peak. In most cases the low level density made it relatively straight forward to decide which energy levels in the final nucleus were populated. To check level assignments and determine excitation energies and Q values, the CDC-7600 computer program LORNA[49] was used to calculate the reaction kinematics, absorber losses and an energy scale from a least-squares fit to the experimental points.

IV. EXPERIMENTAL RESULTS

A. ^{25}Ne

The ^{26}Mg(^{7}Li,^{8}B)^{25}Ne reaction (Q ~ -22 MeV) was initiated by a 78.9 MeV ^{7}Li^{+2} beam of average intensity approximately 100 nA on target. Each detector telescope, subtending a solid angle of 0.43 msr, consisted of ΔE2, ΔE1, and E detectors of 15, 11, and 200 μm thickness, respectively, plus a reject detector.

Fig. 10 presents a particle identification spectrum showing almost complete separation in the region of ^{8}B. (This figure also indicates that a few ^{10}C particles were identified. However, the yield and selectivity of the ^{26}Mg(^{7}Li,^{10}C)^{23}F reaction were such that no information on ^{23}F could be obtained in these experiments.) To further reduce possible background in the ^{8}B region, a two-dimensional analysis, ΔE2 and ΔE1 versus total energy, was done off line. This corresponds to a check that the PI was optimally adjusted and operating properly. A small percentage of additional events could be eliminated in this manner.

An energy calibration for the ^{8}B data was acquired by observing, concurrently with the ^{8}B nuclei, ^{10}B particles at θ_{lab} = 10, 15, and 20° from the reaction ^{26}Mg(^{7}Li,^{10}B)^{23}Ne. The ^{10}B peaks for each run were corrected to allow for slight electronics gain changes and beam energy shifts. Corrections were also made for projectile and exit particle energy losses in the target and in the detector dead layers. In applying the resultant calibration to the ^{8}B events, all of the above corrections were made to each event individually.

Two independent investigations were made of the reaction ^{26}Mg(^{7}Li,^{8}B)^{25}Ne. The ^{8}B data collected at 10° during run 2 are shown

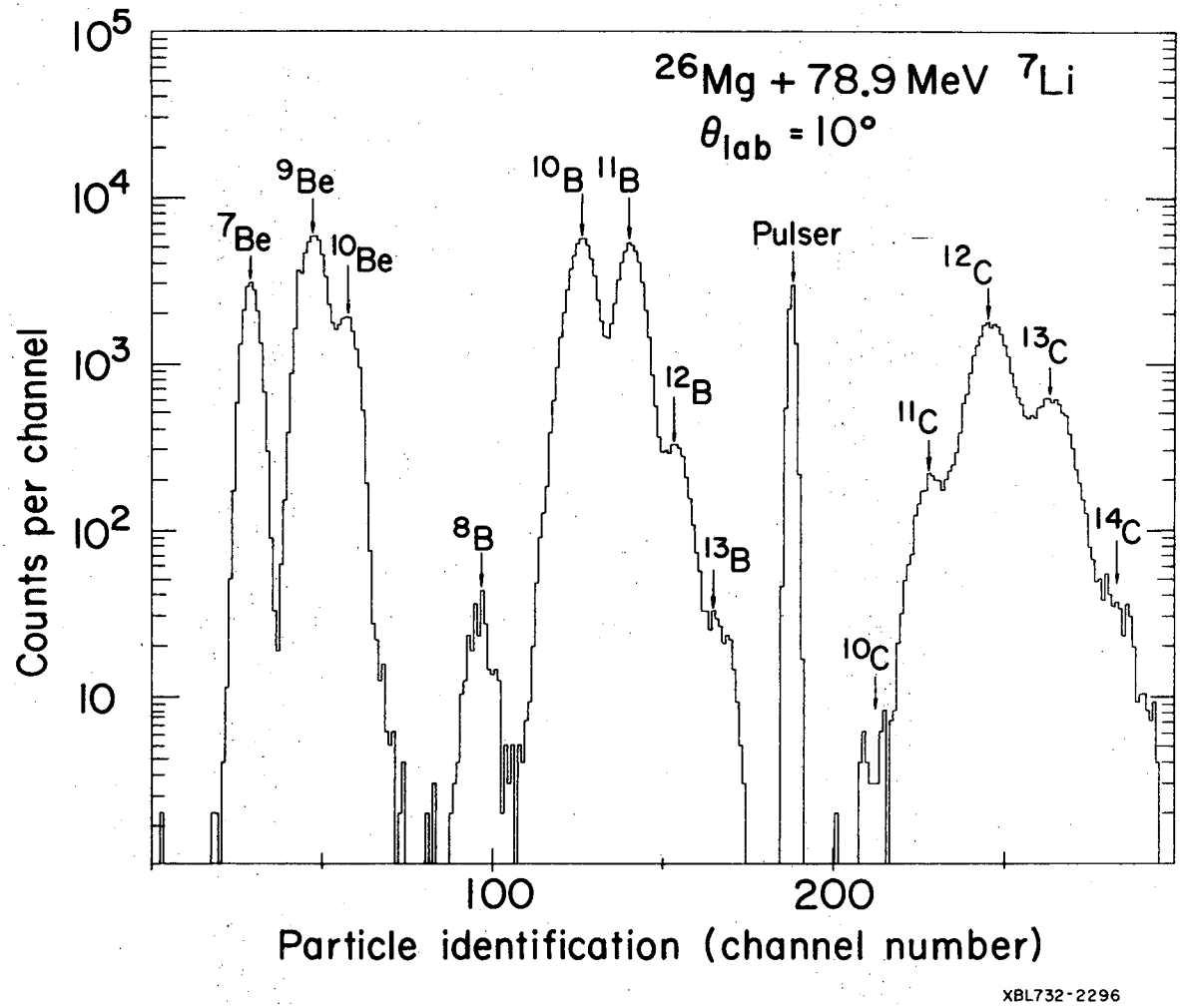

Figure 10. Particle identification spectrum resulting from bombardment of ^{26}Mg by 78.9 MeV ^{7}Li.

in Fig. 11 (a). Fig. 11 (b) is a composite spectrum of these same data plus 15° data taken during both runs 1 and 2 and kinematically corrected to 10°. In addition to the ground state, five excited states of ^{25}Ne can be seen at excitation energies of 1.65 ± 0.05, 2.03 ± 0.05, 3.25 ± 0.08, 4.05 ± 0.08, and 4.7 ± 0.1 MeV. (Counts on the high-energy shoulder of the 3.25-MeV peak are inconsistent with the observed ^{10}B resolution of ~200 keV and are inconclusive evidence for an additional excited state.) Reactions yielding ^{8}B nuclei from possible ^{12}C and ^{16}O contaminants were not seen. Kinematic shifts (from 10° to 15°) of all the observed peaks were only consistent with reactions induced on ^{26}Mg.

Cross sections for population of the ground state at 10° and 15° were similar and were about 350 nb/sr. From the energy of the ^{8}B ground state peak, the Q value for the reaction ^{26}Mg(^{7}Li,^{8}B)^{25}Ne is found to be -22.05 ± 0.10 MeV, corresponding to a mass excess for ^{25}Ne of -2.18 ± 0.10 MeV. This is in good agreement with the two previous experimental results of -1.96 ± 0.30 MeV by Goosman et al.[50] and -2.2 ± 0.3 MeV by Kabachenko et al.[51] (see discussion in ref. 50), both from β end-point measurements arising in the decay of ^{25}Ne. No previous measurements of the level structure of ^{25}Ne have been reported.

B. ^{43,45,46}Ar

A beam of 77.7 MeV α particles (~1 μA) was used to study the ^{48}Ca(α,^{7}Be)^{45}Ar reaction (Q~-28 MeV) and the ^{48}Ca(α,^{9}Be)^{43}Ar reaction (Q~-21 MeV), which were measured concurrently. The ^{48}Ca(^{6}Li,^{8}B)^{46}Ar reaction (Q~-23 MeV) was initiated by an 80.1 MeV ^{6}Li^{+2} beam (~100 nA). For the detection of ^{7}Be and ^{9}Be nuclei the counter telescopes, each subtending a solid angle of 0.43 msr, consisted of ΔE detectors of 59

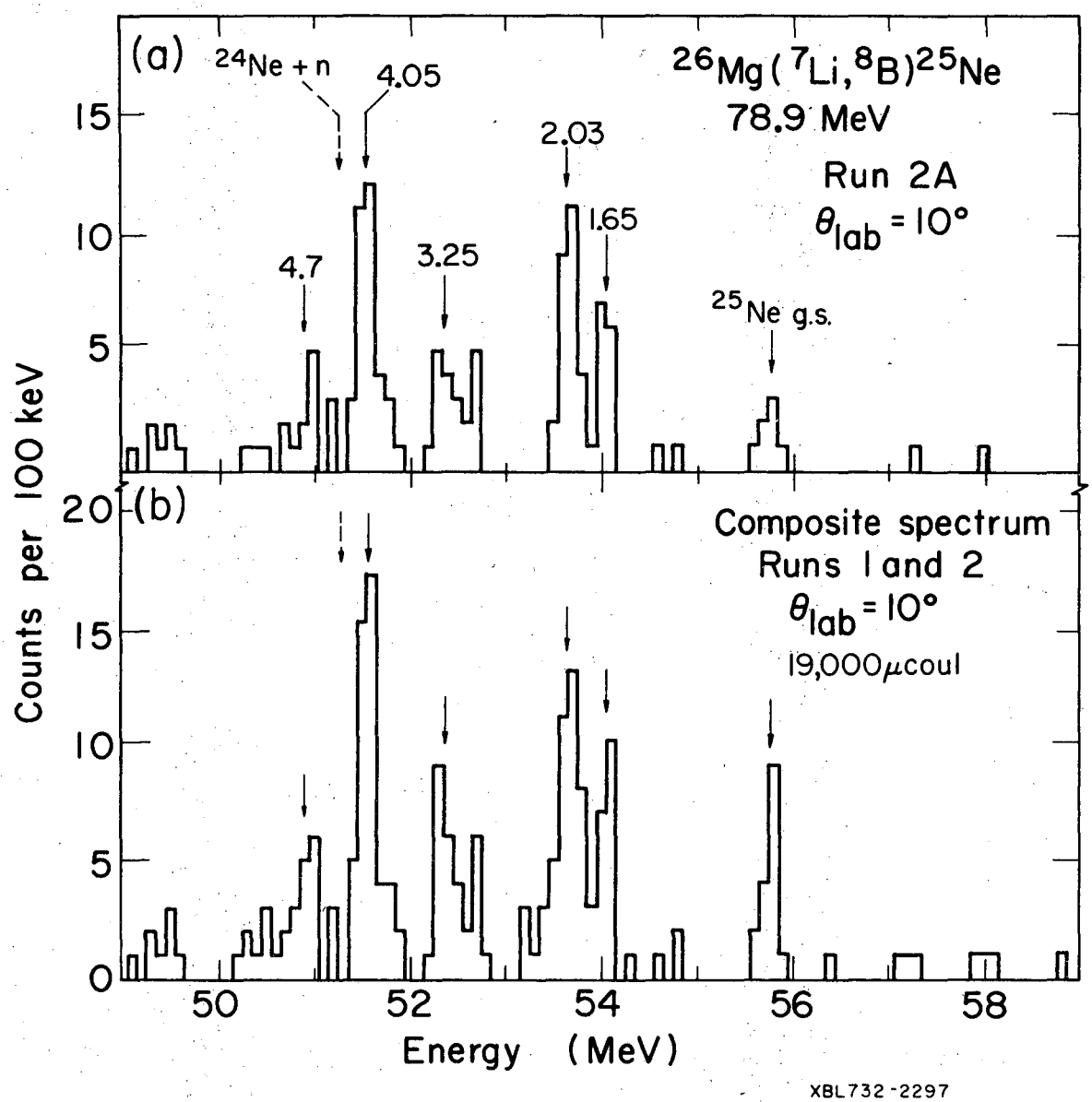

Figure 11. (a) ^{8}B energy spectrum of the ^{26}Mg(^{7}Li,^{8}B)^{25}Ne reaction from run 2 at $\theta_{lab} = 10°$. (b) Composite ^{8}B energy spectrum including data of (a) plus data taken at $\theta_{lab} = 15°$ from runs 1 and 2, kinematically corrected to $\theta_{lab} = 10°$.

and 36 μm thickness and a 260 μm E detector; for the (^{6}Li,^{8}B) experiment the two ΔE detectors were 15 and 11 μm thick and the solid angle subtended was 0.64 msr. The target was normal to the beam.

Fig. 12 shows PI spectra obtained with both the alpha and ^{6}Li beams incident on a ^{48}Ca target. The greater peak separation in the former case is due almost entirely to the use of thicker detectors. This was possible because the thicknesses were optimized for an element of lower Z. In spite of the poorer particle resolution with the ^{6}Li beam, ^{8}B separation is good.

An energy calibration was obtained for the ^{7}Be spectra by recording the ^{40}Ca(α,^{7}Be)^{37}Ar reaction populating the ground state and levels at 1.410 and 2.796 MeV excitation in ^{37}Ar, and the ^{28}Si(α,^{7}Be)^{25}Mg reaction to the ground state and 1.614 MeV levels in ^{25}Mg. Spectra were collected periodically throughout the experiment and included several angles between 18 and 45 degrees. ^{7}Be nuclei were observed in both the ground state and 0.429 MeV first excited state. (All higher states are particle unbound and will not be observed.) Adequate separation between these two levels was obtained for the (α,^{7}Be) reaction on ^{28}Si,^{40}Ca and ^{48}Ca, although not on ^{12}C and ^{16}O impurities, for which the dE/dθ is much higher.

Fig. 13 (a) shows a ^{7}Be energy spectrum from ^{48}Ca measured at 32°. Transitions arising from ^{12}C and ^{16}O contaminants are indicated, as well as peaks (FWHM ~ 250 keV) corresponding to the ground state of ^{45}Ar and to a level at 3.25 MeV excitation. Spectra at several angles between 28 and 45 degrees (see Fig. 13 (b)) were collected, kinematically confirming observation of the reaction ^{48}Ca(α,^{7}Be)^{45}Ar, as well as enabling the region up to 5 MeV excitation to be seen. Over this angular range the cross

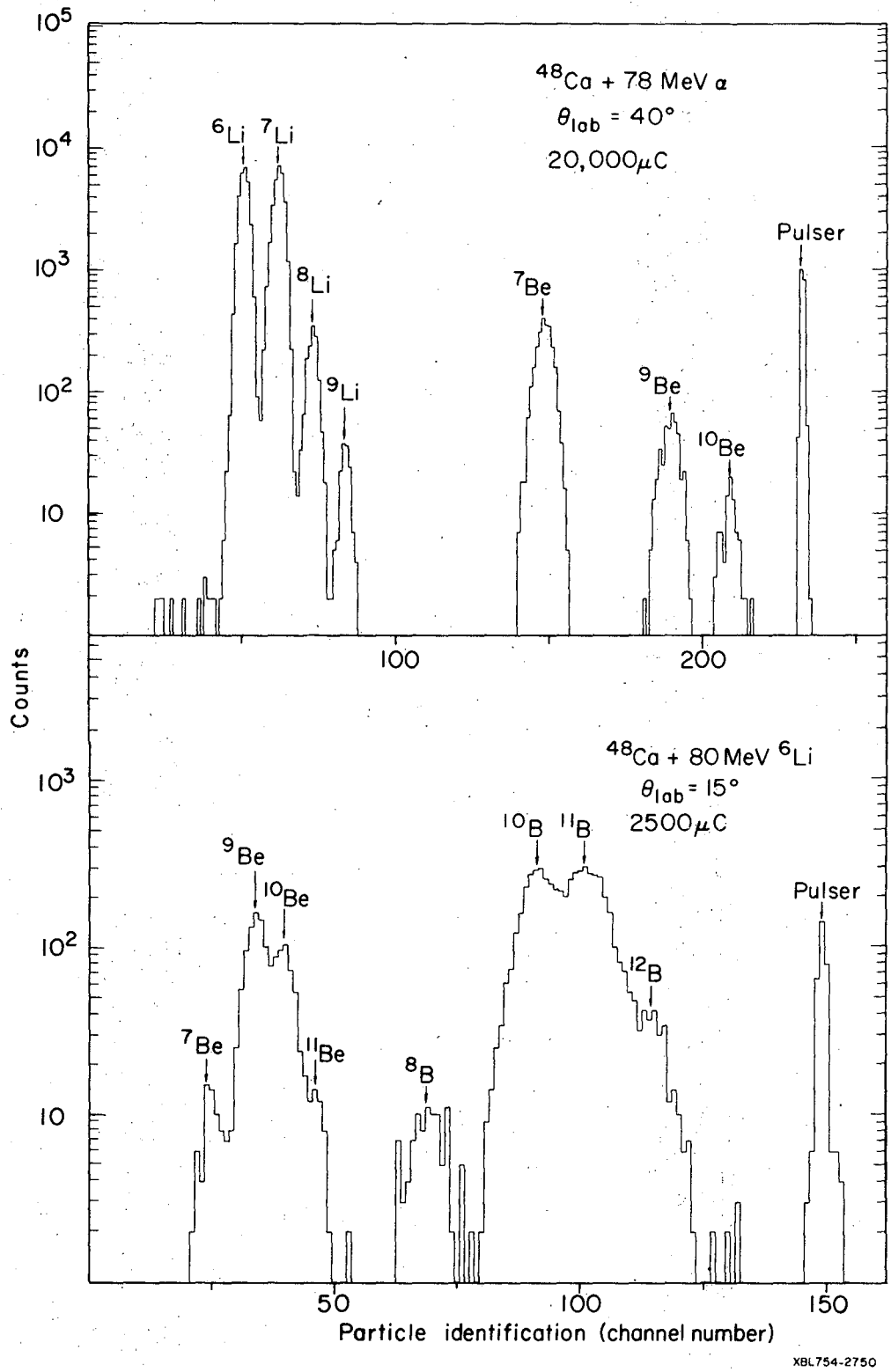

Figure 12. Particle identification spectra resulting from bombardment of ^{48}Ca by (a) 78 MeV α particles, and (b) 80 MeV ^{6}Li.

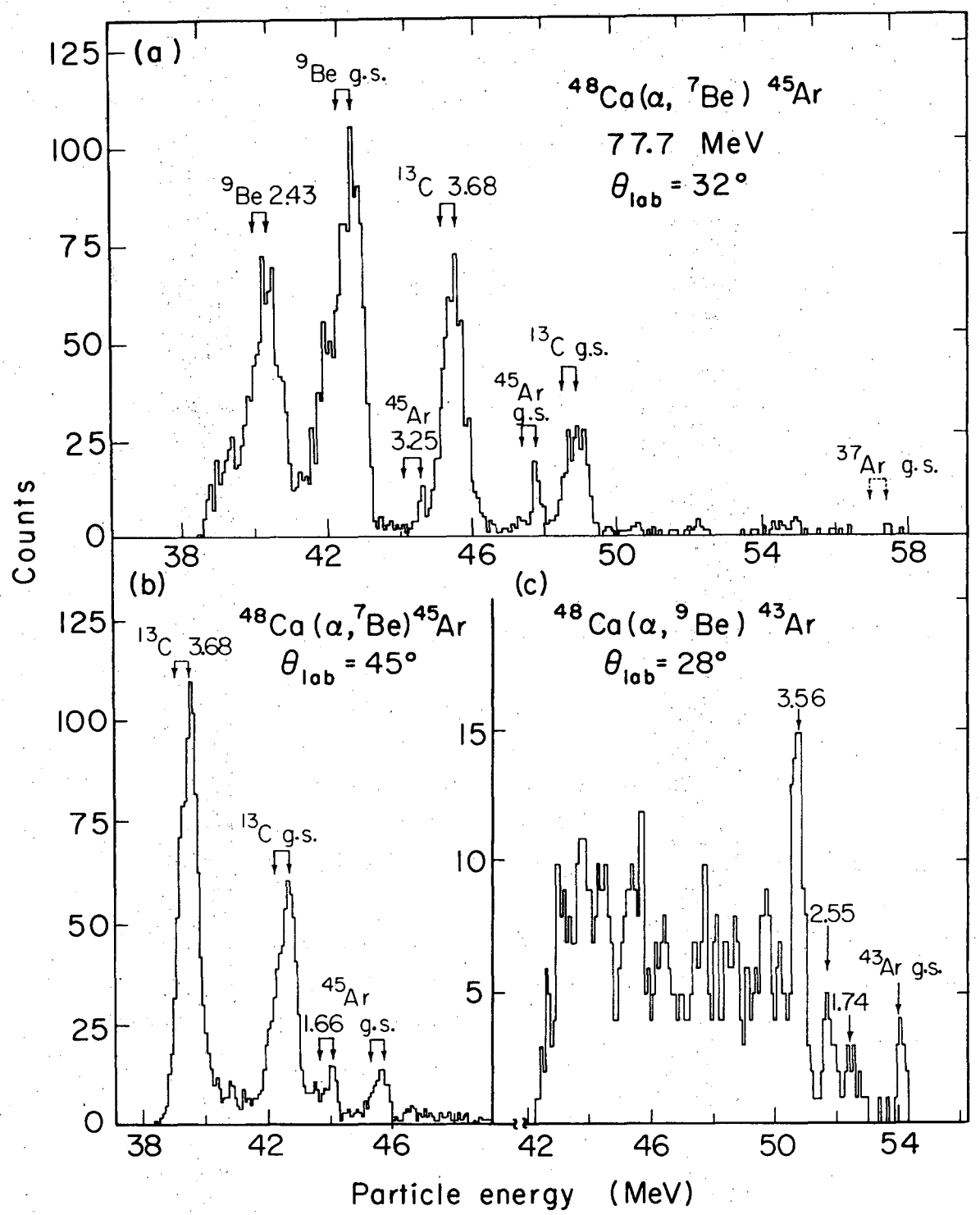

XBL7311-4418

Figure 13. (a) An energy spectrum from the reaction $^{48}Ca(\alpha,{}^{7}Be)^{45}Ar$ at $\theta_{lab} = 32°$ (7250 μC). The double arrows represent ^{7}Be(g.s.) and $^{7}Be^{*}$(0.429) transitions. (b) As (a) but taken at $\theta_{lab} = 45°$ (30,000 μC). (c) A composite spectrum of data taken with one counter telescope at $\theta_{lab} = \pm 28°$ from the reaction $^{48}Ca(\alpha,{}^{9}Be)^{43}Ar$ (17,000 μC). Contributions to this spectrum from the (α, ^{9}Be) reaction on ^{12}C and ^{16}O fall below ∿ 46 MeV.

section to the ground state of ^{45}Ar varied between 1.4 and 0.5 μb/sr, and transitions to levels an 1.66 ± 0.05, 2.42 ± 0.05, and 3.25 ± 0.07 MeV excitation were identified. All states were seen at more than one angle.

For the ^{9}Be spectra the ^{7}Be energy calibration was used as a primary reference since it was well determined in the region of interest. Analysis of ^{9}Be energy spectra from ^{12}C, SiO_2 and ^{40}Ca targets showed that the ground state of the residual nucleus was always populated. ^{9}Be has no particle-bound excited states, so the "shadow" peak problem encountered with the ^{7}Be spectra is not present. A ^{9}Be energy spectrum from ^{48}Ca at 28° is shown in Fig. 13 (c). Peaks are indicated corresponding to the ground state ($d\sigma/d\Omega \sim 100$ nb/sr) and excited states at 1.74 ± 0.05, 2.55 ± 0.05, and 3.56 ± 0.07 MeV excitation in ^{43}Ar. These and a state at 4.74 ± 0.10 MeV were all seen at more than one angle. (For a discussion of the assignment of the ground state peak, see Section V.)

For the $^{48}Ca(^{6}Li,^{8}B)^{46}Ar$ data, an energy calibration was obtained by periodically collecting spectra from a carbon target, and from the position of the $^{16}O(^{6}Li,^{8}B)^{14}C$ ground state peak arising from slight oxidation of the ^{48}Ca target. A ^{8}B energy spectrum from ^{48}Ca at 15° is shown in Fig. 14 (a). Identification of the peaks followed from comparison with spectra taken at 15° on ^{40}Ca, ^{12}C and SiO_2 (as an oxygen target). Spectra from ^{12}C and SiO_2 are shown in Figs. 14 (b) and 14 (c), respectively. (As was the case for the lighter targets, the level most strongly populated in the $^{40}Ca(^{6}Li,^{8}B)^{38}Ar$ reaction was the ground state.) Observed kinematic shifts between 10° and 17° provided additional confirmation of peak assignments. The cross section to the ground state of ^{46}Ar was found to be ~1 μb/sr at forward angles. No transitions to excited states of ^{46}Ar

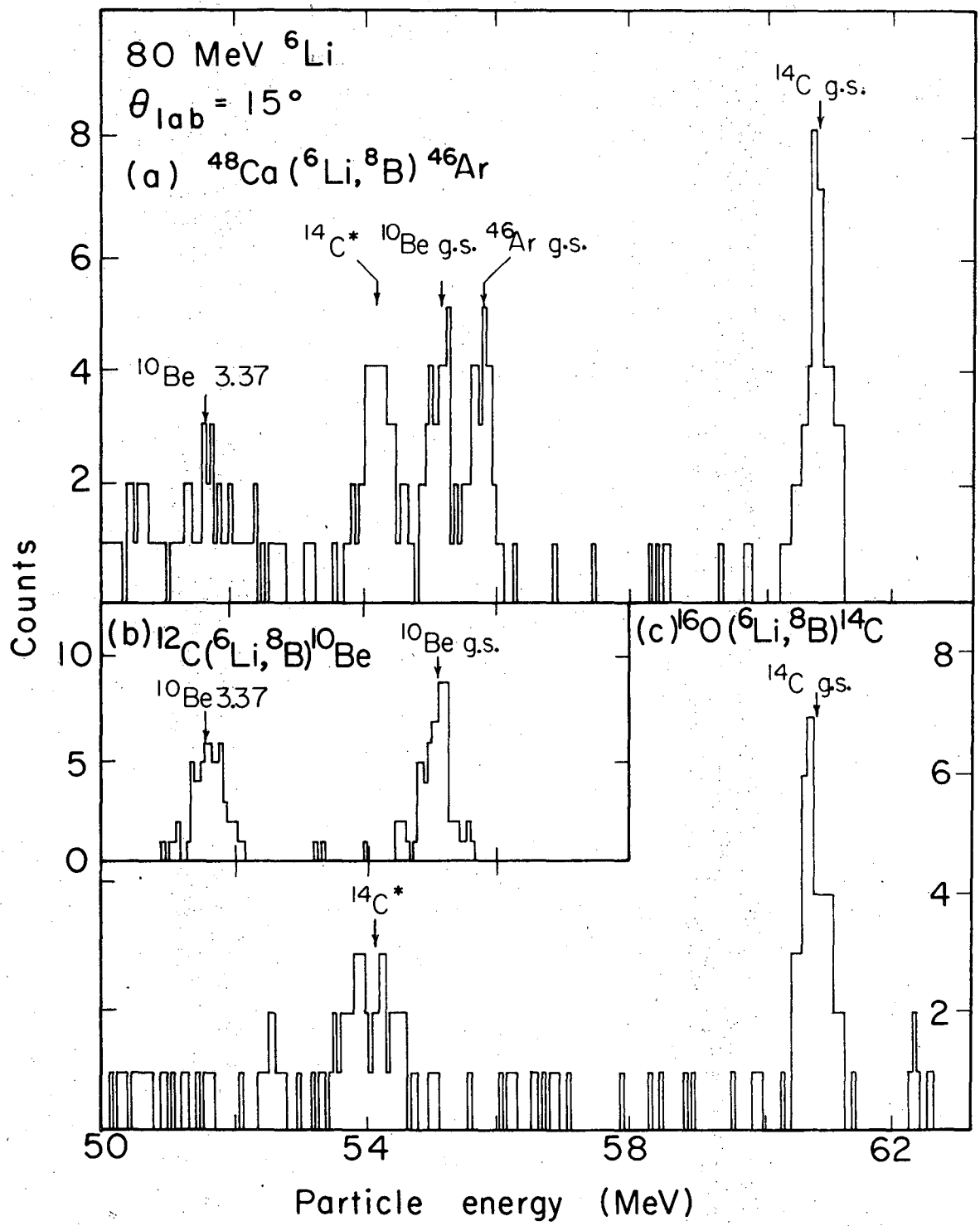

Figure 14. Energy spectra from the (^{6}Li,^{8}B) reaction taken at θ_{lab} = 15° on (a) ^{48}Ca (6300 μC); (b) ^{12}C, and; (c) ^{16}O. All are displayed with the same ^{8}B energy scale.

were observed; shell-model calculations[52] predict the first excited state to be at ~2 MeV excitation.

Analysis of the data gave Q values for the formation of ^{43}Ar, ^{45}Ar and ^{46}Ar of -21.17 ± 0.07, -27.84 ± 0.06, and -23.33 ± 0.07 MeV, respectively. These correspond to mass excesses of ^{43}Ar = -31.98 ± 0.07 MeV, ^{45}Ar = -29.727 ± 0.06 MeV, and ^{46}Ar = -29.732 ± 0.07 MeV. Comparisons are made with theory in Section V.

C. Cl and S Isotopes

Due to the successful observation of ^{43,45,46}Ar, we irradiated a ^{48}Ca target with a 110 MeV alpha beam and observed the ^{8,10,11}B and $^{10-13}$C exit particles, which populate the residual nuclei ^{44,42,41}Cl and $^{42-39}$S, respectively. The masses of all these residual nuclei are unknown. Ground state Q values for the reactions vary from about -20 to -44 MeV.

The ΔE2, ΔE1 and E counters were 48, 27 and 340 μm thick, respectively, for the boron telescope, and 29, 14 and 289 μm for the carbon telescope. Solid angles subtended were 0.17 and 0.43 msr, respectively. Boron isotopes were measured at 10 and 30 degrees and carbon isotopes at 10 and 35 degrees. Beam intensities varied from about 0.3 μA at 10 degrees to 2 μA at backward angles.

Fig. 15 shows PI spectra of the boron isotopes obtained from the thick telescope and of the carbon isotopes obtained from the thin telescope. Particle separation is seen to be very good.

The energy region of interest for ^{8}B and ^{10,11}C at 10° was obscured by the large contribution from ^{12}C and ^{16}O impurities on the target. For the other reactions, the predicted position for formation of the Cl or S isotope in its ground state fell higher in energy than contaminant

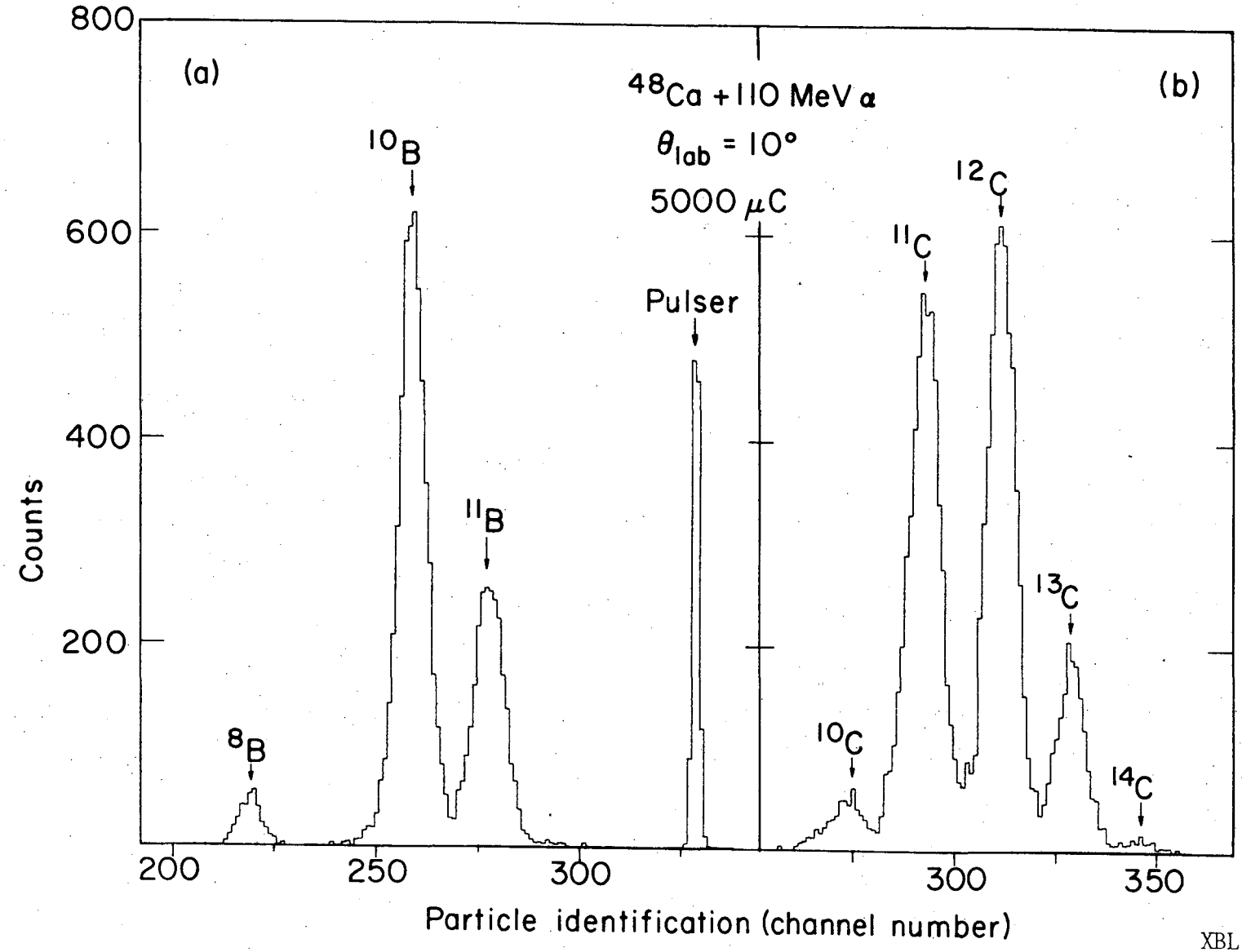

XBL 754-2749

Figure 15. Particle identification spectrum resulting from bombardment of ^{48}Ca by 110 MeV α particles. (a) Boron isotopes seen in the thick detector telescope. (b) Carbon isotopes seen in the thin detector telescope.

contributions. Nevertheless, no positively-identifiable peaks were seen for formation of any of the Cl or S isotopes.

Energy spectra of ^{10}B exit particles at 10° and 30°, and of ^{8}B particles at 30°, are shown in Fig. 16. Peaks arising from ^{12}C and ^{16}O contaminants are indicated, as well as the expected positions of the ^{42}Cl and ^{44}Cl ground states. Fig. 17 presents spectra of ^{11}C taken at 35° and of ^{12}C and ^{13}C taken at 10°. Expected ground state positions of $^{41,40,39}S$ residual nuclei are indicated. The other B and C spectra were similar but, generally speaking, showed even less.

The very low count level in the region of most of the Cl and S isotopes permitted the determination of strict upper limits for the cross sections of these reactions populating the ground state. These cross section limits are given to the nearest 5 nb/sr in Table II. The very large angular momentum mismatches involved (5-8ħ as calculated semi-classically, including the Coulomb potential) may have contributed to extremely low cross sections for many of these reactions.

D. ^{10}Li

A 121 MeV $^{9}Be^{+3}$ beam was used to initiate the reaction $^{9}Be(^{9}Be,^{8}B)^{10}Li$ ($Q \sim -34$ MeV). The ^{8}B telescope, subtending a solid angle of 0.3 msr, consisted of $\Delta E2$, $\Delta E1$, and E detectors of 53, 45, and 210 μm thickness, respectively, and was cooled to -20°C. The recoil telescope contained 11 and 48 μm ΔE and E counters, respectively, and subtended 15 msr. The data were obtained at a ^{8}B detection angle of 14° and a recoil angle of 33° in the lab, and with the target rotated normal to the latter in order to minimize the energy loss of the recoils in the target. (Although this does increase the target thickness for ^{8}B exit particles, it does not

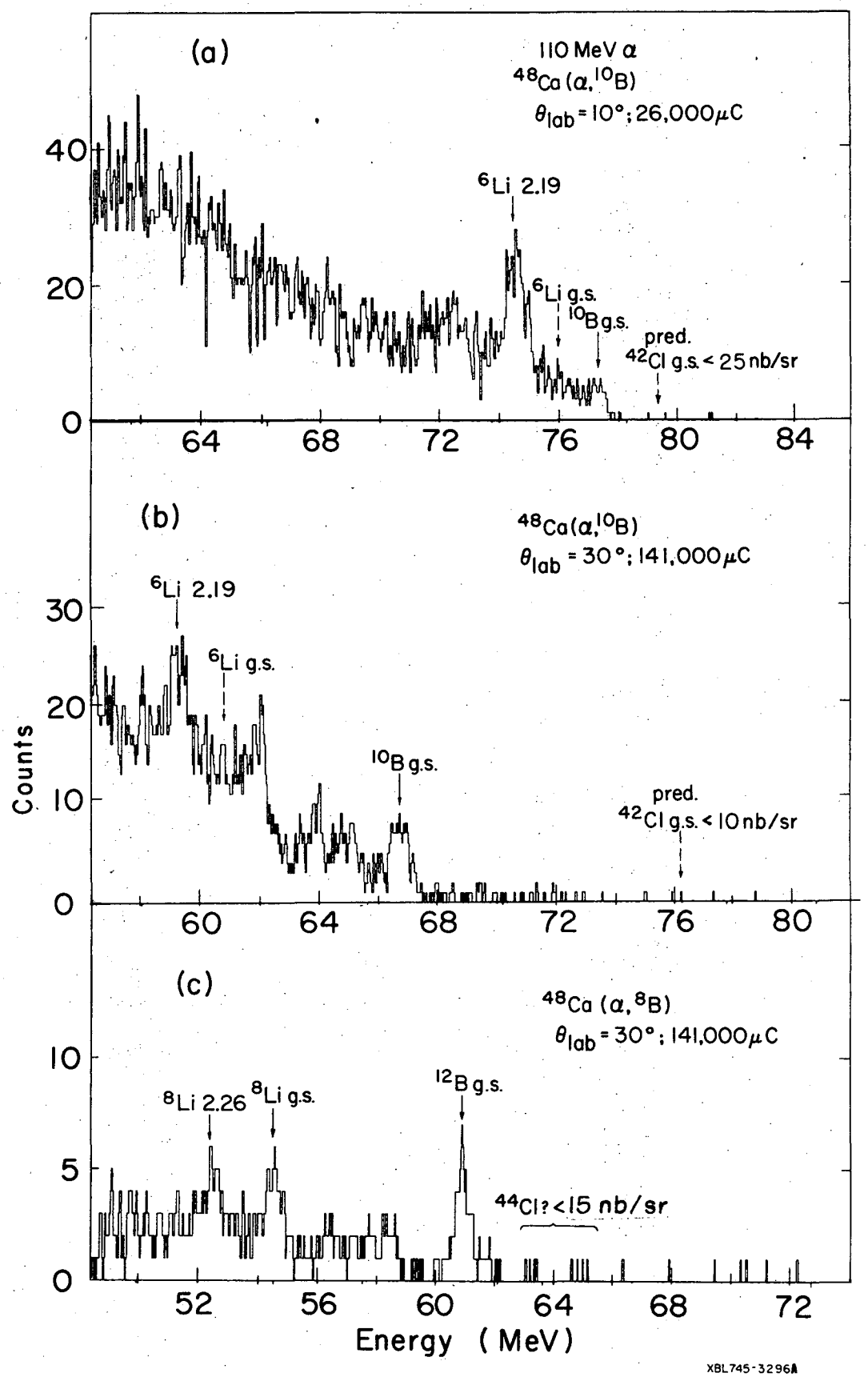

Figure 16 Energy spectra of the $^{48}Ca(\alpha,^{10}B)^{42}Cl$ reaction (a) at 10° and (b) at 30°, and of the $^{48}Ca(\alpha,^{8}B)^{44}Cl$ reaction (c) at 30°. Predicted ground state positions are indicated for ^{42}Cl and ^{44}Cl.

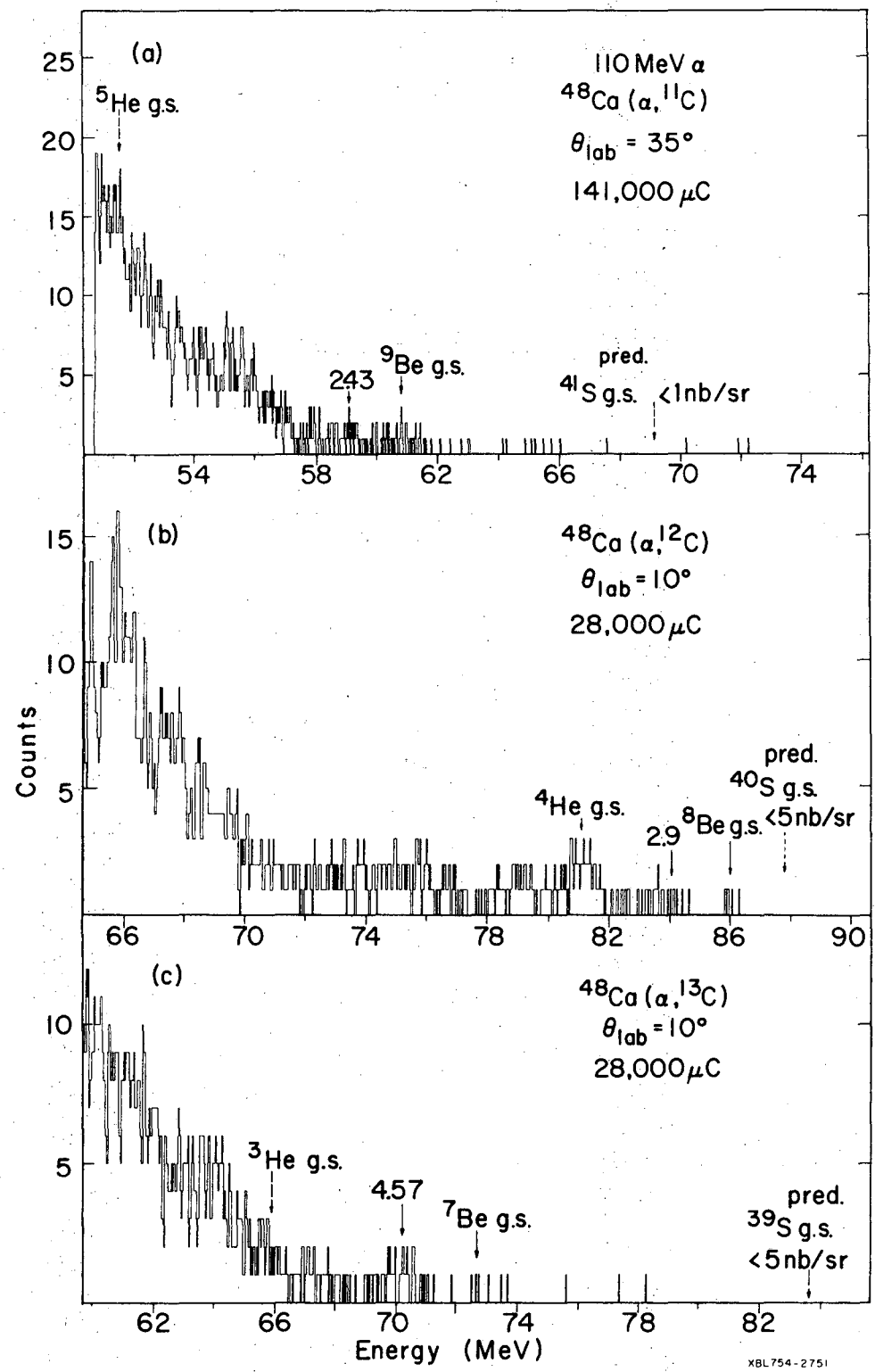

Figure 17 Energy spectra of (a) the $^{48}Ca(\alpha,^{11}C)^{41}S$ reaction at 35°, (b) the $^{48}Ca(\alpha,^{12}C)^{40}S$ reaction at 10°, and (c) the $^{48}Ca(\alpha,^{13}C)^{39}S$ reaction at 10°. Predicted ground state positions are indicated for $^{41,40,39}S$.

	^{39}S	^{40}S	^{41}S	^{42}S
10°	5	5	—	—
35°	1	1	1	5

	^{41}Cl	^{42}Cl	^{44}Cl
10°	15	25	—
30°	5	10	15

XBL754-2753A

Table II. Center-of-mass cross sections in nb/sr (given to nearest 5) for the α-induced reactions on ^{48}Ca at the laboratory angles indicated. First row gives residual nucleus populated.

significantly decrease their energy resolution, which is heavily dominated by angular acceptance effects.) Typical counting rates were 5000/sec in the ^{8}B $\Delta E2$ counter and 50,000/sec in the recoil ΔE counter. Bipolar signal shaping in the recoil electronics enabled these rates to be maintained without excessive pulse pileup ($\leqslant$ 4%).

Fig. 18 presents a particle identification spectrum taken with the ^{9}Be target. The insert shows the ^{8}B region on an expanded scale. (Note that it contains a larger number of counts than the main figure.) Those events which also had a recoil coincidence are shown cross-hatched. It is seen that ^{10}B events tailing into the ^{8}B region are totally eliminated by this requirement.

The source of the small peak between the ^{8}B and ^{10}B regions seen in both parts of Fig. 18 is not definitely established. These counts have an energy spectrum with the same shape as the main ^{10}B peak. If some ^{10}B particles stopped in the rear dead layer of the E detector or lost insufficient energy in the anticoincidence detector to trigger its threshold, their PI signals would be shifted downwards and might form a noticeable peak. However, the energy spectrum of such a peak would be very restricted in width and not resemble the observed spectrum of the peak in question. Similarly, pulse pileup from the simultaneous detection of two lighter particles, a phenomenon which sometimes produces an extra peak in a PI spectrum, would be expected to produce an energy spectrum markedly differing from that observed. The extra peak thus appears to be some aberration of the detection system or electronics which acts on a small random sampling of all ^{10}B events.

No(^{9}Be,^{8}B) reactions are known which produce unambiguously-assignable

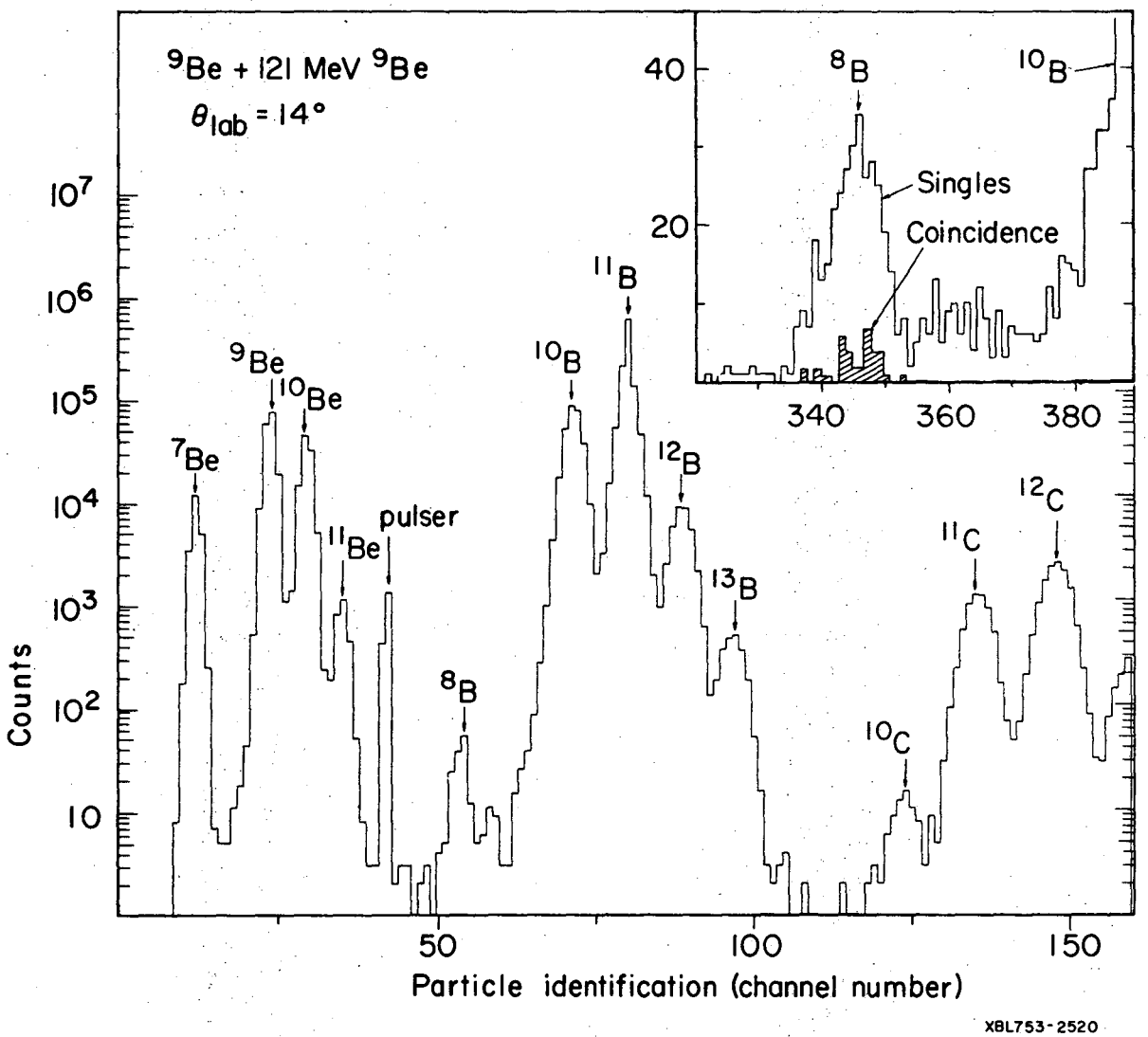

Figure 18. Particle identification spectrum resulting from the bombardment of ^{9}Be by 121 MeV ^{9}Be. Insert shows the ^{8}B region on an expanded scale, with the events which had a recoil coincidence cross-hatched.

states with sufficiently large cross sections to serve as an energy calibration for the $^{9}Be(^{9}Be,^{8}B)^{10}Li$ data. The one-proton pickup reaction $(^{9}Be,^{10}B)$, which could be expected to have a much higher cross section, produces states about 20 MeV higher in energy than the ^{8}B nuclei of interest, much too far away to be useful for calibration purposes. A calibration was instead obtained by observing at 12° the $^{40}Ca(^{6}Li,^{8}B)^{38}Ar$ reaction to the ground and first excited (2.17 MeV) states of ^{38}Ar, and the $^{28}Si(^{6}Li,^{8}B)^{26}Mg$ ground state reaction, initiated with an 80 MeV $^{6}Li^{+2}$ beam. These previously-studied[53] reactions have reasonably-large cross sections (5-10 μb/sr) and populate discrete states with ^{8}B energies between 65 and 71 MeV, close to the ^{8}B energy of 75 MeV from the $^{9}Be(^{9}Be,^{8}B)^{10}Li$ ground state reaction at 14°. In addition, the ^{6}Li beam at the 88-Inch Cyclotron has a higher average intensity and greater dependability than the ^{9}Be beam.

Such a calibration procedure is possible because 80 MeV $^{6}Li^{+2}$ and 120 MeV $^{9}Be^{+3}$ have essentially the same magnetic rigidity and charge-to-mass ratio Q/M, and therefore the same cyclotron field and frequency and beam transport magnet currents. Nothing affecting beam energy need be changed in switching between these two beams (although a very small frequency change is required because Q/M changes by about 1 part in 10^{3}). Measuring the energy of one of the two beams therefore determines just as precisely the energy of the other, by the relationship that beam energy is proportional to Q^{2}/M. Thus 120 MeV $^{9}Be^{+3}$, for example, corresponds to 79.907 MeV $^{6}Li^{+2}$.

It was desirable to obtain an experimental point above the ^{8}B energy of 75 MeV in order to avoid the possibility of an extrapolation error in determining the mass of ^{10}Li. The $^{12}C(^{9}Be,^{8}B)^{13}B$ reaction was used for

this purpose, since it was necessary to investigate this reaction anyway in order to be able to identify any peaks that might arise from ^{12}C contamination of the ^{9}Be target.

A ^{8}B energy spectrum from the $^{12}C(^{9}Be,^{8}B)^{13}B$ reaction at 14° is shown in Fig. 19 (a). Unfortunately, the ground state population is too low to be used for calibration purposes. There are two doublet states[54] in ^{13}B at 3.48 and 3.54 MeV, and 3.68 and 3.71 MeV excitation, corresponding to the region of the sharp peak at 81 MeV. It can not be said which state or states are populated in this spectrum. A value was therefore arbitrarily assumed midway between the extremes, and an uncertainty assigned large enough to encompass all four states. Because the ^{8}B energy corresponding to ^{10}Li ground state production is closer to the $(^{6}Li,^{8}B)$ calibration points than to the $(^{9}Be,^{8}B)$ point, the uncertainty in the ^{10}Li mass resulting from this assumption is much less than the uncertainty in the ^{13}B point itself. It is interesting to note that the 300 keV width observed for this peak is just what would be expected from detection geometry considerations for a single, narrow state. This suggests that only one of the two doublets is being populated to any significant degree.

A spectrum of all the ^{8}B data from the ^{9}Be target, representing 2750 μCoul of ^{9}Be beam (fully stripped), is shown in Fig. 19 (c). The same data, with the additional requirement that each event be in coincidence with a count in the recoil detector, are seen in Fig. 19 (b). With this requirement, elimination of the ^{10}B's and of the ^{8}B's arising from ^{12}C contamination is essentially complete, demonstrating the high effectiveness of the recoil telescope technique. A comparison of spectra 19 (b) and 19 (c)

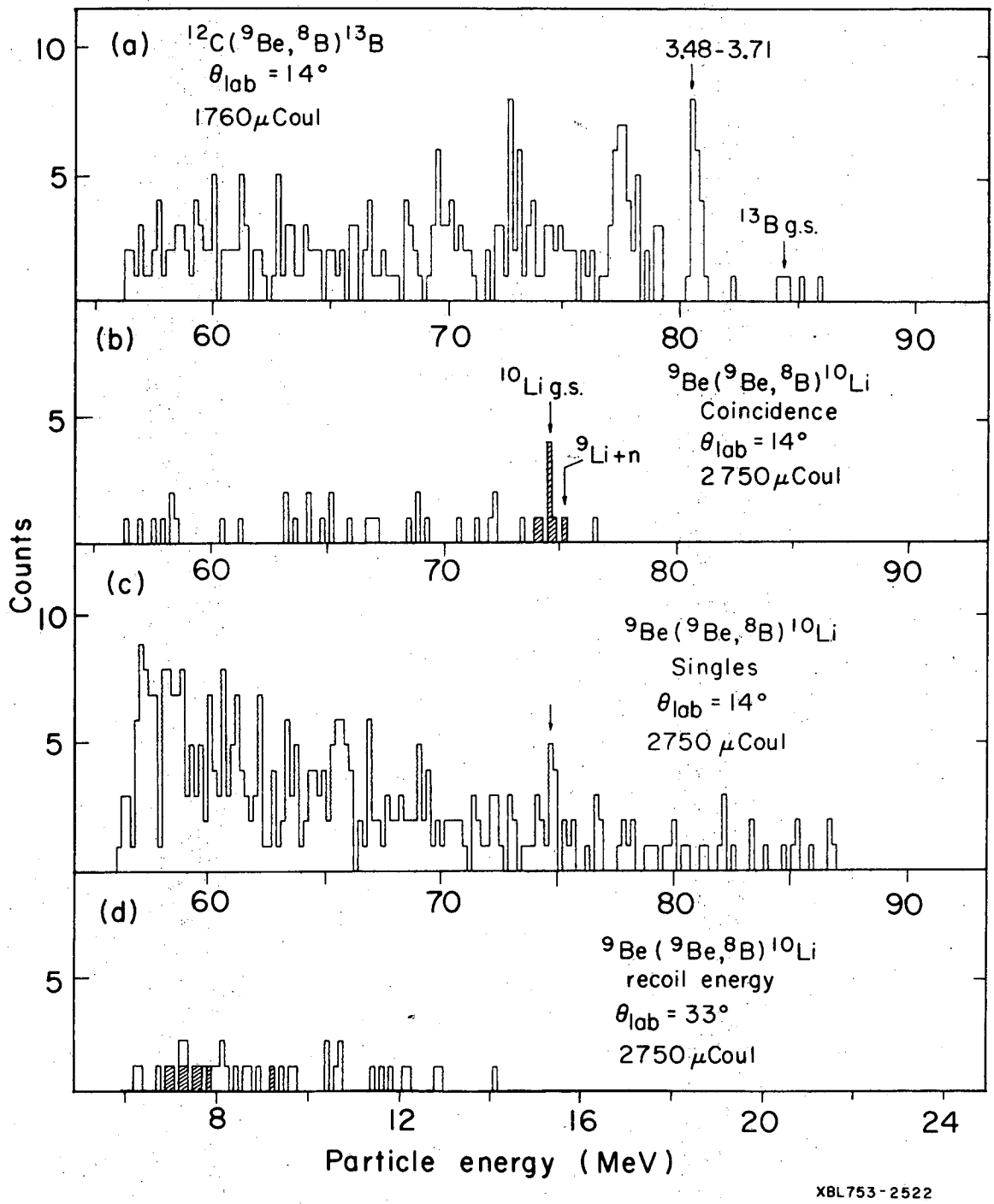

Figure 19 Energy spectra of (a) the $^{12}C(^{9}Be,^{8}B)^{13}B$ reaction; (b) the $^{9}Be(^{9}Be,^{8}B)^{10}Li$ reaction coincidence events, showing binding-energy threshold of ^{9}Li + n; (c) the $^{9}Be(^{9}Be,^{8}B)^{10}Li$ reaction singles events; and (d) the recoil energy of the $^{9}Be(^{9}Be,^{8}B)^{10}Li$ reaction coincidence events. The events assigned to the ^{10}Li ground state and their associated recoils are cross-hatched in parts (b) and (d), respectively.

also indicates that the efficiency for detecting the ^{9}Li decay products of ^{10}Li ground state recoils was high.

As discussed in Section III E, coincident events were accepted which had a ΔTOF signal (the difference in detection time between the ^{8}B and its coincident recoil) in a region that encompassed the real peak (the particle and its coincidence occurring in the same beam burst) and one chance coincidence peak (the particle and its recoil in adjacent beam bursts). A ΔTOF spectrum is shown in Fig. 20 for events of all particle types which had a recoil coincidence. Requiring the further restriction that a ^{8}B event must have a recoil coincidence, all but three of the events in the chance coincidence peak for the entire experiment were eliminated, and they corresponded to ^{8}B events well outside of the energy region of interest. Since the chance contribution should be the same in all ΔTOF peaks, we can reliably conclude that the chance contribution to the data in Fig. 19 (b) is negligible. The ΔTOF parameter of the data in Fig. 19 (b) is shown cross-hatched in Fig. 20.

A further indication that the data in Fig. 19 (b) have been correctly attributed to the ^{9}Be(^{9}Be,^{8}B)^{10}Li reaction comes from the recoil PI spectrum. Although isotope resolution is poor, it is sufficiently good to show that all the events under consideration are grouped together in roughly the region that would be expected for ^{9}Li nuclei.

The events assigned to the ^{10}Li ground state are cross-hatched in Fig. 19 (b). The width of this peak appears somewhat narrower than would be expected for a single unbound state on the basis of a neutron tunneling calculation, although the statistics are too poor to determine the width definitively. A recoil energy spectrum of the coincidence data, with the

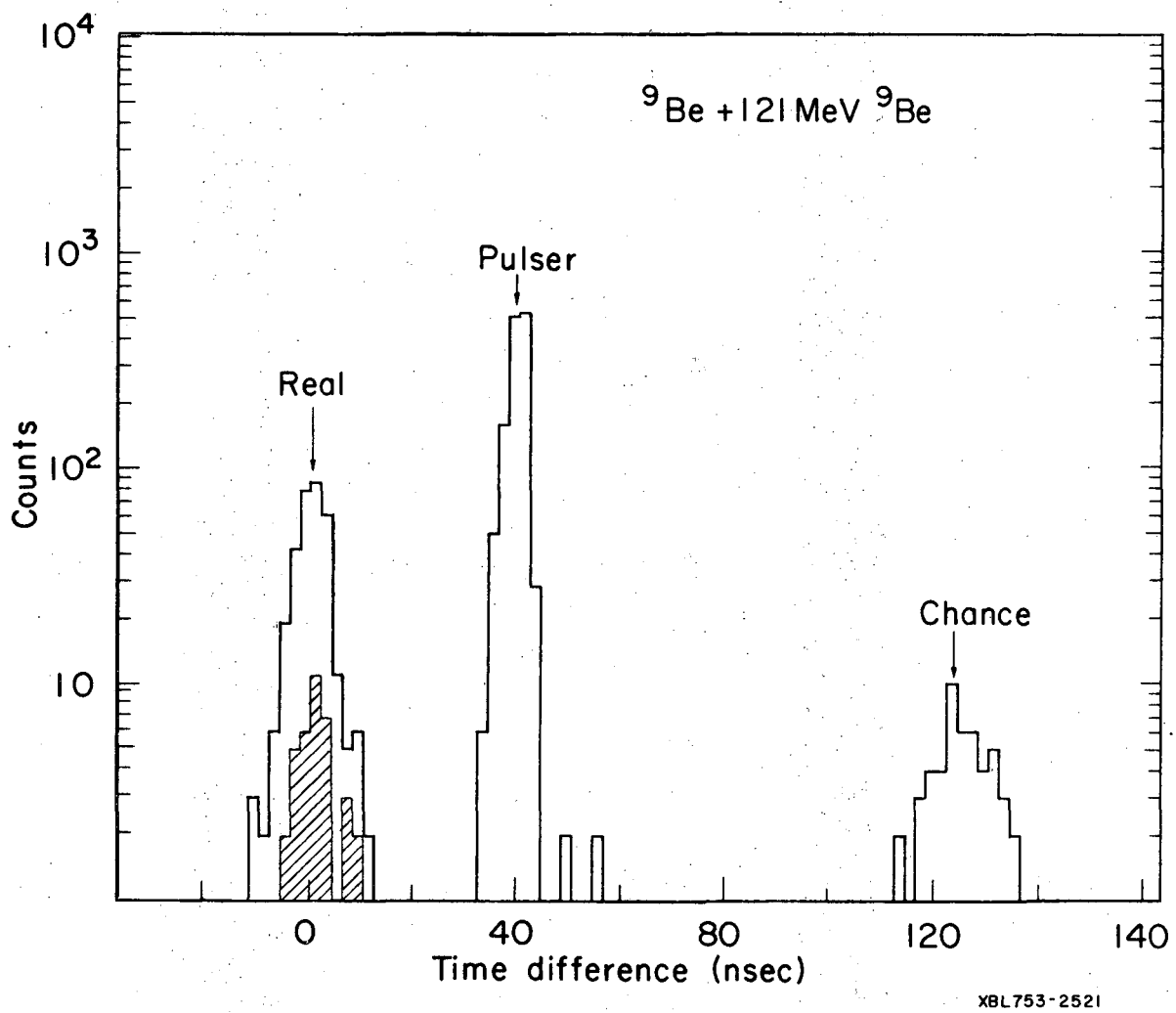

Figure 20. A TAC spectrum showing the difference in flight time between detected particles and their coincident recoils. The real coincidence peak is from particle and recoil in the same burst; the chance coincidence peak is from recoils one beam burst later. Cross-hatched counts are ^{8}B particles with a coincidence (the events in Fig. 19(b)).

same events cross-hatched, is shown in Fig. 19 (d). Again, the cross-hatched events occur in the expected energy region. (It may be interesting to note that as the ^{10}Li excitation energy increases, so does its kinetic energy.)

The observed Q value for the ^{9}Be(^{9}Be,^{8}B)^{10}Li ground state reaction based on Fig. 19 and a recent confirming reinvestigation is -34.06 ± 0.25 MeV, corresponding to a mass excess for ^{10}Li of 33.83 ± 0.25 MeV. ^{10}Li is thus unbound to ^{9}Li plus a neutron by 0.80 MeV, compared to a prediction of 0.21 MeV unbound based on the Garvey-Kelson method. This suggests the possibility that we are actually observing a low-level excited state of ^{10}Li. Based on particle-particle, hole-hole theorems of the nucleus, the low level structure of ^{10}Li should be very similar to that of ^{12}B, which has one proton hole in the $p_{3/2}$ shell rather than one $p_{3/2}$ particle. The first excited state of ^{12}B is 0.953 MeV. Since ^{10}Li is experimentally known[55] to be particle unbound, if the observed level were an excited state of ^{10}Li, it would have to be at less than 0.80 MeV excitation, which is unlikely.

The reaction cross section to the ground state of ^{10}Li at 14° is 30 nb/sr c.m. That the background is essentially nonexistent in such a low cross section reaction demonstrates the extreme effectiveness of the experimental technique employed.

The only previously-published[56] experimental results on the direct mass measurement of ^{10}Li, also from this laboratory, used the same reaction but a less-sophisticated technique. Particle separation was very much poorer, and the energy spectra had a high background. The "possible evidence" cited in that report for the observation of ^{10}Li should be considered as superseded by the present results.

E. ^{15}B

A 120 MeV $^{9}Be^{+3}$ beam (~ 100 nA on target) was used to initiate the $^{14}C(^{9}Be,^{8}B)^{15}B$ reaction. Fig. 2 illustrates schematically the detection setup, which consisted of a telescope of 55, 45, and 230 μm detectors (ΔE2, ΔE1, E), and a recoil detector of 15 μm. The ^{8}B telescope was at 14° and subtended an angle of 0.8° horizontally by 1.9° vertically, for a solid angle of 0.4 msr. The recoil counter, positioned at 32°, had an acceptance of 8.4° horizontally by 5.6° vertically, corresponding to a 13 msr solid angle. To allow detection of particles over an energy range of 5 MeV excitation in ^{15}B, the acceptance of the recoil detector in the reaction plane was made larger than its vertical acceptance.

Knowledge of the distribution of recoil particles corresponding to the detected ^{8}B particles is necessary in choosing the recoil detection geometry. An accurate calculation is difficult because of the many variables involved. For a particle-stable recoil nucleus, such as ^{15}B in its ground state, the distribution depends in a fairly straightforward way on the beam spot geometry (which can not be known precisely in advance) and the ^{8}B detection geometry.

The recoil distribution is much more complicated for ^{13}B recoils arising from reactions on ^{12}C nuclei in the target. This is because, at the angle at which ground state ^{15}B recoils are detected, the ^{13}B nuclei are emitted in particle-unbound excited states. (Refer to Section III B.) The maximum possible opening angle of the resultant ^{12}B decay-product cone can be calculated by a vector summation of the forward motion due to the ^{13}B kinetic energy and the maximum deflection due to the ^{13}B breakup energy. (A three-body calculation gave essentially the same results.)

Both of these quantities vary for a given ^{13}B emission angle. The ^{13}B kinetic energy depends significantly on where in the target the reaction occurred because the dE/dx in the target is large (about 5 MeV/mg-cm^2). Available breakup energy depends on which states in the ^{12}B daughter are populated by the decaying recoil, information which is not known. Assuming reasonable values for these variables, the ^{12}B maximum cone angle would be about 21° for "average" conditions.

These considerations are appropriate for ^{13}B recoils emitted at the precise angle where ^{15}B ground state recoils are expected. However, an angle of several degrees is subtended by the recoil detector, and thus a wide recoil energy and excitation range can be observed. A considerable variation of the maximum breakup cone angle across the detector results.

There is a tendency for the recoil decay products to be preferentially located near the outer edge of the cone. (Projecting a spherical breakup geometry in the center of mass onto a two-dimensional detector in the lab accounts for this phenomenon.) This tendency, in conjunction with the fact that the ^{12}B breakup cone is much larger than the recoil collimator, makes it apparent that most of the ^{12}B daughters will fall outside of the chosen detection geometry, as desired.

Recoil detection efficiency for bound particles was tested with the elastic scattering of ^{9}Be from a 200 μg/cm^2 ^{12}C target. With the ^{9}Be detection angle fixed, the percentage of detected elastically-scattered ^{9}Be nuclei which had a coincident ^{12}C recoil was measured at a series of recoil detection angles. As expected, elastic recoils were detected over approximately an 8° range of settings, corresponding to the angular acceptance of the recoil collimator. Over this 8° range the measured efficiency

was flat at about 50%, and dropped sharply to zero on either side. The principal loss of efficiency is due to the vertical acceptance of the recoil counter being inadequate. (A sufficiently large detector was not available because the vertical dimension of the recoil distribution is very large.) The angle observed to be the center of the recoil distribution agreed very well with the calculated value, indicating that the detection angles were properly calibrated.

The use of a TAC to generate a ΔTOF signal was discussed in Section III G. Pulser ΔTOF resolution was 150 psec. ΔTOF resolution for real particles was measured by $^{9}Be + ^{12}C$ elastic scattering to be about 600 psec. By measuring the scattering at several angles, calibrations for the ΔTOF and recoil energy spectra were simultaneously produced.

From nonrelativistic equations of motion we find that the flight time for a particle of energy E and mass M is given by

$$t = \frac{d}{c}\sqrt{\frac{M}{2E}} ,$$

where c is the speed of light and d is the flight path (15.3 cm for the three-counter telescope and 5.5 cm for the recoil detector). For flight paths this short, flight times are in the range of 3 to 6 nsec. Calculations of ΔTOF yield 1.7 nsec for the reaction producing ^{15}B in its ground state. For ^{13}B of 8.4 MeV excitation (which comes at the same angle as the ^{15}B ground state prediction), ΔTOF values vary from 0.1 to 1.5 nsec, depending on whether the neutron is emitted directly backward or forward, respectively. To this must be added the spreading effects of producing ^{13}B in different excited states, and of recoil losses in the target.

Fig. 21 presents a particle identification spectrum, showing very good ^{8}B separation. A ^{8}B energy calibration was obtained by the (^{6}Li,^{8}B) reaction at 80 MeV. (See Section IV D.) Various angles were measured on ^{12}C, SiO_2, and ^{40}Ca targets to produce the ground states of ^{10}Be, ^{26}Mg, ^{14}C and ^{38}Ar. The amount of ^{12}C in (and on) the ^{14}C target was determined by comparison between the $^{12}C(^{9}Be,^{10}B)^{11}B$ reaction measured for a given integrated number of beam particles on the ^{14}C target and on a ^{12}C target of known thickness. Initially the ^{14}C target contained about 20 $\mu g/cm^2$ of ^{12}C and 80 $\mu g/cm^2$ of ^{14}C, but after a prolonged period of bombardment the ^{12}C had built up to nearly 50 $\mu g/cm^2$.

Fig. 22 (a) and 22 (b) show ^{8}B energy spectra from the ^{14}C target, collected for 7900 μCoul; part (a) contains all ^{8}B events (singles and coincidence), part (b) only those with a recoil coincidence. The reduction in counts by adding the coincidence requirement is indeed striking. Recoil events from reactions on ^{12}C producing ^{13}B near its ground state will be eliminated because the ^{13}B angle is outside the range of recoil acceptance. Events will begin to appear as the ^{13}B excitation energy increases and the ^{13}B angle approaches the ^{15}B angle. However, at about this point ^{13}B becomes particle unbound, and as its excitation energy increases its breakup cone angle rapidly becomes so large that nearly all the ^{12}B nuclei are not detected. Most events which are accepted should therefore be near the ^{12}B + n threshold, as is observed in Fig. 22 (b). ^{15}B ground state predictions from the transverse (T) and modified shell model (M) mass equations are indicated.

Fig. 22 (c) presents for comparison a spectrum from a ^{12}C target taken so as to equalize the ^{13}B yield from both targets. An enhancement

0 0 0 0 4 3 0 7 2 5 9

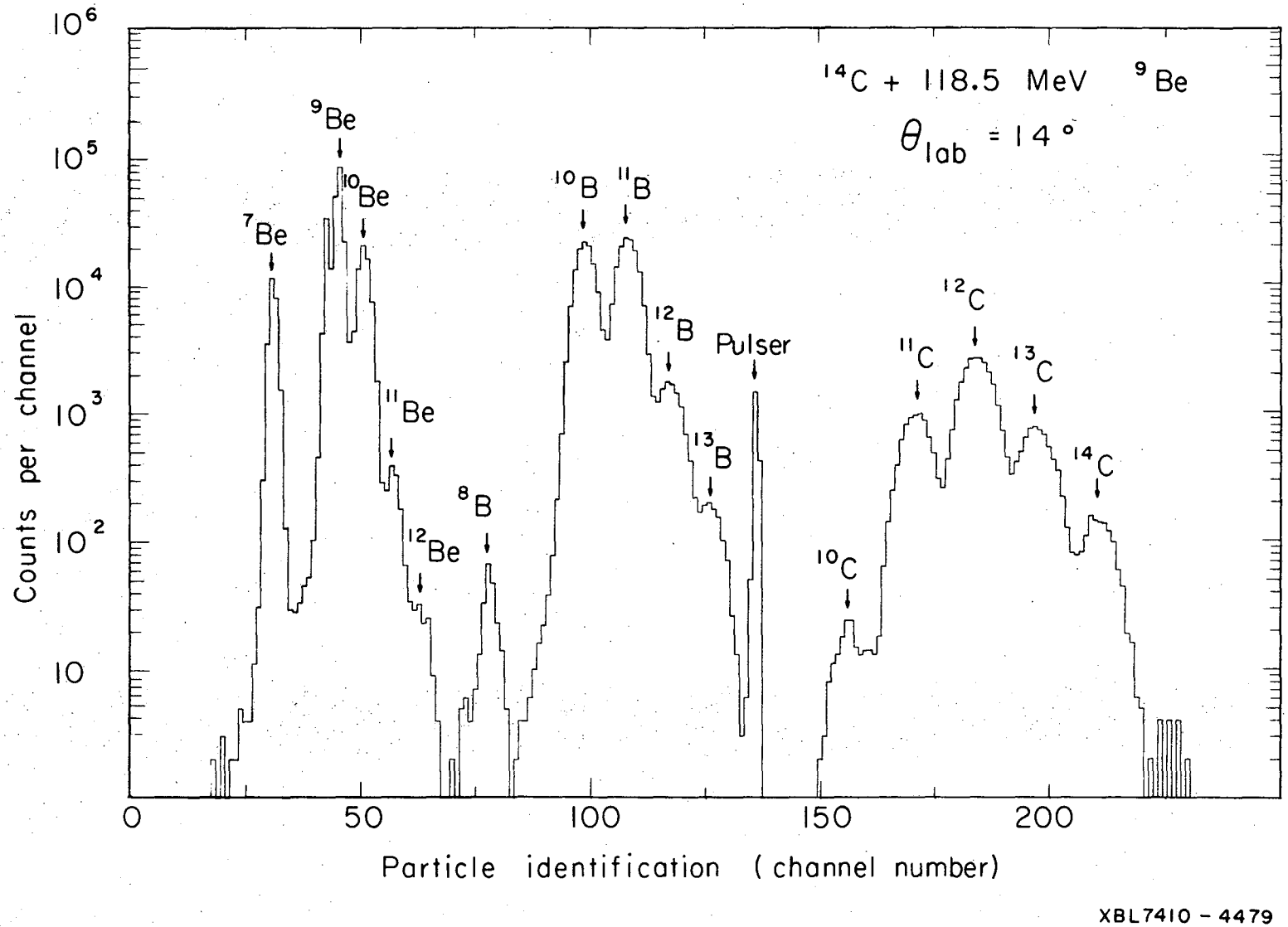

Figure 21. Particle identification spectrum resulting from bombardment of a ^{14}C target by 118.5 MeV ^{9}Be.

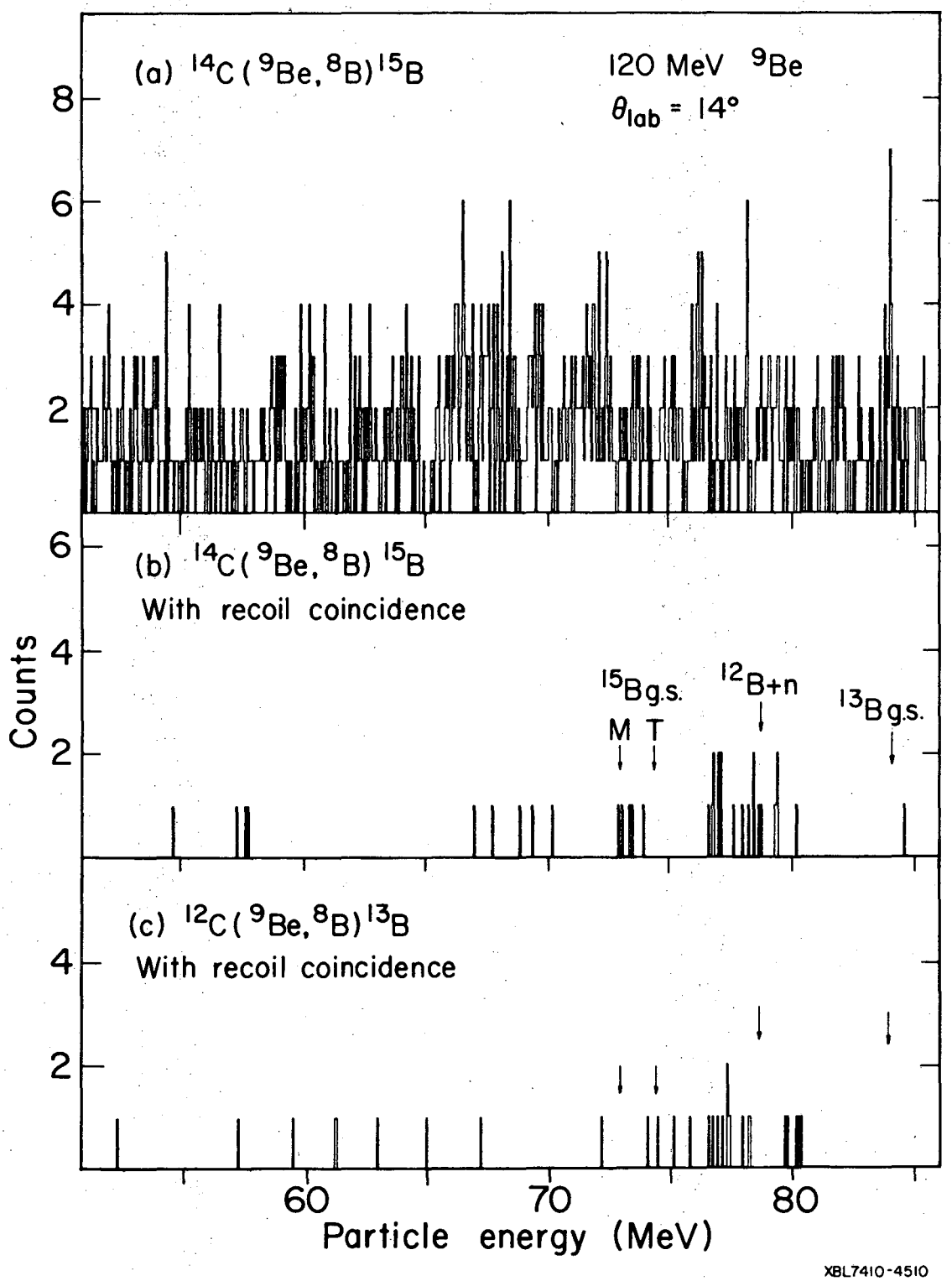

Figure 22. Energy spectra of (a) the $^{14}C(^{9}Be,^{8}B)^{15}B$ reaction, singles events; (b) the $^{14}C(^{9}Be,^{8}B)^{15}B$ reaction, coincidence events; and (c) the $^{12}C(^{9}Be,^{8}B)^{13}B$ reaction, coincidence events. Indicated are the threshold for breakup of ^{13}B into ^{12}B + n and the ^{15}B ground state positions predicted by M and T.

of counts in the ^{15}B region of Fig. 22 (b) is seen over what would be expected from comparison with Fig. 22 (c). If the 5 counts seen were indeed due to the formation of ^{15}B in its ground state, they would correspond to a mass-excess of 29.64 ± 0.21 MeV and a cross section of 120 nb/sr. Mass-excess predictions are 28.75 MeV by the transverse relationship and 29.89 MeV by the modified shell model.

The statistics are sufficiently low, however, that it is highly desirable to have additional confirming evidence before saying that ^{15}B has been successfully observed. The recoil PI and energy parameters for the five candidate events and for the ^{13}B events seen in Fig. 22 (c) were indistinguishable. At the time the data in Fig. 22 were accumulated, the ΔTOF measurement technique had not yet been adopted.

It was decided to reinvestigate the reaction with the addition of the fast timing for time-of-flight information. The motivation was to try to distinguish between ^{13}B (detected as ^{12}B) and ^{15}B recoils in the coincidence spectrum, as well as to generate additional statistics for a more conclusive determination of ^{15}B. A special 25 μm recoil detector of wider area (7 × 10 mm) was made[57] to permit increasing the vertical acceptance for improved ^{15}B detection efficiency. The new angular acceptance was 7.0° radially (slightly decreased from previously) by 10.0° vertically, or a 50% increase in solid angle. Elastic scattering tests showed the recoil detection efficiency for bound particles to be about 100%, compared to the previous 50%.

The ^{8}B energy spectra resulting from the reinvestigation (14,000 μCoul) are shown in Fig. 23, presented in the same format as Fig. 22. Approximately 50% of the events in the region of the ^{13}B 6.42 MeV peak[58]

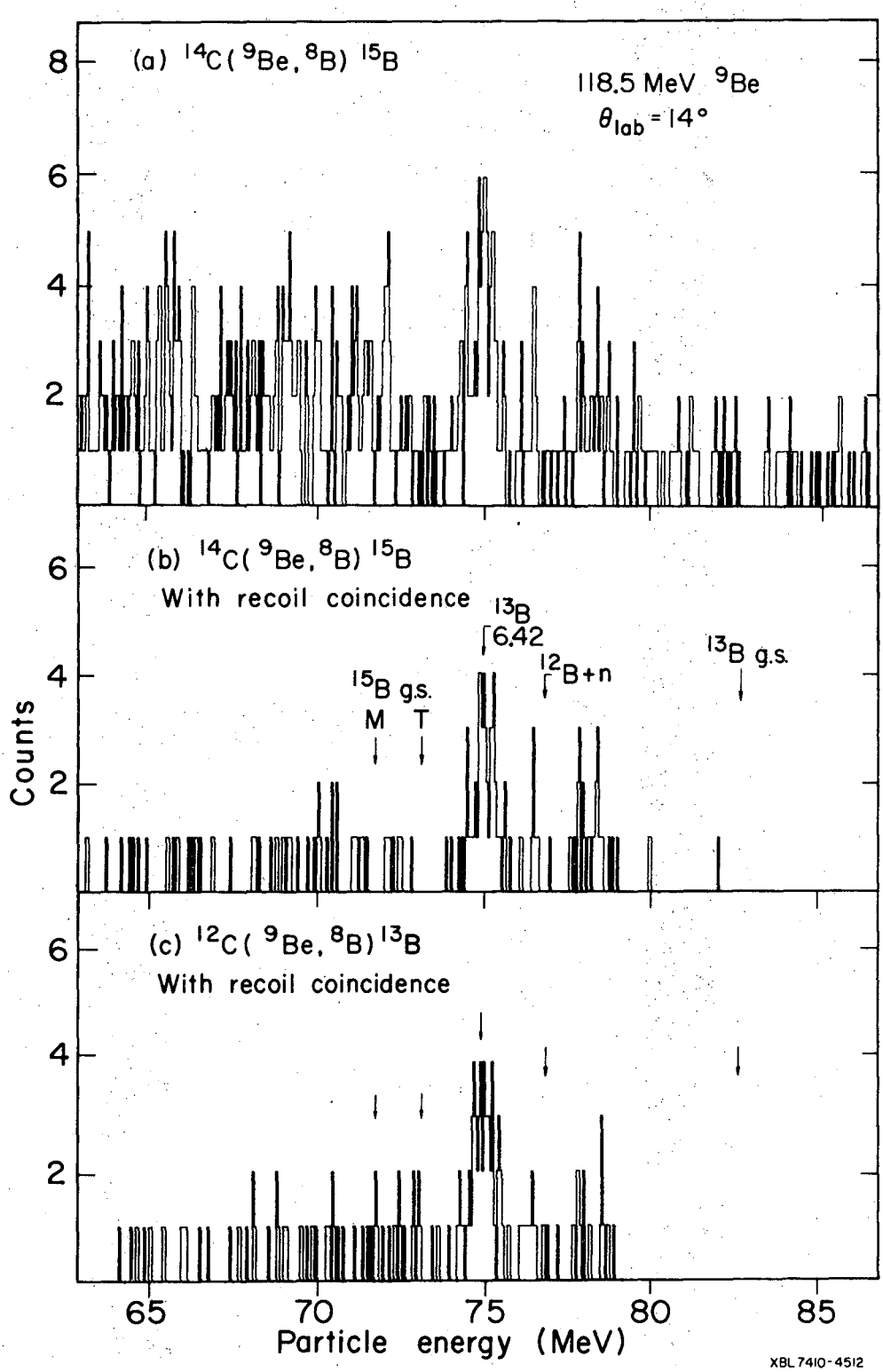

Figure 23 Results of reinvestigation of the $^{14}C(^{9}Be,^{8}B)^{15}B$ reaction, presented in an identical format to Fig. 22.

had a recoil coincidence. This is seemingly much higher than previously, although the percentage in the initial investigation is difficult to determine. Thus ^{13}B rejection is not nearly as complete. An additive effect is the presence of more ^{13}B events in the singles spectrum, since the amount of ^{12}C on the target had approximately doubled, as mentioned earlier.

The shapes of Fig. 22 (a) and Fig. 23 (a) are noticeably different. Since these spectra are independent of the recoil geometry, and the ^{8}B detection system was not changed, the spectra should be very similar. The observed dissimilarity may be due largely to differing target compositions. Fig. 22 (a) was produced with a freshly-made ^{14}C target having an appreciable iodine contamination (see Section III F). A substantial decrease in iodine content may have occurred before Fig. 23 (a) was produced, due to sublimation induced by beam heating. The large increase in ^{12}C contamination of the ^{14}C target is probably an even larger factor contributing to the dissimilarity. Considerations such as these cloud the comparison of ^{12}B rejection efficiencies made in the previous paragraph and complicate the determination of an optimum detection geometry.

In Fig. 23 (b) is seen a group of eleven counts in the same region as the five possible ^{15}B counts of Fig. 22 (b). However, in this case they do not correspond to an enhancement above background. Based on the Fig. 23 (c) comparison spectrum, we would expect about sixteen ^{12}B background counts in this region. Thus, within statistics, the counts in the predicted ^{15}B region of Fig. 23 (b) are consistent with being entirely due to background. These eleven counts correspond to a cross section of approximately 150 nb/sr, about the same as observed for the five candidate

counts in Fig. 22 (b). This casts additional doubt on the observation of ^{15}B in Fig. 22 (b), for a ^{15}B contribution of that size (five counts), in conjunction with the amount of background seen in Fig. 23 (c), would be expected to produce twice as many counts in the ^{15}B region of Fig. 23 (b) as are seen.

The coincident events in the expected ^{15}B region were again examined in detail to see if they differed in any clear way from those known to be due to the production of ^{13}B particles. The recoil energy and ΔTOF peaks were found to be so kinematically broadened that it was impossible to differentiate between ^{15}B and ^{12}B on this basis. When a two-dimensional plot of ΔTOF versus recoil energy was made for all events, a narrow and well-defined band was produced. However, the bands were indistinguishable for the ^{15}B energy region of both ^{12}C and ^{14}C target data.

Two conclusions are possible from these data. Either it is not possible to differentiate between detected ^{15}B and ^{12}B recoils under these experimental conditions, or else ^{15}B was not produced. In either case, no conclusive evidence for the observation of ^{15}B was seen. An upper limit for the yield of the $^{14}C(^{9}Be,^{8}B)^{15}B$ ground state reaction of about 50 nb/sr can be set.

This experiment would probably be feasible with detection geometry optimally designed (to maximize the $^{15}B/^{12}B$ ratio) and with a much lower percentage of ^{12}C in the target (a few percent at most, preferably 1% or less, which is probably unattainable). Otherwise, some method must be devised for differentiating between the ^{15}B and ^{12}B recoils. One possibility is using a large-acceptance spectrometer to detect the recoil particles, thus obtaining recoil mass resolution and better time-of-flight

information.

Due to the low value for the cross section and the magnitude of the contamination problem, this is an extremely difficult experiment. Unfortunately, with present experimental techniques there appear to be few alternative reactions. The major candidates appear to be three-proton pickup on ^{18}O, such as the (^{7}Li,^{10}C) or (^{11}B,^{14}O) reactions; double charge exchange on ^{15}N, such as the (^{9}Be,^{9}C) or (^{18}O,^{18}Ne) reactions; and four-neutron stripping on ^{11}B, such as the (^{18}O,^{14}O) reaction. These reactions all suffer from very serious problems of separating the exit particle from adjacent isotopes of the same Z. Each reaction also has at least one of the following major drawbacks: very highly negative Q values, very large $dE/d\theta$, and very low recoil kinetic energy. Thus the best chance for measuring the mass of ^{15}B may still rest with successfully solving the contamination problems accompanying the $^{14}C(^{9}Be,^{8}B)^{15}B$ reaction.

V. COMPARISON WITH THEORY

A. Masses

^{25}Ne-- The experimental mass-excess of -2.18 ± 0.10 MeV for ^{25}Ne can be compared with predicted values of -1.95 MeV by the transverse relation T and -2.12 MeV by the modified mass relation M, as given in Table I. This comparison has been previously illustrated in Fig. 1. Agreement is seen to be much better with the modified relation.

$^{43-46}$Ar-- In Fig. 24 T and M predictions are compared with the measured mass-excesses of ^{43,45,45}Ar, reported in Sect. IV B. Also included is a recent preliminary experimental result[59] for ^{44}Ar of -32.27 ± 0.04 MeV. Predicted values for $^{43-46}$Ar from M are -31.76, -32.32, -29.65, and -29.67 MeV, respectively, and from T are -31.83, -32.60, -29.81, and -30.23 MeV. Overall agreement with the modified relation is very good; agreement with the transverse relation is decidedly less so.

^{10}Li-- The mass-excess of ^{10}Li was measured to be 33.83 ± 0.25 MeV, corresponding to 0.80 MeV unbound to neutron emission. This is significantly less bound than the transverse prediction of 0.21 MeV unbound, but not unbelievably so. Since ^{10}Li is an odd-odd nucleus, it can not be predicted by the modified mass relation.

Abramovich et al.[60] have observed a resonance in the ^{7}Li(t,p)^{9}Li reaction corresponding to an excitation energy of about 21 MeV in ^{10}Be. On the basis of its narrow width, they assigned it to the T = 2 analogue of the ^{10}Li ground state, thereby deducing that ^{10}Li is unbound by 0.062 ± 0.060 MeV.

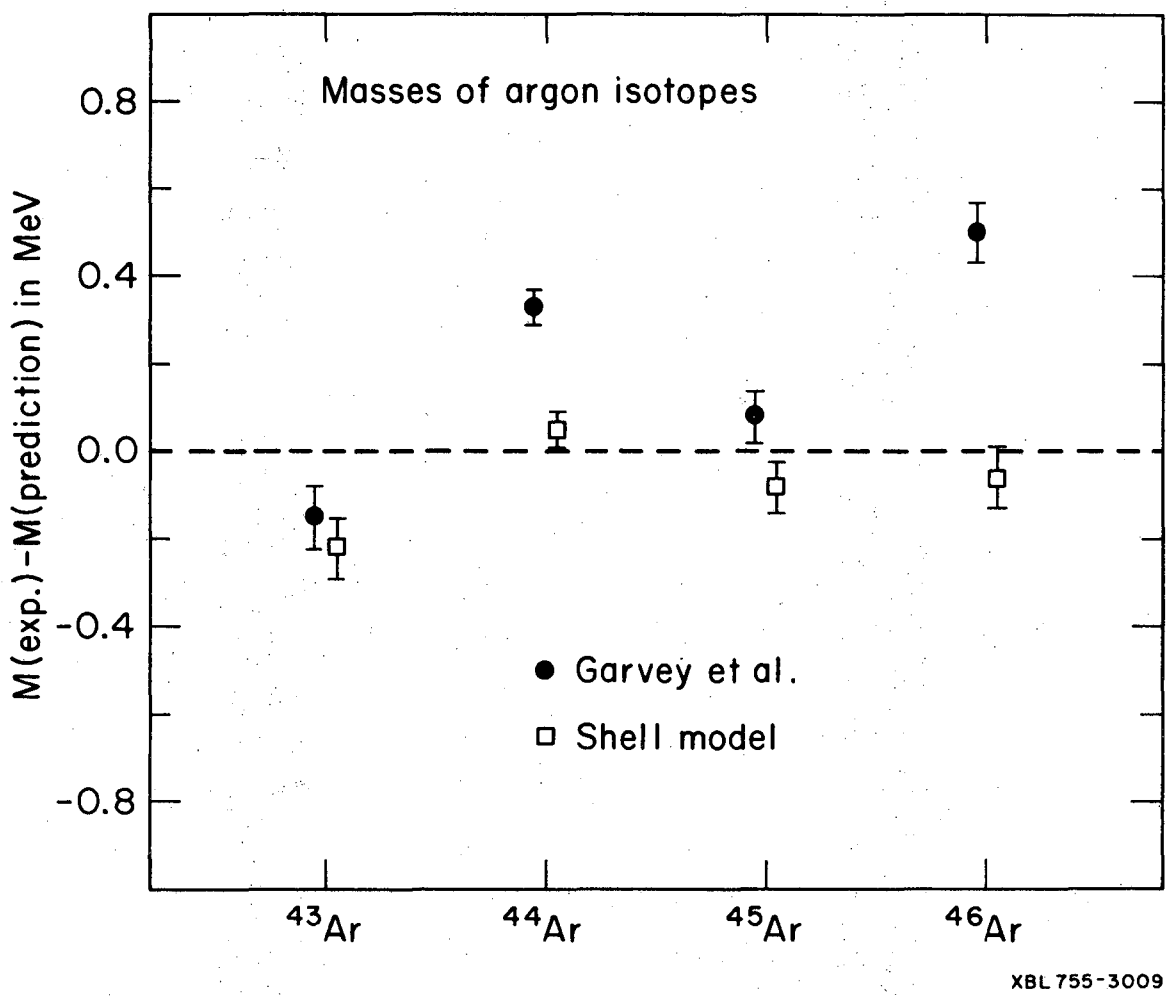

Figure 24. Comparison of the differences between the measured mass-excesses and predictions for the argon isotopes $^{43-46}$Ar by the Garvey-Kelson transverse relation (circles) and modified shell model mass relation (squares).

B. Level Schemes

^{25}Ne-- The low-lying structure of ^{25}Ne has been calculated by Cole et al.[1] as part of a larger study in the sd shell. Untruncated shell-model calculations were carried out using the procedure of Whitehead,[61] with particles distributed in the $d_{5/2}$, $s_{1/2}$, and $d_{3/2}$ levels, restricted only by the Pauli principle. The two-body interaction of Preedom and Wildenthal[62] was used.

Fig. 25 shows the results of this calculation compared to the observed levels, normalized to the ground states. (Cole et al.[1] obtained a mass-excess of -2.24 MeV for ^{25}Ne.) The calculated ground state spin of 1/2 + agrees with the 1/2 + (3/2 +) measured by Goosman et al..[50] If the assumption is made that the observed levels at 3.25 and 4.05 MeV are unresolved doublets (or that not all states were populated), then the agreement with theory would be quite good indeed.

^{43,45}Ar-- Large-basis shell-model calculations for ^{43}Ar and ^{45}Ar are available from other authors.[52,63] Gloeckner et al.[52] calculated the levels in ^{43}Ar up to 3.5 MeV, compared in Fig. 26 to the observed levels. Interaction parameters from a previous study[64] among the lighter Ar isotopes were used in conjunction with a $(\pi d_{3/2})^{-2}$ $(\nu f_{7/2}, \nu p_{3/2})^{n}$ model space.

Perhaps the most striking conclusion from Fig. 26 is the high selectivity of the ^{48}Ca(α,^{9}Be)^{43}Ar reaction. This selectivity can be understood from the large angular momentum mismatch of the reaction, about[52] $\Delta L \doteq 6\hbar$. Consequently, only high-spin states should be populated. Indeed, wherever a level is experimentally observed, a high-spin state is predicted to occur.

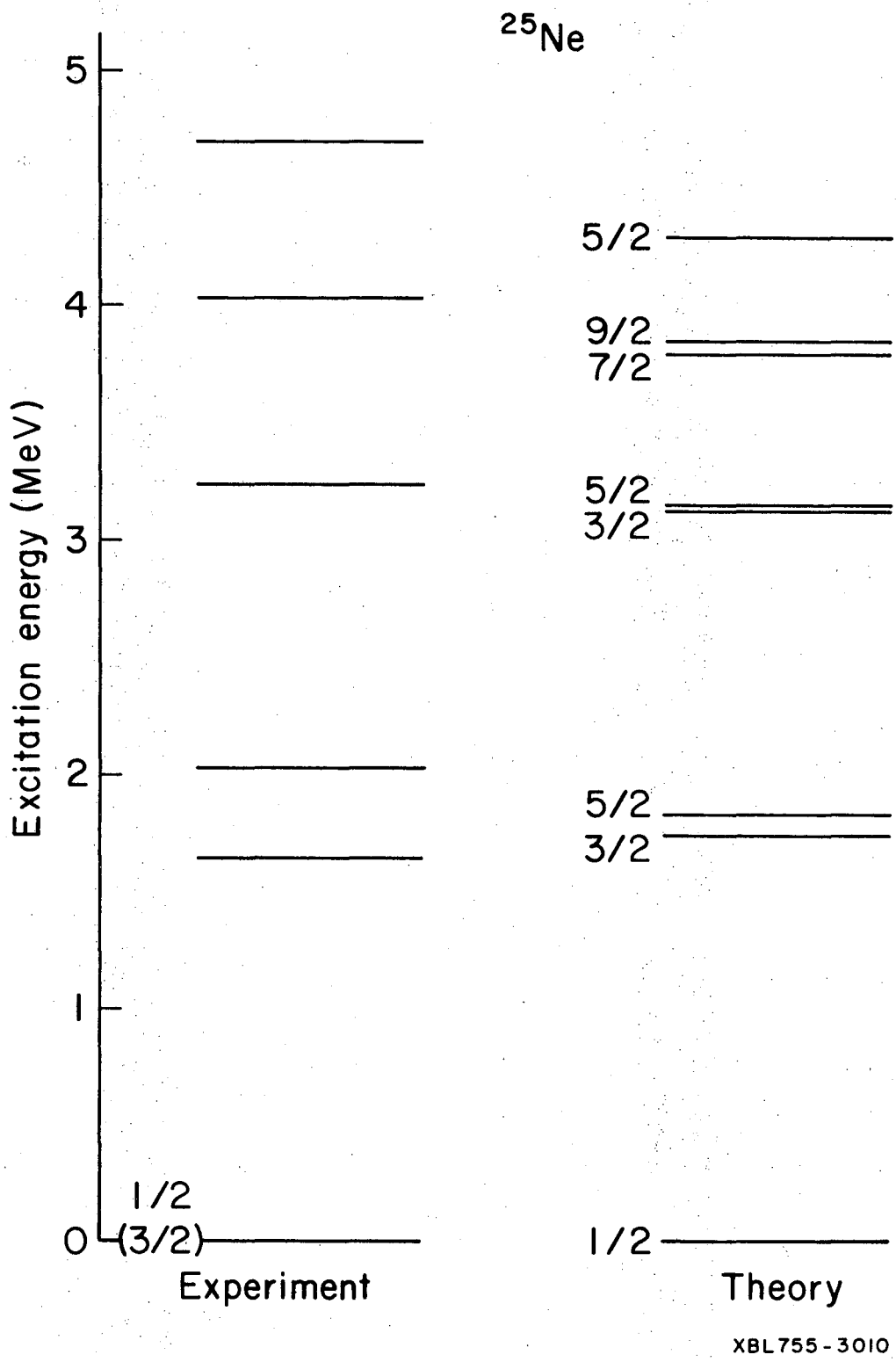

Figure 25. Experimental level scheme of ^{25}Ne compared to the calculation of Cole et al.[1]

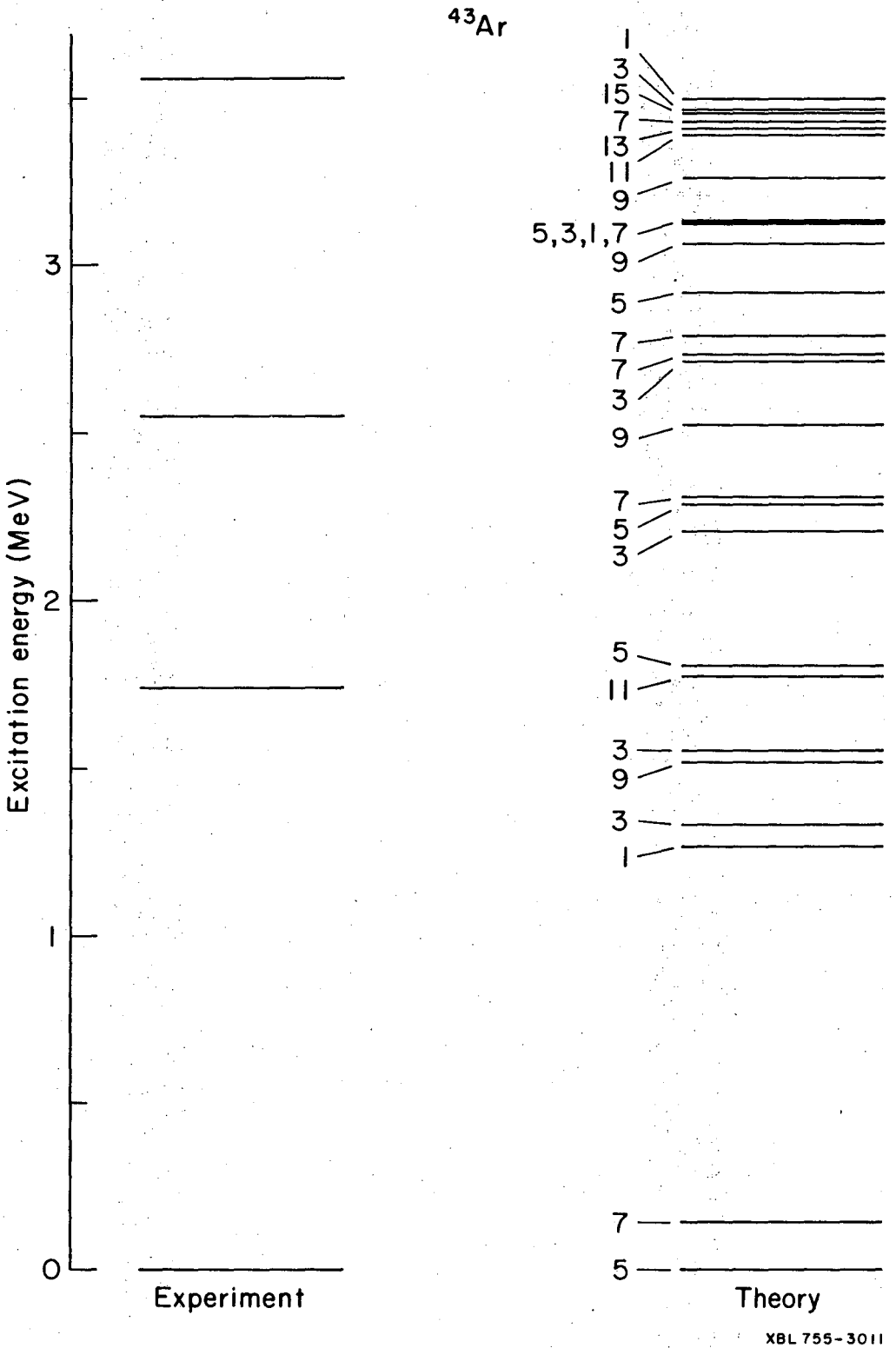

Figure 26. Experimental level scheme of ^{43}Ar compared to the calculation of Gloeckner et al.[52] The numbers to the left of the theoretical levels are $|2J|$.

A further consequence of this reasoning is that the $7/2^-$ state predicted to lie at about 0.15 MeV should be more strongly populated than the nearby $5/2^-$ state, casting doubt on the assignment of the highest-energy observed peak entirely to the ground state. However, there is uncertainty in the calculation of which state should fall lowest in energy; Evwaraye et al.[63] have predicted the $7/2^-$ level to be the ground state, as it is known to be[65] in ^{41}Ar. We have therefore assumed[66] on the basis of reaction systematics that the highest-energy peak corresponds predominantly to population of the ground state of ^{43}Ar. The comparison, given in Fig. 24, of the ^{43}Ar ground-state mass with either of the predicted values reinforces this assumption.

The model of Gloeckner et al.[52] can therefore be used to understand the ^{43}Ar data. However, it breaks down for ^{45}Ar and heavier isotopes, and has not been used to describe those results. Both models,[52,63] nevertheless, do demonstrate a qualitative similarity between ^{45}Ar and ^{39}Ar, as would be expected on the basis of simple particle-hole theorems. Excited states should thus begin above about 1 MeV, consistent with experiment.

VI. CONCLUSION

Multiparticle transfer reactions involving heavy ions have been shown to be a suitable tool for measuring the masses and excited states of light nuclei far from β-stability. Ground state masses were reported for ^{25}Ne, ^{43,45,56}Ar, and ^{10}Li. Several excited levels were also measured for ^{25}Ne and ^{43,45}Ar, and compared with theory. Very low ground state cross section upper limits were set for ^{15}B and for several highly neutron-excess isotopes of Cl and S.

A recoil coincidence system has been developed which can partially separate bound from unbound recoils when contamination problems are particularly severe. A modification involving recoil particle identification was introduced that is applicable when the recoils from desired and contaminant reactions are of different Z. This technique proved to be very effective.

A simple modified shell model mass relation has been derived, and predictions presented for the masses and particle-stability of neutron-excess light nuclei. The fit to known masses and the predictive ability of this model were compared with an updated recalculation by the Garvey-Kelson approach. The modified shell model was shown to better account for the masses of many nuclei of high neutron-excess. Thus it is a useful alternative to Garvey-Kelson for very neutron-rich light nuclei.

Many additional masses of interest could be measured by these techniques. ^{9}He, ^{13}Be (both particle-unbound), ^{15}B, and ^{19}N are particularly interesting because their masses as predicted by the modified relation and by Garvey-Kelson differ by more than 750 keV. Experimental masses for these nuclei would permit a more stringent test and comparison of

the two models in the very light nuclei. Other desirable experiments would include measuring the mass of ^{17}C and reinvestigating ^{21}O and ^{22}O.

ACKNOWLEDGMENTS

My deepest thanks and appreciation to Dr. Joseph Cerny, my research director, for many years of unflagging interest in and help with the travails of a graduate student, even from "Down Under."

I would like to acknowledge the contributions of the following individuals:

postdocs Hans Harney, Rick Gough, Nick Jelley, Mike Zisman, and Danny Ashery;

present and past graduate students John Esterl, Joe Sherman, George Goth for introducing a very green grad student to The Big World of the Nucleus, Rich Sextro (and his wife Joan) for several great hikes through deserts and over mountains, Gordon Wozniak for yeoman's service as a thesis-reader and electronic trouble-shooter, my faithful office-mate of many years John Macdonald, Bob Weisenmiller for help with physics and for other things too numerous to mention, Dave Vieira, Dieter Stahel, Leonard Ho, and Brian Jeltema.

I owe my special thanks to:

Nick Jelley for a lion's share of the work on mass relations;

Creve Maples for writing several invaluable computer programs and answering panic calls for help;

Mike Zisman for going the extra mile to prepare me for orals and the German language exam;

Claude Ellsworth and Leonard Ho for providing the targets used in these experiments;

the cyclotron crew, the shops, and the other excellent support personnel;

0 0 0 0 4 3 0 7 2 6 7

Fred Goulding, Don Landis, Ed Lampo, and their trusty cohorts for designing and maintaining the electronic equipment;

Bob Lothrop and Jack Walton for providing the detectors;

and all those others who gave generously of their expertise and enthusiasms.

Grateful thanks are also due for the special assistance and good times provided by Roy Burton, Don Stiver, Dick Perkins, and, of course, Ann Macdonald.

APPENDIX I

Predicted mass-excesses and one- and two-proton binding energies (in MeV) of the T_z = -2, -5/2, and -3 nuclei through the titanium isotopes. The method of Kelson and Garvey[35] was employed (see discussion at the end of Sect. II C). In similar fashion to their work, the letter in parentheses beside the nuclear species specifies the type of information available on the neutron-excess isotope used in the prediction, with D or X signifying a nuclide whose mass is known or unknown, respectively. For the latter, the mass predicted by the transverse mass relation (and listed in Table I) was assumed.

TZ = -2
****

NUC.	MASS EXCESS	BINDING ENERGY 1P	BINDING ENERGY 2P
8C (D)	35.77	-.15	-2.44
10N (X)	39.38	-3.21	-1.92
12O (D)	33.06	-.32	-2.82
14F (D)	33.37	-2.56	-1.22
16NE(D)	24.67	.23	-2.09
18NA(D)	25.57	-1.66	.20
20MG(D)	17.40	2.76	2.39
22AL(D)	17.95	.14	3.40
24SI(D)	10.75	3.28	3.41
26P (D)	11.19	-.11	3.31
28S (D)	4.46	2.28	3.00
30CL(D)	4.89	-.62	2.59
32AR(D)	-2.16	2.47	2.69
34K (D)	-1.41	-.65	2.71
36CA(D)	-6.45	2.59	2.64
38SC(D)	-4.67	-1.17	1.84
40TI(D)	-9.01	2.23	1.55

TZ = -5/2
****

NUC.	MASS EXCESS	BINDING ENERGY 1P	BINDING ENERGY 2P
17NA(X)	35.79	-3.83	-3.60
19MG(X)	32.63	.23	-1.43
21AL(X)	26.62	-1.93	.84
23SI(D)	23.29	1.95	2.08
25P (D)	19.48	-1.44	1.83
27S (D)	17.91	.57	.46
29CL(D)	14.31	-2.56	-.28
31AR(D)	11.73	.45	-.17
33K (D)	7.51	-2.38	.09
35CA(D)	4.73	1.16	.51
37SC(D)	3.81	-2.97	-.38
39TI(D)	2.19	.43	-.74

TZ = -3
****

NUC.	MASS EXCESS	BINDING ENERGY 1P	BINDING ENERGY 2P
18MG(X)	44.08	-1.00	-4.83
20AL(X)	42.23	-2.31	-2.08
22SI(X)	32.11	1.79	-.13
24P (X)	32.91	-2.33	-.38
26S (X)	27.25	-.48	-1.93
28CL(D)	27.98	-2.78	-2.21
30AR(X)	21.65	-.05	-2.61
32K (X)	21.75	-2.73	-2.28
34CA(X)	14.03	.77	-1.61
36SC(X)	15.28	-3.26	-2.10
38TI(D)	10.72	.38	-2.59

0 0 0 4 3 0 7 2 9 8

APPENDIX II

Experimental ground-state cross sections of some low-cross section multiparticle transfer reactions are presented. Only reactions with $|\Delta T_z| \geqslant 3/2$ and $d\sigma/d\Omega < 10$ μb/sr are included. Cross sections are quoted in the center of mass, except for references d, i, and l, which do not indicate the frame of reference used.

projectile ΔT_z	reaction	ref.	beam energy (MeV)	lab angle (deg)	$d\sigma/d\Omega$ ($\mu b/sr$)
	$^{16}O(^{7}Li,^{8}B)^{15}C$	a	78.9	15	2.1
	$^{26}Mg(\quad)^{25}Ne$	b	78.9	15	0.35
	$^{12}C(^{7}Li,^{10}C)^{9}Li$	c	80	7.4	0.6
	$^{16}O(\quad)^{13}B$	c	80	7.4	0.4
- 3/2	$^{7}Li(^{7}Li,2p)^{12}Be$	d	~30	30	2.9
	$^{9}Be(^{9}Be,^{8}B)^{10}Li$	e	121	14.4	0.030
	$^{12}C(\quad)^{13}B$	a	121	14.4	0.13
	$^{26}Mg(^{11}B,^{8}B)^{29}Mg$	f	86	11	0.015
	$^{28}Si(\quad)^{31}Si$	f	86	11	0.08
	$^{14}N(p,^{6}He)^{9}C$	g	54.7	14.1	0.16
	$^{24}Mg(\quad)^{19}Na$	g	54.7	14.1	0.12
	$^{28}Si(\quad)^{23}Al$	g	54.7	14.1	~ 0.05
	$^{10}B(^{3}He,^{6}He)^{7}B$	h	50	14.1	0.56
+ 3/2	$^{11}B(\quad)^{8}B$	h	50	14.1	1.44
	$^{12}C(\quad)^{9}C$	i	68.5	10.5	2.8
	$^{16}O(\quad)^{13}O$	j	65.3	10.6	0.76
	$^{20}Ne(\quad)^{17}Ne$	k	62.6	10	0.1
	$^{24}Mg(\quad)^{21}Mg$	j	55.9	14.1	0.84
	$^{28}Si(\quad)^{25}Si$	l	70	10	0.9
	$^{40}Ca(\quad)^{37}Ca$	j	55.9	11.2	0.175
	$^{12}C(\alpha,^{8}He)^{8}C$	m	156	2	0.06
+ 2	$^{24}Mg(\quad)^{20}Mg$	m	156	2	0.004
	$^{26}Mg(\quad)^{22}Mg$	n	110.6	10	0.06

References for Appendix II

a. K. H. Wilcox, unpublished data.

b. Ref. 2; and this work.

c. J. Cerny, R. B. Weisenmiller, N. A. Jelley, K. H. Wilcox, and G. J. Wozniak, Phys. Letters 53B, 247 (1974); and R. B. Weisenmiller, private communication.

d. H. H. Howard, R. H. Stokes and B. H. Erkkila, Phys. Rev. Letters 27, 1086 (1971).

e. This work.

f. Ref. 3.

g. J. Cerny, R. A. Mendelson, Jr., G. J. Wozniak, J. E. Esterl, and J. C. Hardy, Phys. Rev. Letters 22, 612 (1969).

h. R. L. McGrath, J. Cerny, and E. Norbeck, Phys. Rev. Letters 19, 1442 (1967).

i. G. F. Trentelman, B. M. Preedom, and E. Kashy, Phys. Rev. C6, 2205 (1971).

j. G. W. Butler, J. Cerny, S. W. Cosper, and R. L. McGrath, Phys. Rev. 166, 1096 (1968).

k. G. J. Wozniak, unpublished data.

l. G. F. Trentelman and I. D. Proctor, Phys. Letters 35B, 570 (1971).

m. R. G. H. Robertson, S. Martin, W. R. Falk, D. Ingham, and A. Djaloeis, Phys. Rev. Letters 32, 1207 (1974).

n. J. Cerny, N. A. Jelley, D. L. Hendrie, C. F. Maguire, J. Mahoney, D. K. Scott, and R. B. Weisenmiller, Phys. Rev. C10, 2654 (1974).

REFERENCES

1. B. J. Cole, A. Watt, and R. R. Whitehead, J. Phys. (London) A 7, 1399 (1974).

2. K. H. Wilcox, N. A. Jelley, G. J. Wozniak, R. B. Weisenmiller, H. L. Harney, and Joseph Cerny, Phys. Rev. Letters 30, 866 (1973).

3. D. K. Scott, B. G. Harvey, D. L. Hendrie, L. Kraus, C. F. Maguire, J. Mahoney, Y. Terrien, and K. Yagi, Phys. Rev. Letters 33, 1343 (1974).

4. S. Cohen and D. Kurath, Nucl. Phys. 73, 1 (1965).

5. G. T. Garvey, Ann. Rev. Nucl. Sci. 19, 433 (1969).

6. N. Zeldes, Ark. Fys. 36, 361 (1967).

7. M. Bolsterli, E. O. Fiset, J. R. Nix, and J. L. Norton, Phys. Rev. C5, 1050 (1972).

8. M. Brack, J. Damgaard, A. S. Jensen, H. C. Pauli, V. M. Strutinsky, and C. Y. Wong, Rev. Mod. Phys. 44, 320 (1972).

9. V. M. Strutinsky, Yadern. Fiz. 3, 614 (1966) (transl: Soviet J. Nucl. Phys. 3, 449 (1966)).

10. V. M. Strutinsky, Nucl. Phys. A95, 420 (1967).

11. V. M. Strutinsky, Nucl. Phys. A122, 1 (1968).

12. E. Comay, S. Liran, J. Wagman, and N. Zeldes, Proc. Int. Conf. Prop. Nuclei Far from the Region of Beta-Stability, Leysin, 1970 (CERN, 1970), Vol. 1, p. 165.

13. J. Wing, Proc. 3rd Int. Conf. on Atomic Masses, Winnipeg, 1967, ed. R. C. Barber (Univ. of Manitoba Press, 1967), p. 194.

14. J. Wing, Nucl. Phys. A120, 369 (1968).

15. N. Zeldes, M. Gronau, and A. Lev, Nucl. Phys. 63, 1 (1965).

16. N. Zeldes, A. Grill, and A. Simievic, Mat. Fys. Skr. Danske Vid. Selsk. 3, No. 5 (1967).

17. S. Liran and N. Zeldes, Proc. Int. Conf. on Nucl. Phys., Munich, 1973, ed. J. de Boer and H. J. Mang (North-Holland/American Elsevier, Amsterdam, 1973), Vol. 1, p. 322.

18. G. T. Garvey, W. J. Gerace, R. L. Jaffe, I. Talmi, and I. Kelson, Rev. Mod. Phys. 41, S1 (1969).

19. G. T. Garvey and I. Kelson, Phys. Rev. Letters 16, 197 (1966).

20. J. Jänecke and H. Behrens, Z. Phys. 256, 236 (1972).

21. J. Jänecke and H. Behrens, Proc. Int. Conf. on Nucl. Phys., Munich, 1973, ed. J. de Boer and H. J. Mang (North-Holland/American Elsevier, Amsterdam, 1973), Vol. 1, p. 321.

22. J. Jänecke and H. Behrens, Phys. Rev. C9, 1276 (1974).

23. M. K. Basu and D. Banerjee, Phys. Rev. C3, 992 (1971).

24. J. Jänecke, Phys. Rev. C6, 467 (1972).

25. J. Jänecke and B. P. Eynon, Nucl. Phys. A243, 326 (1975).

26. W. H. Bassichis and S. S. Ali, Phys. Letters 52B, 282 (1974).

27. S. Goldstein and I. Talmi, Phys. Rev. 105, 995 (1957).

28. A. de-Shalit and I. Talmi, Nuclear Shell Theory (Academic, New York, 1963).

29. C. Thibault and R. Klapisch, Phys. Rev. C9, 793 (1974).

30. N. A. Jelley, J. Cerny, D. P. Stahel, and K. H. Wilcox, Lawrence Berkeley Laboratory Report No. LBL-3414 (unpublished).

31. Masses were generally taken from A. H. Wapstra and N. B. Gove, Nucl. Data A9, 265 (1971). References to most new masses of interest are given in Table I; a few other new or revised masses (for ^{34}P, ^{38}S, and ^{58}Mn) are cited in Ref. 30. In addition, in order to determine all the parameters, it was necessary to use the mass of the particle-unstable nuclide ^{7}He.

32. J. D. Bowman, A. M. Poskanzer, R. G. Korteling, and G. W. Butler, Phys. Rev. C9, 836 (1974).

33. A. G. Artukh, G. F. Gridnev, V. L. Mikheev, V. V. Volkov, and J. Wilczynski, Nucl. Phys. A192, 170 (1972).

34. R. Klapisch, C. Thibault, C. Rigaud, A. M. Poskanzer, L. Lessard, and W. Reisdorf, Proc. Int. Conf. on Nucl. Phys., Munich, 1973, ed. J. de Boer and H. J. Mang (North-Holland/American Elsevier, Amsterdam, 1973), Vol. 1, p. 325; and C. Thibault, R. Klapsich, C. Rigaud, A. M. Poskanzer, R.Prieels, L. Lessard, and W. Reisdorf, Phys. Rev. C14 (to be published).

35. I. Kelson and G. T. Garvey, Phys. Letters 23, 689 (1966).

36. Fig. 16 in Ref. 32 presents those neutron-deficient nuclei expected to lie on the edge of stability, based on minor updating of Ref. 35. ^{33}K and ^{34}K are incorrectly shown therein[32] as nucleon stable due to an error in the proof of Ref. 35.

37. Dhom Products, 11120 Compton, N. Nollywood, CA 91603.

38. D. J. Clark, J. Stayaert, J. Bowen, A. Carneiro, and D. Morris, AIP Conf. Proc. No. 9, Cyclotrons--1972 (Proc. 6th Int. Cyclotron Conf., Vancouver, 1972), ed. J. J. Burgerjon and A. Strathdee (AIP, N.Y. 1972), p. 265.

39. K. W. Ehlers, Nucl. Instr. and Meth. 18, 571 (1962).

40. R. E. Hintz, F. B. Selph, W. S. Flood, B. G. Harvey, F. G. Resmini, and E. A. McClatchie, Nucl. Instr. and Meth. 72, 61 (1969).

41. Leonard Ho, private communication.

42. J. L. Gallant, Nucl. Instr. and Meth. 102, 477 (1972).

43. F. S. Goulding, D. A. Landis, J. Cerny, and R. H. Pehl, IEEE Trans. Nucl. Sci. 13, 514 (1966).

44. J. Cerny, S. W. Cosper, G. W. Butler, H. Brunnader, R. L. McGrath, and F. S. Goulding, Nucl. Instr. and Meth. 45, 337 (1966).

45. Approximate values for b are 1.6 for Li-B, 1.5 for C, 1.4 for Ne, and 1.2 for Ar. Exact values depend (among other things) on the

thicknesses of the ΔE detectors used. Dr. A. M. Poskanzer, private communication.

46. F. S. Goulding, D. A. Landis, J. Cerny, and R. H. Pehl, Nucl. Instr. and Meth. 31, 1 (1964).

47. ORTEC, Inc., 100 Midland Rd., Oak Ridge, Tenn. 37830.

48. FORTRAN program CHAOS, provided by Dr. C. C. Maples .

49. C. C. Maples, Lawrence Berkeley Laboratory Report No. LBL-253 (Ph.D. Thesis), Sept. 1971 (unpublished).

50. D. R. Goosman and D. E. Alburger, Phys. Rev. C7, 1133 (1973).

51. A. P. Kabachenko, I. B. Kyznetzov, K. Sivek-Vilchinka, E. A. Skakun, and N. I. Tarantin, Joint Institute for Nuclear Research, Dubna, Report No. D7-5769, 1971 (unpublished), p. 204 (transl: Brookhaven National Laboratory Report No. BNL-tr-511 (unpublished)).

52. D. H. Gloeckner, R. D. Lawson, and F. J. D. Serduke, Phys. Rev. C9, 2071 (1974).

53. R. B. Weisenmiller, private communication (to be published).

54. F. Ajzenberg-Selove, Nucl. Phys. A152, 1 (1970).

55. J. D. Bowman, A. M. Poskanzer, R. G. Korteling, and G. W. Butler, Phys. Rev. C9, 836 (1974).

56. J. Cerny, Proc. Int. Conf. Reactions between Complex Nuclei, Nashville, 1974, ed. R. L. Robinson, F. K. McGowan, J. B. Ball, and J. H. Hamilton (North-Holland/American Elsevier, Amsterdam, 1974), Vol. 2, p. 483.

57. Made by Mr. Jack Walton, Lawrence Berkeley Laboratory.

58. H. W. Wyborny, Nucl. Phys. A185, 669 (1972).

59. W. F. Steele, G. M. Crawley, and S. Maripuu, Michigan State Univ. Cyclotron Laboratory Report No. MSUCL-98 (1973); and Phys. Letters (to be published).

60. S. N. Abramovich, B. Ya. Guzhovsky, A. G. Zvenigorodsky, and S. V. Trusillo, Izv. Akad. Nauk SSSR, Ser. Fiz. 37, 1967 (1973).

61. R. R. Whitehead, Nucl. Phys. A182, 290 (1972).

62. B. M. Preedom and B. H. Wildenthal, Phys. Rev. C6, 1633 (1972).

63. A. O. Evwaraye and S. Maripuu, Bull. Am. Phys. Soc. 18, 577 (1973); and private communication.

64. D. H. Gloeckner, R. D. Lawson, and F. J. D. Serduke, Phys. Rev. C7, 1913 (1973).

65. P. M. Endt and C. van der Leun, Nucl. Phys. A214, 1 (1973).

66. N. A. Jelley, K. H. Wilcox, R. B. Weisenmiller, G. J. Wozniak, and Joseph Cerny, Phys. Rev. C9, 2067 (1974).

0 0 0 3 4 3 0 7 2 7 3

LEGAL NOTICE

This report was prepared as an account of work sponsored by the United States Government. Neither the United States nor the United States Energy Research and Development Administration, nor any of their employees, nor any of their contractors, subcontractors, or their employees, makes any warranty, express or implied, or assumes any legal liability or responsibility for the accuracy, completeness or usefulness of any information, apparatus, product or process disclosed, or represents that its use would not infringe privately owned rights.

TECHNICAL INFORMATION DIVISION
LAWRENCE BERKELEY LABORATORY
UNIVERSITY OF CALIFORNIA
BERKELEY, CALIFORNIA 94720